University of Tasmania

The Investigation of High Quality Surfing Waves Generated by a Moving Pressure Source

by

Mohammadreza Javanmardi

National Centre for Maritime Engineering and Hydrodynamics

Australian Maritime College

Submitted for fulfilment of PhD Candidature

Supervisors:

A/Professor Jonathan Binns

Professor Giles Thomas

Professor Martin Renilson

June 2015

Declaration of originality

This thesis contains no material which has been accepted for a degree or diploma by the University of Tasmania or any other institution, and to the best of my knowledge and belief no material previously published or written by another person except where due acknowledgement is made in the text of the thesis.

Mohammadreza Javanmardi 01 June 2015

Statement of Authority of Access

This thesis is not to be made available for loan or copying for two years following the date this statement was signed. Following that time the thesis may be made available for loan and limited photocopying in accordance with the Copyright Act 1968.

Mohammadreza Javanmardi 01 June 2015

Abstract

This thesis reports on an investigation into a novel method for generating surfable waves. This is a new surf pool concept to generate continuous surfable waves, with one or more pressure sources being rotated within an annular pool to generate waves. The circular channel has sloping bathymetry with the outer side being deeper; the waves are generated in the deep water and break in the shallow water on the inner island. Whilst previous experimental studies proved that it is possible to generate the surfable waves with this method, due to a lack of knowledge concerning waves generated in such a restricted environment, the influence of many parameters on the generated waves required investigation.

The research was conducted to better understand the wave generated by moving pressure sources, the waves' propagation and the effect of bathymetry on the wave quality for surfing. Studying all these parameters by experimental means would be exceptionally time consuming and expensive, so computational fluid dynamics was proposed as an effective alternative approach. Since previously proposed numerical methods were not able to predict the behaviour of these waves accurately, the main aim of the research described within this thesis was to investigate whether a new numerical method could be used as a research tool to gain insight into the production of highly controlled waves suitable for surfing and subsequently for proposed designs.

Experimental tests were conducted at the Australian Maritime College's towing tank and model test basin to investigate wave generation, improve the wave quality for surfing and provide validation data for the numerical investigation. A brief description of these experiments and the derived conclusions are presented. The towing tank test series mainly focused on the pressure source effect on the wave generated and the model test basin series considered the bathymetry effect on the wave propagation and control breaking point.

To investigate whether a numerical method could be used as a design tool for proposed designs, the finite volume approach was chosen to predict the wave generation and breaking characteristics. The accuracy and stability of the numerical scheme were firstly investigated. The numerical results for different configurations were compared with the experimental data. It was found that the numerical approach used is capable of accurately predicting wave height, propagation and forces on the pressure sources.

A grid study was conducted to optimise the simulation cost and accuracy. In this mesh study, the effect of aspect ratio, the number of cells per wave length and wave height were also investigated. It was shown that mesh quality has a significant effect on wave height prediction.

To better understand the effect of channel bathymetry on the wave breaking location, wave breaking intensity, peel angle and wave wall length for different channels were numerically examined at full scale. It was shown that high quality continuous breaking waves with the desired plunging shape and long wave length were able to be generated and it is possible to create waves suitable for surfers from beginner to expert level by changing the pressure source speed. From the channels studied it was concluded that channel shape does not have a significant effect on the maximum wave height, but the width of the deep section of the channel has a significant influence on the breaking location and the channel slope has an effect on the breaking intensity. The wave wall length was longest in the channel with the widest deep-section.

To determine the influence of the pressure source parameters on generating high quality surfable waves, different pressure source shapes were modelled. By comparing the results, the effects of

wavedozer parameters were investigated. The effects of wavedozer parameters such as draught, angle of attack and beam were investigated and it was shown that increasing the draught, angle of attack and beam increases the height of the generated waves. It was showed that increasing the beam is more effective than increasing draught in terms of increasing the wave height. The waves generated by a higher attack angle wavedozer were found to be larger than the lower attack angle, but the quality of the waves generated by the lower angle of attack was better.

Acknowledgment

I would like to express my special appreciation to my supervisors Dr Jonathan Binns, Associate Professor Giles Thomas and Professor Martin Renilson.

Jonathan you have been a tremendous mentor for me. I would like to thank you for your encouragement and helping me to grow both personally and as a research scientist. Your advice on both research as well as on my career have been priceless. You have been supportive since the day I came to Australia even to improve my English.

I take this opportunity to thank Greg Webber, whose idea of making a continuously breaking surfing wave pool sent me on this journey of discovery.

Thanks to Steven Schmied who has contributed in the experimental part of my project. Further, I thank all the staff at UTAS AMC who have been so welcoming and supportive, especially the technical support staff: Dr Gregor Macfarlane, Kirk Meyer, Liam Honeychurch, Mike Underhill and Peter Tomic.

I would like to thank the Australian Research Council (ARC) for awarding a Linkage Project grant to the joint Liquid Time Pty Ltd and UTAS AMC team.

Hearty thanks to Jalal Rafie Shahraki whom I know from the first day in undergraduate school. His supports helped me to never feel how far I am from home.

A special thanks to my family. Words cannot express how grateful I am to my sibling for all of the sacrifices that they have made, on my behalf, taking care of my lovely mother. Your prayer for me was what sustained me thus far. I would also like to thank all of my friends in Launceston whom created an enjoyable time for me during my studies.

Table of Contents

Table of Figures

Table of Tables

Nomenclature

α	Volume fraction value
ε	Turbulence dissipation rate
θ	Vortex breaking angle
k	Turbulence kinetic energy
κ	Blockage factor
λ	Wavelength
λ_s	Wavelength perpendicular to the beach slope
v	Cell volume
ϑ	The kinematic viscosity
ξ	Irribarren number
ρ	Density
∇	Displacement
A	Area
A_c	Channel cross section area
AMC	Australian Maritime College
A_s	Pressure source cross section area
ASR	Artificial Surfing Reef
B	Beam of model
BC	Boundary Condition
C_d	Drag coefficient
CFD	Computational Fluids Dynamics
C_l	Lift coefficient
C_p	Pressure force coefficient
d	Draught
f_i	External force
FDM	Finite Difference Method
Fr_h	Depth Froude number
FVM	Finite Volume Method
g	Acceleration of gravity
GIS	Grid-independent solution
h	Water depth

H	The trough to crest height of the first significant wave
H_{beach}	Wave height at the start of the beach
HRIC	High Resolution Interface Capturing scheme
l	Vortex length
LWL	Length of Water Line
MTB	Model Test Basin
P	Pressure
PRESTO	Pressure Staggering Option
s	Beach slope
SIMPLE	Semi-Implicit Method for Pressure-Linked Equations
T	Wave period
TT	Towing Tank
u	Velocity
$\overline{\acute{u}_i \acute{u}_j}$	Reynolds stress
V	Vessel speed
w	Vortex width
W	Width of channel
WL	Wave wall length
WP	Wave Prob
χ	Scale factor
x	Longitudinal coordinate
y	Lateral coordinate
y_{beach}	Beach Lateral start point
z	Vertical coordinate
z_{beach}	Beach start step size

Publications Relevant to the Thesis

The publications are as follows:

- Javanmardi, M., Binns, J., Renilson, M. R., Thomas, G., Schmied, S., Huijsmans, R., "The Formation of Surfable Waves in a Circular Wave Pool- Comparison of Numerical and Experimental", proceeding of the ASME 2012 31st International Conference on Ocean, Offshore and Arctic Engineering OMAE2012, July 1-6, Rio de Janeiro, Brazil.
- Javanmardi, M., Binns, J., Renilson, M. R., Thomas, G., " The Prediction of Moving Body Wave Patterns in a Confined Channel at Large Distances from the Body", 18th Australasian Fluid Mechanics Conference, 3-7 December 2012, Launceston, Australia.
- Javanmardi, M., Binns, J., Renilson, M. R., Thomas, G., "Prediction of Water Wave Propagation Using Computational Fluid Dynamics", proceeding of the ASME 2013 32nd International Conference on Ocean, Offshore and Arctic Engineering OMAE2013, June 9-14, 2013, Nantes, France.
- M. Javanmardi, J. Binns, G. Thomas, M. Renilson, "An investigation into the effect of pressure source parameters and water depth on the wake wash wave generated", International Journal of Engineering for the Maritime Environment, submitted 20- May- 2015.
- Javanmardi, M., Binns, J., Thomas, G., Renilson, M. R., "Mesh quality effects on the accuracy of water wave propagation from a moving body", International Journal of Computational Fluid Dynamics, submitted 21- May-2015.
- Javanmardi, M., Binns, J., Thomas, G., Renilson, M. R., "Influence of channel shape on wave generated parameters by a pressure source in shallow water", International Journal of Waterway, Port, Coastal and Ocean Engineering, submitted 21- May-2015.

1. Introduction

Surfing is a popular sport at many coastal locations around the world. The number of surfers worldwide is estimated at 23 million and in 2010 the revenue of the global surfing industry stood at $6.24 billion [1]. According to the research of Sweeney [2], there are approximately 2.5 million recreational surfers in Australia with 420,000 participating in surf schools annually. 107 affiliated surf schools operate at more than 550 beaches around Australia [3]. This interest in surfing is on the increase. Although surfers need only a surf board and an appropriate beach, locations with a suitable environment are limited. Indeed, surf breaks that consistently produce world class surfing conditions are rare [4] and are often overcrowded. In addition, weather conditions are not always suitable for surfing. The growth of surfing, along with the environmental limitations, has led to a new concept: the surfing pool.

1.1. Surfing pool

A surfing pool is a basin of water in which waves are generated to allow someone to surf. It provides an opportunity for surfing every day, independent of both weather and location, even for people who live far from the sea. Since sea waves are random from surfer's point of view, it is rare to find a place that is suited to all surfers from beginner to expert. However it is possible to generate artificial waves with different parameters in the surf pool and the level of safety is much higher than surfing in the sea.

The Wembley swimming pool in London, constructed in 1934 [5], contained the first artificial wave maker used for surfing. In 1966, indoor surfing was made possible in a wave pool in Tokyo, Japan [5]. Of the many surfing pools constructed, several different approaches have been implemented to create surfing conditions. The most commonly used wave makers are the flap- and piston-type wave makers. A flap-type wave maker utilises a hinged board which oscillates around a rotation point. A piston-type wave maker uses a paddle with a linear actuator to generate waves. Figure 1-1 shows the piston- and flap-type wave makers schematically. Another method of generating waves is a thin layer of water injected onto a wave-shaped surface, this type of wave pool is shown in Figure 1-2.

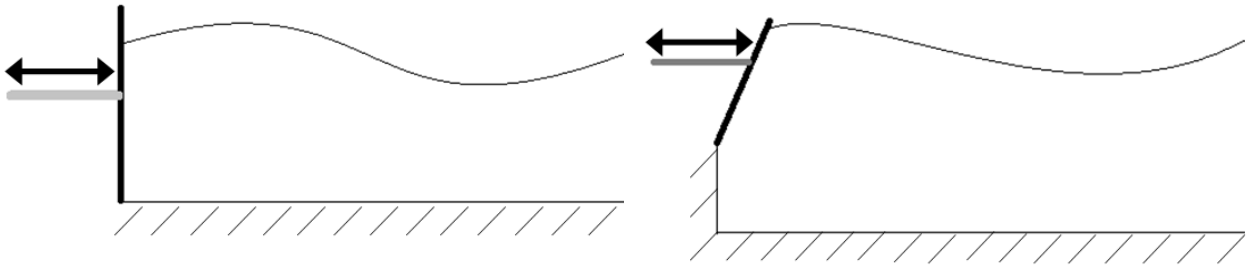

Figure 1-1: Piston and flap-type wave-maker

Figure 1-2: A type of surf pool [6]

A new surf pool concept was developed by Greg Webber and his idea to produce continuous breaking waves was patented [7, 8] by Liquid Time Pty Ltd. This invention is based on a circular pool in which the surfing waves are created continuously along the banks of the pool [9]. The idea was born from Webber's experiences surfing in the Clarence River on waves generated behind a fishing boat as shown in Figure 1-3.

Webber's idea is based on one or more pressure sources being rotated within an annular wave pool to generate waves. A pressure source is any object that disrupts the water's surface and creates a wave. The circular channel has sloping bathymetry with the outer side being deeper; the waves are generated in the deep water and break in the shallow water on the inner island. A circular wave pool is capable of providing a theoretically infinitely long ride around a central island which is not possible in the conventional style of surfing pools. The pool should be capable of creating waves from beginner to expert level and providing a safe learning environment for novice surfers. Figure 1-4 shows the concept design of the circular wave pool.

Figure 1-3: Surfing in the Clarence river on waves generated by a fishing boat [10]

Figure 1-4: Greg Webber's circular wave pool concept [9]

1.2. Background

The related topics of creating the perfect surfing wave can be separated into four different categories: wave generation; shallow water waves; Artificial Surfing Reef (ASR) design; and previous studies of the circular wave pool.

The wake pattern which is produced by a moving point across the surface of deep water was first explained mathematically by Lord Kelvin (William Thomson) [11] and is known as the Kelvin wake pattern. Kelvin's theory was later refined through experiments on waves generated by a moving vessel in deep and shallow waters [12, 13]. All vessels operating in deep water produce a Kelvin type wave pattern consisting of two kinds of waves: transverse waves which crest across the ship track and divergent waves which crests roughly parallel to the ship track, moving outward. The waves are

confined to a wedge shaped region behind the ship, and the half angle of the wedge is 19.5 degrees. This angle is independent of the ship speed as long as the deep water condition is satisfied. The classical Kelvin wave pattern is generated at depth Froude number of less than 0.57 [14], where the Depth Froude number (Fr_h) is defined as the ratio of vessel speed to the wave propagation speed in shallow water:

$$Fr_h = \frac{V}{\sqrt{gh}}$$

where V(m/s) is the vessel speed, g (m/s^2) is the acceleration of gravity, and h (m) is the water depth. Figure 1-5 illustrates the Kelvin wave pattern.

As the Depth Froude number approaches 1.0, the vessel speed becomes equal to the maximum wave propagation speed in the given water depth. This speed is often called the 'critical speed'. At this stage, all transverse waves are pushed in front of the vessel, resulting in a wave building perpendicular to the vessel and all diverging waves form behind this critical wave.

As a deep water wave approaches the velocity orbits become flattened circles, or ellipses (Figure 1-6). The wave begins to 'feel' the bottom, and the resulting friction and compression of the orbits reduce the forward speed of the wave. The speed of the wave is equal to the wavelength divided by period.

$$C = \frac{\lambda}{T}$$

Where λ is wavelength and T is wave period. As the period of a wave does not change, therefore, when the wave 'feels the bottom', it slows, and the accompanying reduction in the wavelength and speed results in increased height and steepness as the wave's energy is condensed in a smaller water volume.

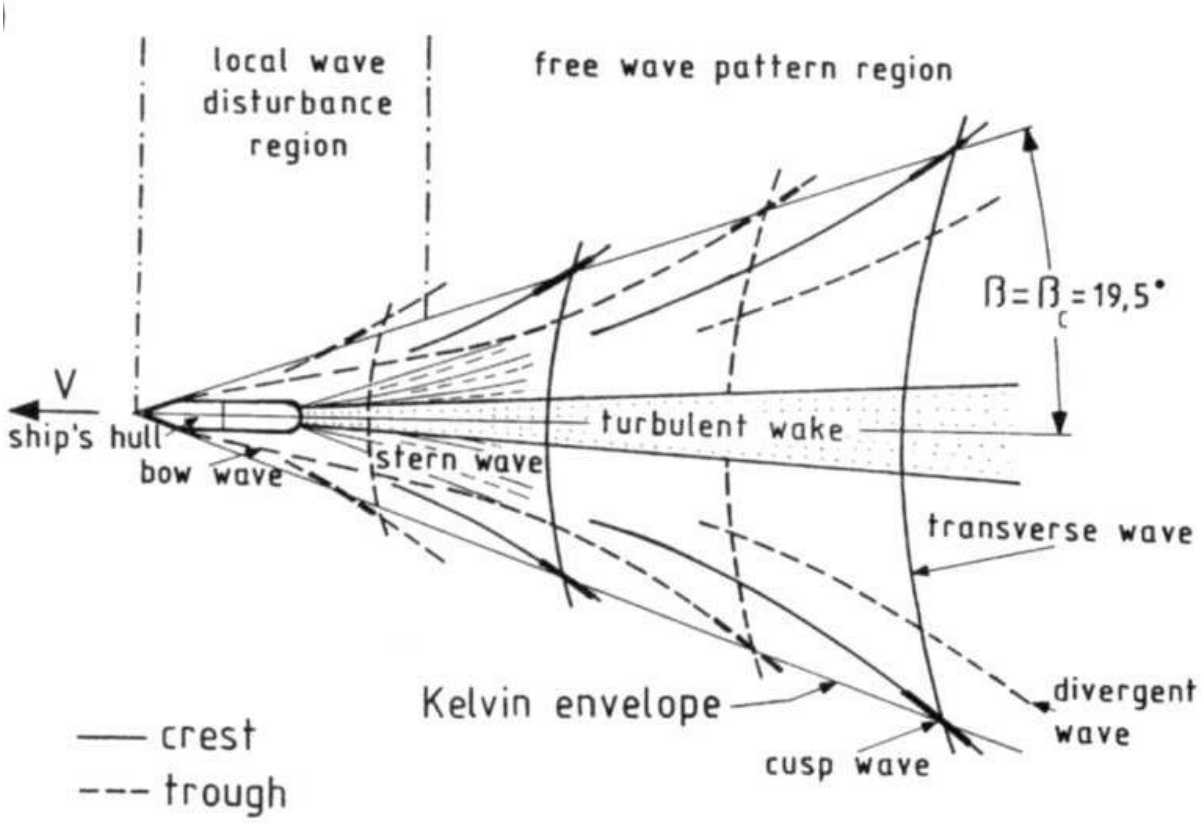

Figure 1-5: Kelvin wake pattern [15]

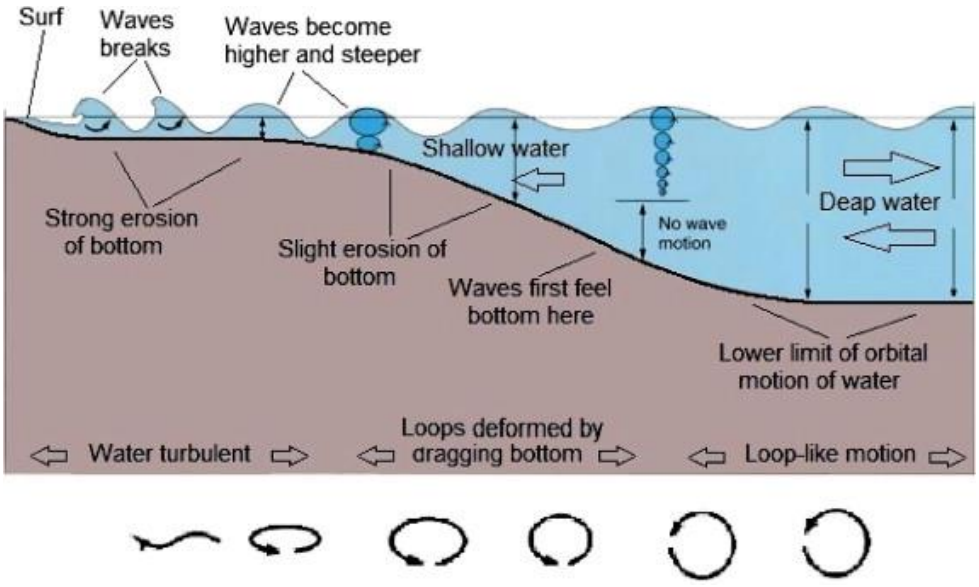

Figure 1-6: motion of water particles in different water depths [16]

In deep water the wave celerity is a function of the wavelength, while in shallow water the water depth limits the wave celerity. Water depths of more than half the wavelength can be considered as deep water, whereas water depth less than $1/20^{th}$ the wave length is commonly regarded as shallow water [17]. There are some processes that can affect the wave propagation into coastal and shallow water areas such as: refraction, diffraction, shoaling, breaking, friction and reflection. Many studies

have been conducted into the effect of waves on vessels operating in shallow and restricted waterways, for example [18-21]. In addition, significant research has been conducted into wash wave impacts on ecology and the environment, and vessel operation in shallow water close to the coastline [22-24]

As mentioned previously, the number of surfers has dramatically increased over recent years. Although there are thousands of kilometres of coastline around the world, there are only a small number of high-quality surfing breaks on these coasts [25]. Interest in creating ASRs has increased in response to demands on the existing breaks due to increased participation in the sport [25, 26]. The concept of multipurpose reefs has been developed recently [4, 27], so that these artificial reefs are also utilised for coastal protection, ecological restoration, fisheries enhancement and habitats for marine organisms.

Although much information has been available on using reefs for habitat enhancement and coastal protection, very little information is available on what makes a high-quality surfing break. In terms of surfing, waves require some special characteristics. The wave must be steep faced to produce high surfboard speed, but it must also have a well-defined breaking point. That is, waves must peel as they break, so the surfer can utilise the unbroken face of the wave close to the breaking part. The peel angle is a term used to describe the speed that a surfer is required to travel to successfully traverse across the face of a wave. The peel angle is the most useful parameter with respect to ASR design [25]. Walker defined the scheme used to classify the important waves parameters based on surfing skill [26]. Hutt[28] investigated the wave peel angle at Raglan Point in New Zealand and developed a new surfing skill classification scheme using wave angles and wave height. By changing the seabed slope, the shape of breaking changes [29]. Among the four classified wave breaking intensities (spilling, plunging, collapsing and surging), spilling and especially plunging waves are required for surfing [25]. Some investigators have tried to develop a method to predict the wave breaking intensity [30, 31]. Mead and Black [4] classified surfing wave breaking intensity based on reef gradient. Since the reef shape dictates the wave peel angle and wave breaking intensity, studies have been conducted to replicate reef shape. Recent advances in Computational Fluid Dynamics (CFD) modelling have made it possible to investigate a wide range of coastal projects. Some numerical studies have been conducted to design artificial reefs [32, 33]. There are many investigations have been conducted to define some functional reef components [34] (such as: ramp, focus, platform, wedge, and ridge) and tried to optimise the reef shape. There is much research need to optimise the wide variety of conditions. This research will add to the knowledge of the reefs performances.

The first attempt to prove the circular wave pool concept was by using a fishing vessel to generate waves in a river estuary, where the vessel travelled in a straight line close to the bank [35]. The test demonstrated that this approach could be used to create waves suitable for surfing (see Figure 1-3). In 2007, two master students, Schipper [36]and Vries [37], conducted preliminary numerical analysis

and scale model testing of pressure sources moving along a linear track at the TUDelft University towing tank. The main aim of their experiments was to map the similarities and differences with theory and produce a dataset to validate future numerical modelling. According to Schipper [36], different methods were used, including pressure point modelling, panel method modelling by DELKELV and 3D modelling by Navier Stokes solver FINLAB, which was partly developed at the University of Technology Delft. Schipper concluded that it is not possible to reproduce the experiments by using such a numerical approach.

Schmied conducted experimental research at the Australian Maritime College (AMC) into the surfing pool concept [10]. He proved that it is possible to generate the surfable wave by this method. Schmied tested several different pressure sources in a straight line [38] and a circular track [39]; he also conducted investigations to determine the effect of beach shape on wave breaking parameters. To optimise the pressure source parameters, he tested different pressure sources in the AMC towing tank at different speeds. For circular track testing, a model circular pool was built in the AMC basin. In this set of tests, some beach parameters such as width of channel, beach slope and beach shape were tested to determine their effect on the surfing waves created. He found that the design parameters were in competition, and to determine a balance of limiting values and the wave quality is extremely sensitive to changes in the design parameters. He also used a numerical approach by linear potential flow solver Michlet to predict the wave height. He conducted that Michlet was not able to be used to accurately predict the wave height.

Doyle [40] conducted preliminary numerical investigations to predict the curved path wave pattern, using ANSYS CFX software to predict the wave pattern generated by a parabolic pressure source in a curved track. He modelled the parabolic pressure source on two different radius curved tracks to investigate the relationship between turning radius and amplitude and compared the results with the theoretical approach. He concluded that ANSYS CFX is not capable of reproducing a realistic wave pattern for such a scenario.

Van Essen [41] used a non-linear potential flow code (RAPID), which had been developed by the Maritime Research Institute Netherlands (MARIN), to predict the wave height for waves generated by wavedozer. She found that RAPID was not able to predict the wave height and free surface elevation close to a pressure source and breaking points.

1.3. Numerical methods

Engineers and designers solve fluid dynamics problems for a wide range of industrial areas including hydrodynamics, aerodynamics, civil engineering and biomechanics.

Generally, there are two ways to investigate the free surface problem: experimental and numerical approaches. This section outlines the various options for undertaking such numerical work and concludes with a suggested methodology for this research.

Numerical methods can be categorised into either Lagrangian (material), Eulerian (spatial) or Arbitrary Lagrangian-Eulerian (ALE) frameworks. The Lagrangian formulation describes convection by placing a set of axes over the material particles that move according to the equations of motion. In the Eulerian formulation, axes are fixed in space and convection terms are incorporated into equations describing the fluid transport. Therefore, solid structures are usually described by Lagrangian formulations, while fluids are usually described by Eulerian formulations. Combining these approaches is generally accomplished through an ALE formulation.

The finite element method (FEM) is generally used for structural solutions, while the finite difference method (FDM) and the finite volume method (FVM) are used for fluid solutions. The advantage of a Lagrangian formulation is its capacity to simulate breaking waves or separated drops without free surface modelling.

The finite volume method is a discretisation method that is well suited for numerical simulations of various types of conservation laws. It has been used in several engineering fields, such as fluid mechanics, heat and mass transfer and petroleum engineering. The finite volume method can be used on arbitrary geometries, using structured or unstructured meshes and it leads to a robust scheme. The local conservation of the numerical fluxes is another feature of the finite volume method. It means the numerical flux is conserved from one discretisation cell to its neighbours. In fluid mechanics and other studies in which flux is important, researchers prefer to use the finite volume method [42].

Although experimental approaches such as the use of scale models are extremely valuable and a common practice, their limitations make it necessary to develop a numerical tool to assist. Some disadvantages, such as the equipment required, scaling problems, measurement difficulties and operating costs, have meant that numerical approaches have been considered as an alternative. Taking into account the advances in computer technology, the use of Computational Fluid Dynamics (CFD) is becoming a popular choice. Computational analyses in the early stages of design are advantageous and can reduce the number of design alternatives. In addition, operating costs may be cheaper than experimental tests once the computational domain and parameters have been set up. For instance, to change any part of a physical model, the model must be reconstructed, whereas in a numerical approach computer models can be easily reconfigured.

Table 1-1 compares some of advantages and disadvantages of experimental, theoretical and numerical approaches (updated from[43]).

Table 1-1: Comparison of Approaches

Approach	Advantages	Disadvantages
Experimental	1. Capable of being most realistic 2. No restriction to linearity 3. Complicated physics can be treated 4. Time evolution of flow can be obtained	1. Equipment required 2. Scaling problems 3. Measurement difficulties 4. Operating costs
Theoretical	1. Clean, general information, which is usually in formula form	1. Restricted to simple geometry and physics 2. Usually restricted to linear problems
Computational	1. No restriction to linearity 2. Complicated physics can be treated 3. Time evolution of flow can be obtained	1. Truncation errors 2. Boundary condition problems 3. Computer costs

1.4. Research questions and plan

Since there was insufficient knowledge about waves generated by moving a pressure source in a channel, studying all unknown questions experimentally would be excessively expensive and time consuming. In addition, all the previous numerical approaches used to predict wave generated parameters, by different authors and with different numerical methods, were unsuccessful. Schipper [36] used different methods including pressure point modelling, panel method modelling by DELKELV and 3D modelling by Navier Stokes solver FINLAB. Schmied [10] used a linear potential flow tool Michlet. Doyle [40]conducted numerical investigations using ANSYS CFX software and Essen [41] used a non-linear potential flow code (RAPID) to predict the wave generated. Unfortunately, none of the used methods were able to accurately predict the wave height. The most important research question related to the surfing pool is whether numerical methods can be used in the design of the wave making devices which none of the previous research into the numerical approaches has reached an acceptable answer to this question. If the numerical approach can be used to predict the wave parameters accurately, then the next question was: can the numerical method be used to improve the wave pool design. To pursue this final aim two different issues have been numerically investigated: shape of the pressure source and shape of the bathymetry.

In terms of pressure source, the research was focused on the impact of the pressure source parameters on the wave generated shape and propagation, to know how pressure source parameters such as shape, beam, draught and displacement affect the wave generated.

Bathymetric parameters; such as slope shape, size of step and slope angle, also need to be investigated. The channel parameters effect on the wave parameters and propagation should be investigated to produce high quality surfable waves, the peel angle and wave breaking intensity must be considered.

The efficiency of the system is very important and the system should be optimised in terms of energy required to power the pressure source. Scaling should be considered especially when the wave propagation is an issue. In conventional hydrodynamic model testing, the forces and vessel behaviours must be considered, while in this case the wave parameters and propagation must be evaluated accurately. In addition, it is not possible to use a common formula to scale the forces for complicated body shapes. Using a numerical approach in this study can tackle this problem.

Scientifically, the project aims to add to the knowledge of wave mechanics. In particular to develop an understanding of wave generation and transmission for a pressure source moving in a circular track. The outcomes from this work should also be able to be extended to other applications, such as vessel generated waves during manoeuvring and whilst operating in restricted waterways such as canals.

1.5. Contents and outline of the thesis

This section describes the main contents of the thesis and serves as a quick reference outline to the appropriate sections.

Chapter 2 - Validation experiments

The aim of this chapter is to present a brief background about the experimental tests which were conducted at Australian Maritime College since 2009. Two series of scale experiments in the towing tank and model test basin are presented. The towing tank tests were mostly focused on the effect of pressure source on the wave generated, whilst the model test basin series mainly considered the effect of channel parameters on wave breaking. The experimental data was used as validation cases for the later numerical investigations.

Chapter 3 - Numerical verification and validation

Chapter 3 is concerned with the numerical verification and validation. The Computational Fluid Dynamics method employed is discussed in more detail. To investigate the ability of the numerical approach to predict the wave parameters and propagation, some benchmark cases were modelled and the wave results compared with the experimental data. In addition, the drag and vertical forces predicted using the numerical approach were compared with the results obtained from the experiments. A full mesh study, including the grid independency and the mesh quality, are also presented.

Chapter 4 - Output parameters to judge designs

The main emphasis of chapter 4 is the output parameters, which is needed to judge the design. It focuses on the effect of the bathymetry on the breaking wave shape and quality. Wave breaking location, wave breaking intensity, peel angle and wave wall length were investigated for full size channels in different depth Froude numbers for varying beach configurations. In addition, the scale effect on the wave height, propagation and forces (drag and lift) were investigated and the relationships determined.

Chapter 5- Use for design

Chapter 5 addresses the numerical results for the effect of the pressure source parameters and profile shape on the generated waves to improve the wave quality. Results for each of the design parameters are presented. In the second part of this chapter the effect of depth and blockage factor on the generated waves are discussed.

Chapter 6- Conclusions and recommendations

Chapter 6 contains the conclusions and some recommendations for further research.

.

2. Validation experiments

As outlined in the previous chapter, the main aim of this work was to develop a valid numerical technique for modelling breaking waves to aid the design and development of a surfing wave pool. In order to ascertain the validity of the numerical approach a comprehensive set of experimental data was required. Therefore an extensive programme of experiments was undertaken at the Australian Maritime College, commencing in 2009.

This programme of experiments had two main components. Firstly straight line tests in the AMC towing tank to enable the effects of pressure source shape and dimensions on the generated waves to be ascertained, and secondly experiments in the AMC's model test basin on a model of the full circular surfing wave pool to investigate the influence of the curved track and beach parameters.

Two series of straight line tests were conducted: firstly a range of different pressure sources was investigated by co-PhD student Steven Schmied [38] in shallow water (500mm water depth) – results from this initial set of experiments were subsequently reanalysed by this candidate. Secondly this candidate conducted a series of tests to investigate the effect of water depth and determine the drag forces on the pressure sources in deep water (1500mm).

Two test series were conducted in the model test basin jointly by this candidate and co-PhD student Steven Schmied to investigate the influence of the curved track and beach parameter effects on generated waves. In total 64 different conditions were tested in the MTB through 501 runs [39].

It is worth noting that in addition the industry partner for this work, Webber Wavepools, conducted full scale testing in the Clarence River at Yamba in New South Wales (NSW) to prove whether a surfable wave could be generated or not [10]. A fishing boat operating in shallow water was used to generate waves that broke along the river bank. These successful tests clearly demonstrated that vessel-generated waves could be used for surfing.

This chapter details the experimental programmes conducted in both the towing tank and the model test basin. It outlines the experimental set ups including instrumentation used, the various pressure sources and the key results.

2.1. Towing Tank tests

In 2009, the first experimental investigation for generating surfable waves by moving a pressure source was conducted at the AMC Towing Tank by Schmied as a part of his PhD research [10]. In these tests, three pressure sources (two parabolic shapes and a wavedozer) were used. These pressure sources were tested at different water depths, depth Froude numbers and draughts.

2.1.1. Towing Tank Setup

To measure the wave parameters in lateral distances from the centre line, five wave probes were set up in the Towing Tank as shown in Figure 2-1. The array WP1, WP2 and WP3 was used to determine the lateral changes of the waves and the array WP4, WP2 and WP5 was used to determine the longitudinal stability of the waves.

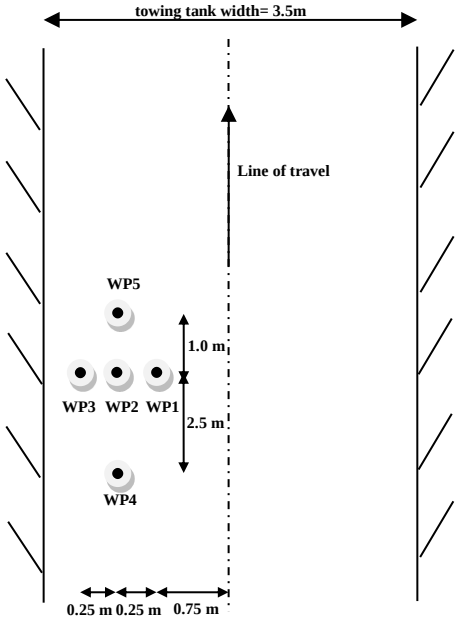

Figure 2-1:Towing Tank setup

2.1.2. Pressure source shape

Initial linear testing of the pressure source was conducted at the AMC Towing Tank in 2009. Two different pressure source shapes, parabolic and wavedozer, were investigated to determine the pressure source shape effect on waves generated for surfing. These two pressure sources were experimentally investigated by Schmied [10]. The ship waves are created by a pressure source where there is a change in the cross-sectional area; therefore the pressure sources with continually changing cross-section area were selected.

Parabolic pressure source

The parabolic shape model was symmetric about its centre line, and the water-plane was constant at different water depth levels. Figure 2-2 illustrates the parabolic models. The first pressure source was a parabolic pressure source of 700mm length, 300mm beam, and 100mm draught (left photo). And the second parabolic pressure source had 700mm length, 600mm beam, and 100mm draught (right photo). The beam effect on wave generation was demonstrated by doubling the model beam. The parabolic pressure sources were tested at different Fr_h.

Wavedozer

A wavedozer is a wedge-shaped body with a constant beam [44]. Table 2-2 shows the main particulars of the wavedozer which were tested in the TT. The angle of attack is the angle between the entry surface and the calm water surface. Figure 2-3 shows the wavedozer attached to the carriage in the AMC Towing Tank prior to a test run. This model was tested at different Fr_h.

Figure 2-2: Parabolic models

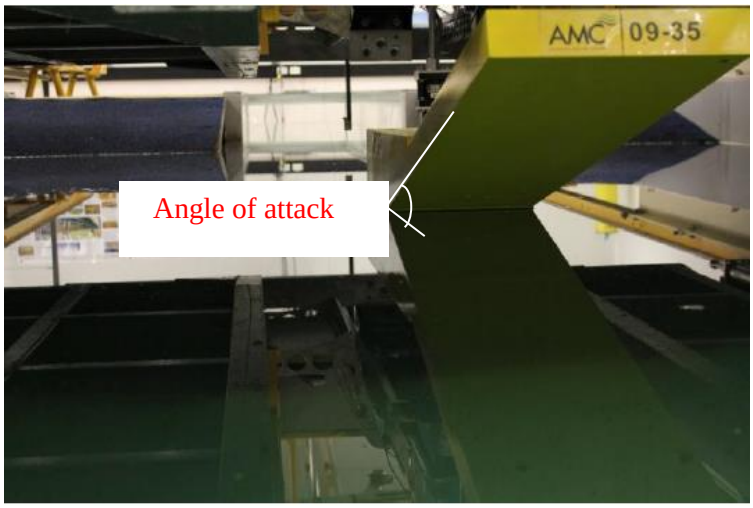

Figure 2-3: Wavedozer model attached to the towing Tank carriage

Table 2-1: Wavedozer Principal Particulars

Length (m)	1.5
Beam (m)	0.3
Angle of attack (deg.)	14
Draught (m)	0.1

2.1.3. Towing Tank Test Series and outcomes

During the towing tank tests series, two parabolic pressures and wavedozer sources were tested at different draughts. The matrix of the test series is shown in Table 2-2. The number of runs in this sequence was 125. By comparing the results for these tests, it was possible to consider the draught, beam and pressure source shape effect on the wave parameters. The longitudinal stability of each test run was determined by comparing the wave amplitudes at WP4, WP2 and WP5. In conclusion, the waves were generally stable for $Fr_h < 0.7$. For parabolic pressure sources instability was increased as Fr_h approached 1. From visual inspection this is due to increased wave breaking with the formation of solitons [38].

Table 2-2: Test Series

series	Pressure source	Beam[mm]	Draught
1	Parabolic	300	100
2	Parabolic	600	100
3	Wavedozer	300	100
4	Parabolic	300	200
5	Parabolic	600	200
6	Wavedozer	300	200
7	Parabolic	300	150
8	Parabolic	600	150
9	Wavedozer	300	150
10	Wavedozer	300	300
11	Wavedozer	300	250

In terms of wave height, the wave generated by the parabolic pressure source was higher than the wavedozer, but they were broken across the entire width of channel for $Fr_h > 0.75$. Soliton generation causes extremely unstable wave systems (Figure 2-4), and speeds of $Fr_h > 1.0$ were not tested. Comparing the results for different pressure sources (parabolic and wavedozer) with same parameters shows that the pressure source type has significant effect on the wave quality.

Figure 2-4: Breaking Bow wave and Soliton

The parabolic pressure source shapes are not ideal for generating surfable waves. It was concluded that the waves generated by the parabolic method always broke across the entire width of the channel for depth Froude numbers $Fr_h > 0.75$. In contrast, minimal to no breaking occurred in the wavedozer generated waves for $Fr_h < 0.95$. Therefore, the wavedozer was selected as the most suitable pressure source for future investigations.

In 2012, a new test series was conducted to measure the drag and vertical force of the system by author. The wavedozer was used as the pressure source during this experiment. A water depth of 1500mm and draught of 100mm was maintained for all of the tests. Three wave probes were positioned at different lateral distances, WP1, WP2 and WP3 in Figure 2-1. Two load cells were installed on the model to measure the vertical and drag forces as shown in Figure 2-5. The model was tested for various Depth Froude numbers from 0.26 to 0.99. The Figure 2-6 and Figure 2-7 show the drag and vertical forces for different depth Froude numbers.

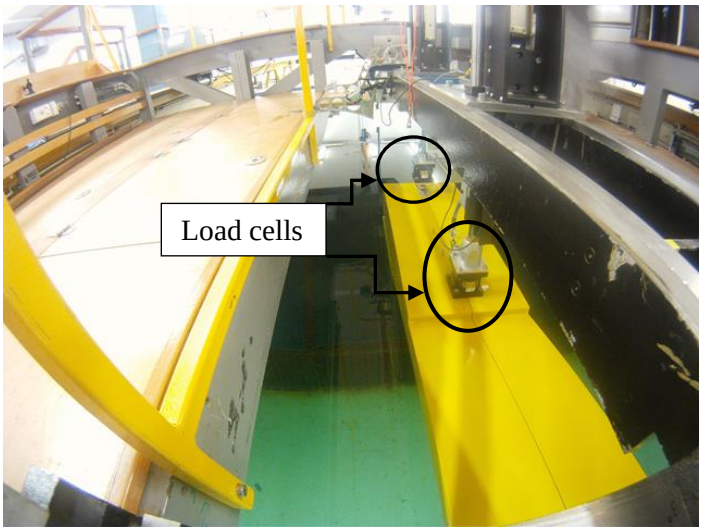

Figure 2-5: Load cells positions

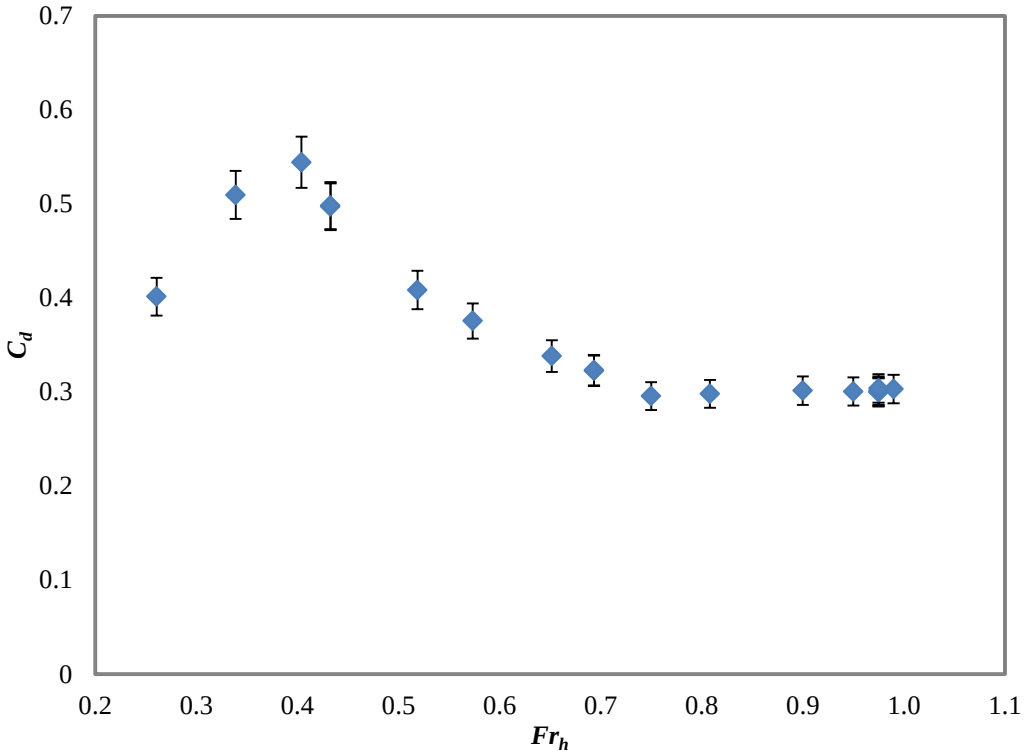

Figure 2-6: The drag coefficients for different depth Froude numbers

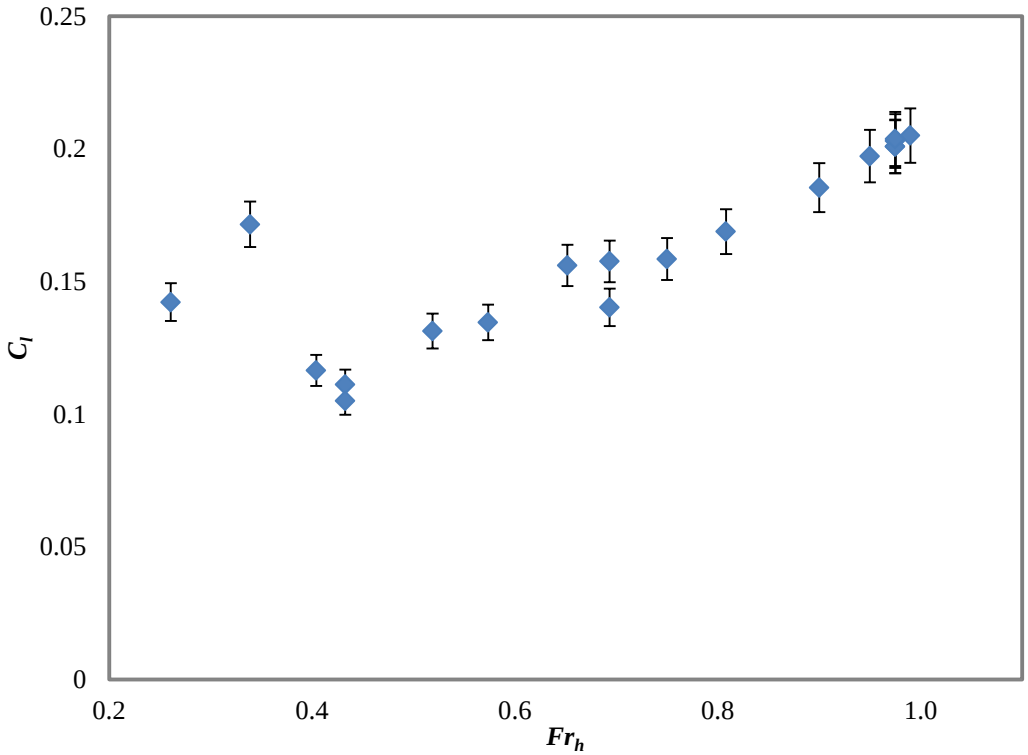

Figure 2-7: The vertical coefficients for different depth Froude numbers

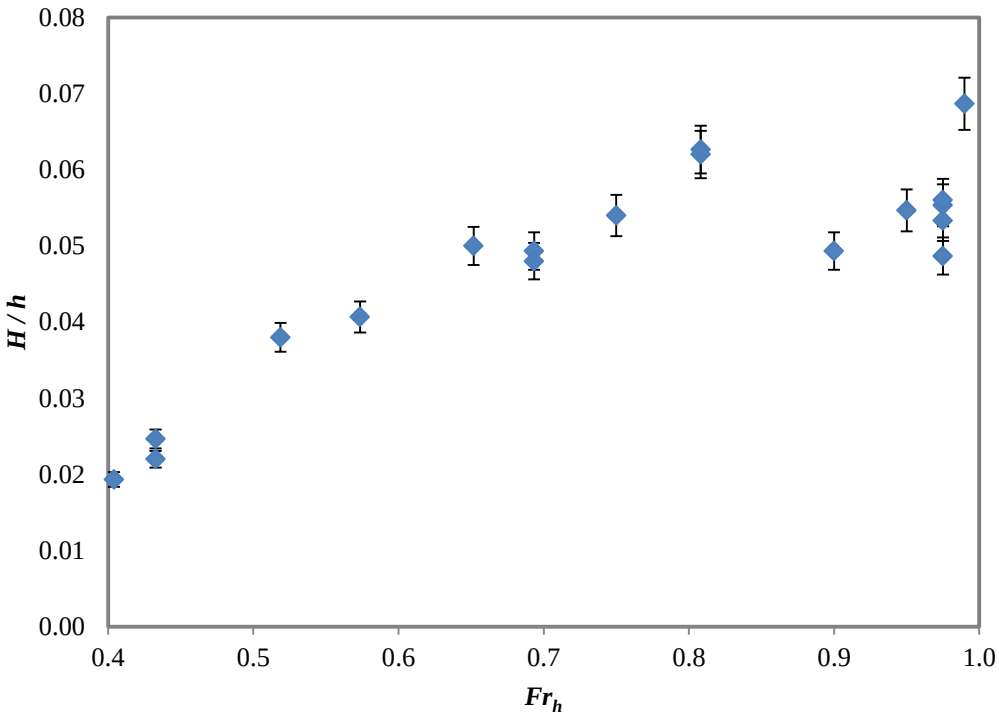

Figure 2-8: The experimental wave height data for varying depth Froude numbers at 0.75 lateral distance

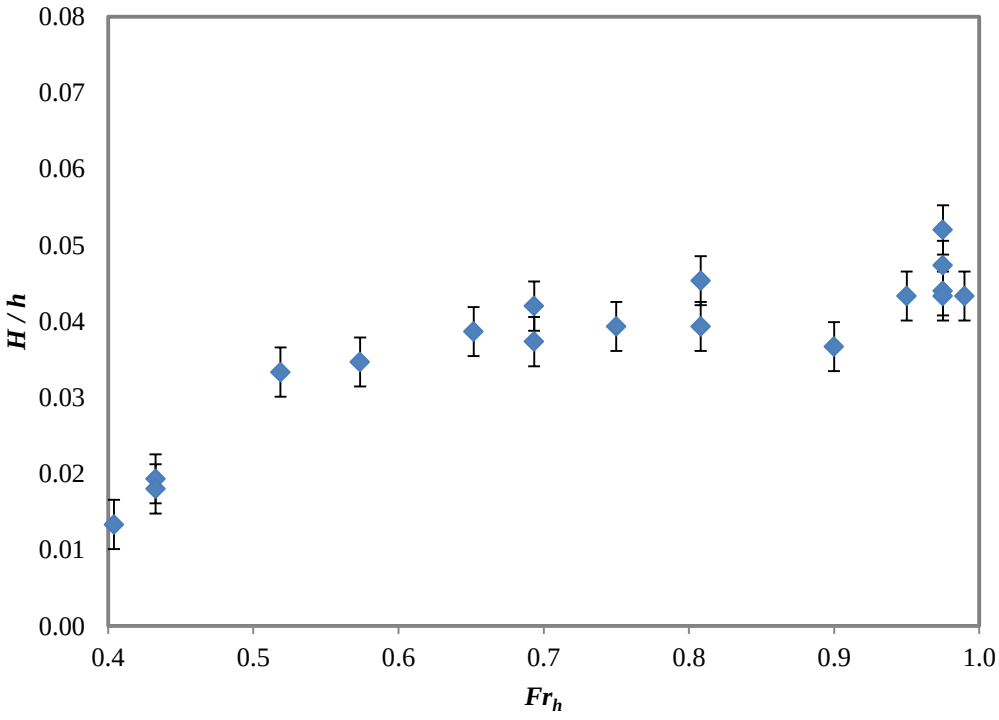

Figure 2-9: The experimental wave height data for varying depth Froude numbers at 1.0 lateral distance

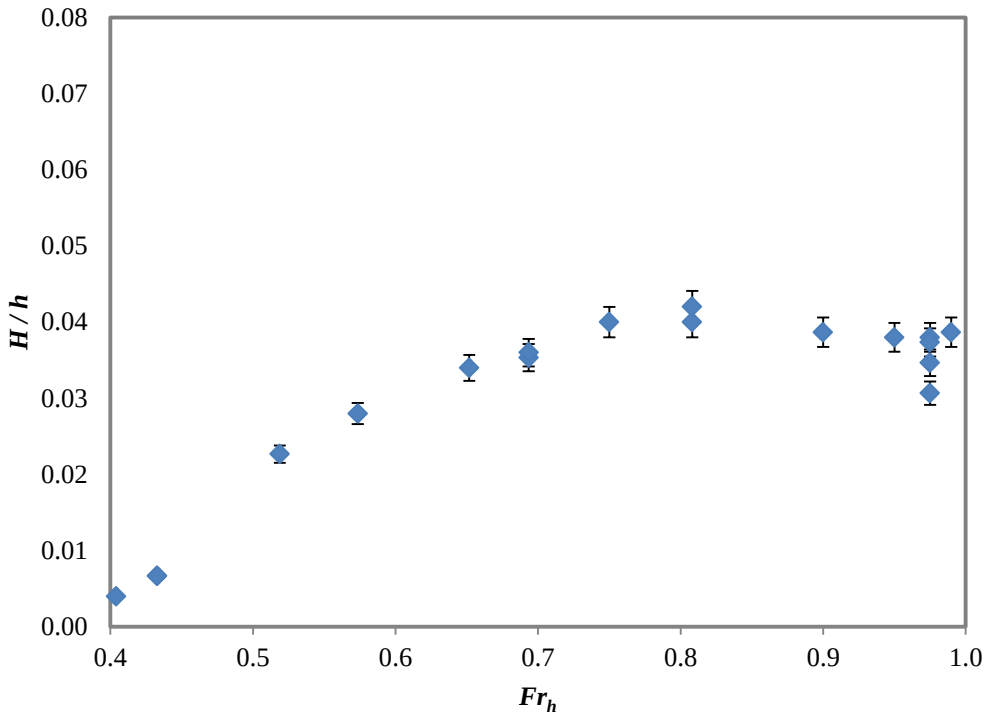

Figure 2-10: The experimental wave height data for varying depth Froude numbers at 1.25 lateral distance

The new deepwater tests were compared to the shallow water results for the wavedozer. By comparing wave heights at various wavedozer speeds in two different water depths (Figure 2-11), it is clear that the wave heights generated at the lower water depth is higher at high speeds. From Figure 2-11 the results are the same until V=1.99 m/s, for which the shallow water run has a depth Froude number of 0.99 while the deep run has a depth Froude number of 0.52. This means that the 500mm water depth experiences shallow water effects at this speed, while 1500mm water depth is still in the deepwater condition. In other words, the results are dependent on depth Froude number. Therefore, it is possible to generate higher waves for given speed by decreasing the water depth. The blockage factor (κ) must be considered, where blockage factor is the ratio of model section area over channel section area. This study was conducted numerically and will be presented in chapter 5.

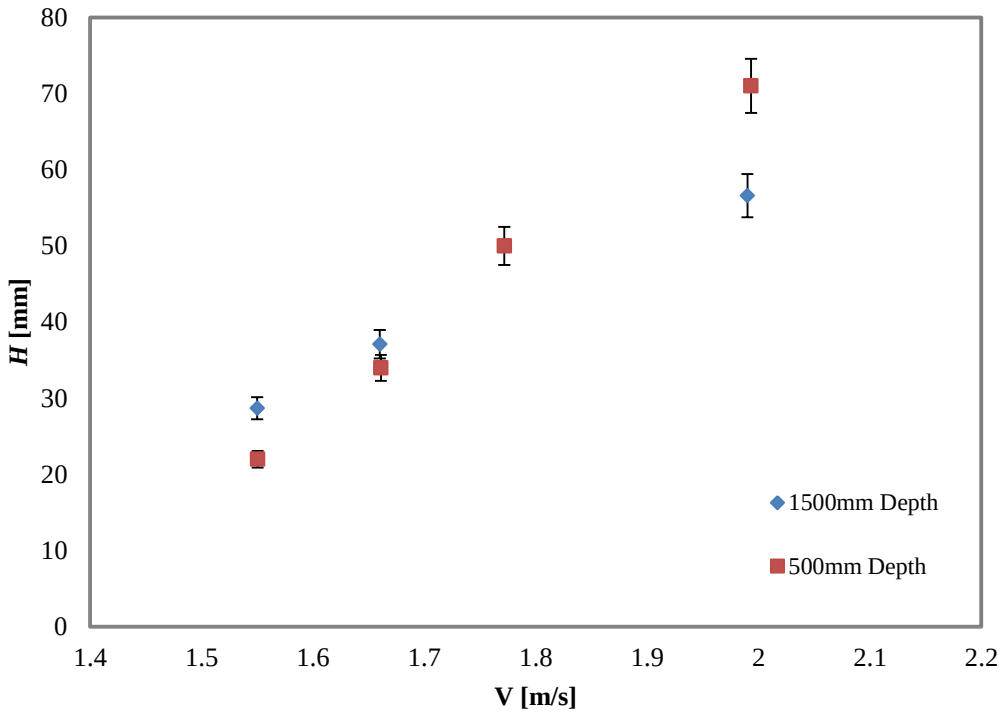

Figure 2-11:Wave heights comparison at different speeds for two water depth for wavedozer pressure source

2.2. Model Test Basin Tests

The second stage of the experimental investigation into generating surfable waves was conducted jointly by author and co-student; Steven Schmied in the Model Test Basin at the AMC in 2010 and 2011. The aim of these tests was to investigate the generation and transformation of the waves developed by pressure sources travelling along a curved track. During these tests, different pressure sources were used and different channel configurations were built. Wave height, breaking point location, breaking wave shape, the relationship between pressure source speed and the wave height, pressure source and the beach parameter effects were the main issues investigated in this stage.

For this study, a scale model of a circular wave pool was built in the MTB at the AMC. The scale model is shown in Figure 2-12. The circular wave pool diameter was 10 meters. Thirteen wave probes were installed to record wave parameters as shown in Figure 2-13. Wave probes 6 and 7 were installed to determine the longitudinal stability by comparing the wave amplitude time trace at WP1, WP6 and WP7. The rest of the wave probes were used to determine the lateral transformation of the waves.

Figure 2-12: Scale model of circular wave pool

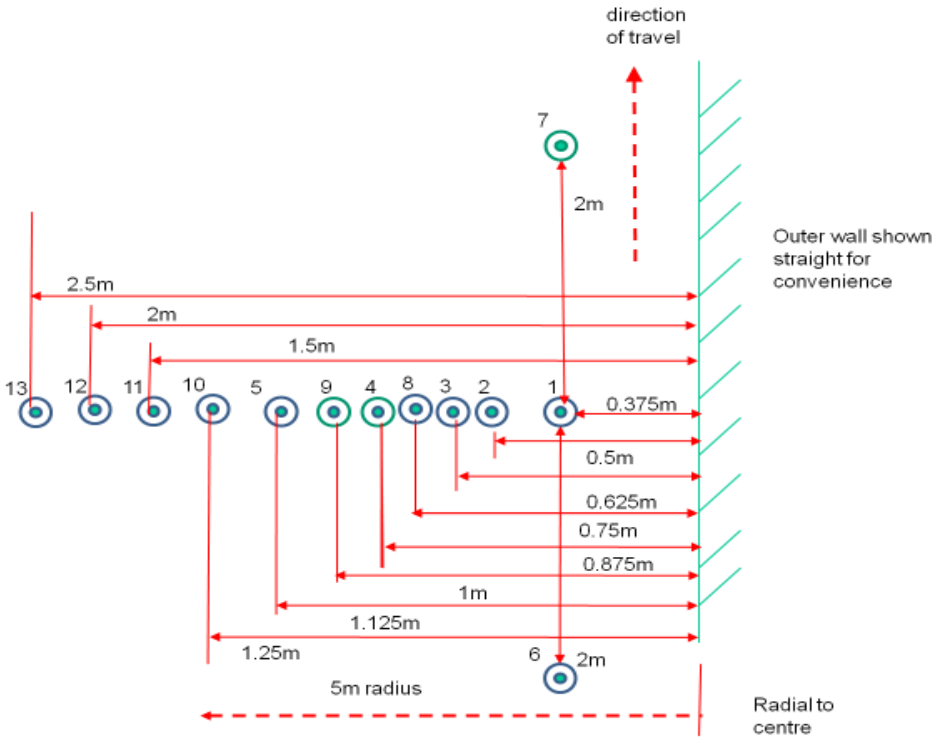

Figure 2-13: wave pool model wave probe array

The scope of testing was to provide additional experimental data to support ongoing investigations of optimum pressure sources to efficiently generate continuously breaking waves. The tested pressure sources MTB were:

- **Model 1** - an asymmetrical wavedozer of 1002mm length, 75mm beam and 50mm draught. The angle of attack was 14 degrees. Model 1 was a half scale version of the wavedozer tested in the linear Towing Tank.
- **Model 2** - an asymmetrical wavedozer of 1002mm length, double the beam of model 1.
- **Model 3** - a symmetrical version of model 1. It was equivalent to model 1 and mirrored about the stern, which allowed the pressure source to be driven both clockwise and counter-clockwise.
- **Model 4** - a symmetrical wavedozer equivalent to model 1 and mirrored about the stern.
- **Model 5** - a curved asymmetrical wavedozer of 75mm beam, 602mm length and 50mm draught. This was equivalent to a curved 1:2 scale model of the wavedozer tested in the linear Towing Tank.
- **Model 6** - a curved asymmetrical wavedozer of 175mm beam, 602mm length and 50mm draught. This model was the second in the series to test the relationship between the pressure source beam and the wave height.
- **Model 7** - a curved asymmetrical wavedozer of 275mm beam, 602mm length and 50mm draught. This was the third in the series to test the relationship between the pressure source beam and the wave height.

The Towing Tank test series was replicated by building a curved TT scaled channel in order to confirm the similarity of waves generated by a pressure source in a straight line and a circular track. The Towing Tank has a rectangular cross-section with a width of 3550mm. The wavedozer tested in the Towing Tank was symmetrical about the centre line of track and measurements were only taken on the port side. Firstly, to replicate the Towing Tank tests in a curved track, the towing cross-section was modelled in half scale and only one side of the centreline as a curved track (width 888mm); Figure 2-14. Model 1 was used for these tests.

Secondly, to measure the effect of the inner wall on the waves, half of the inner wall close to the wave probes was removed. The other half was retained to minimise wave interaction across the pool; Figure 2-15. Figure 2-16 shows the results for straight and curved tracks. It is clear that track shape does not have a significant effect on wave height. Therefore it is possible to use the straight track for future wave height investigations. Figure 2-17 illustrates the results for three different pool configurations with wall at 888mm from perimeter; no wall in the pool and with wall far from wave probes. The generated wave height in $Fr_h \geq 0.85$ for configuration with wall was higher than the two other conditions.

Figure 2-14: Scale model with wall at 888mm from perimeter and no beach fitted

Figure 2-15: Scale model with the wall at 888mm from the perimeter and the wall removed near the wave probes

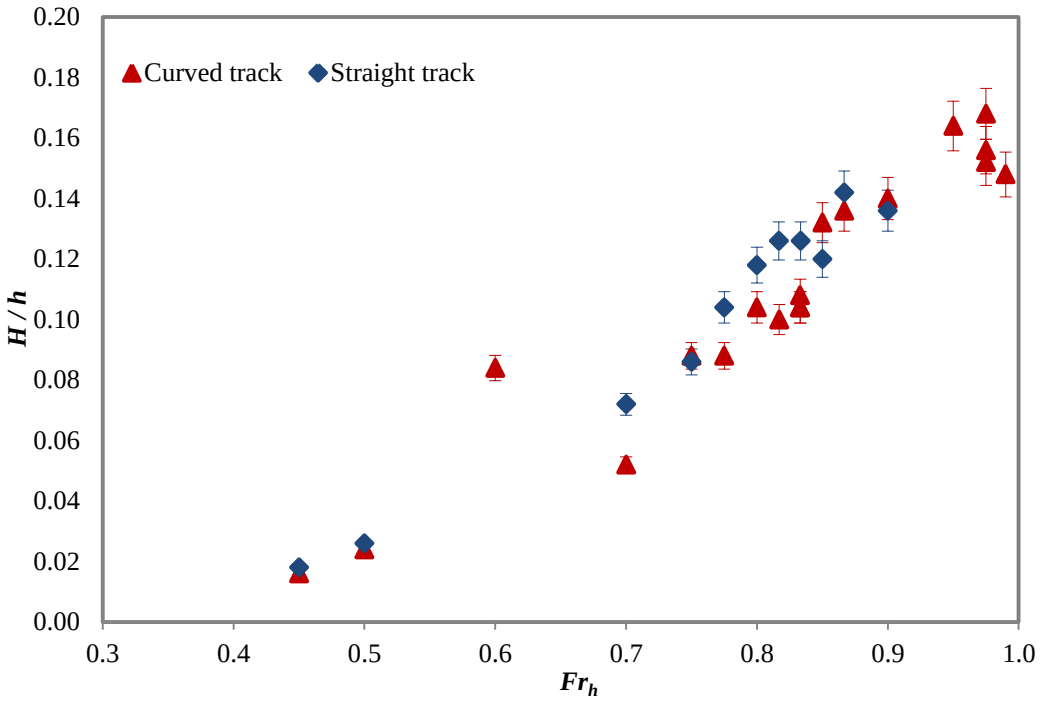

Figure 2-16: Straight and curved tracks wave height comparison; curved track: 75mm constant beam, 250mm water depth and 50mm draught; Straight track: 300mm constant beam, 500mm water depth and 100mm draught

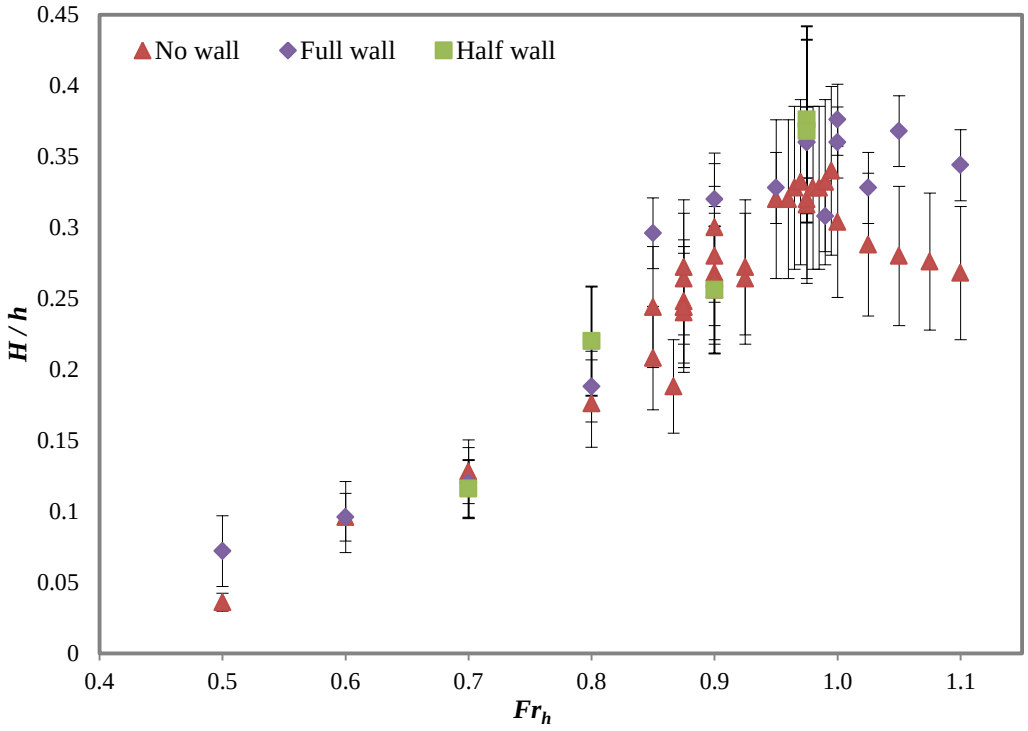

Figure 2-17: Comparions of wave height at 375 mm distance from outer wall for model1 in three different conditions; No wall: with out any wall inside the pool; Full wall: there is a wall at 888mm from the perimeter; Half wall: there is wall at 888mm from the perimeter and the wall removed near the wave probes

2.2.1. Model beam

To determine the model beam effect on wave height, models 5, 6 and 7 with 75, 175 and 275mm beam respectively were tested. In this step, there was no wall inside the circle. The models' draught was 50mm and the water depth was kept 500mm in all tests. The results are shown in Figure 2-18. It was shown that by increasing the beam, wave height increases.

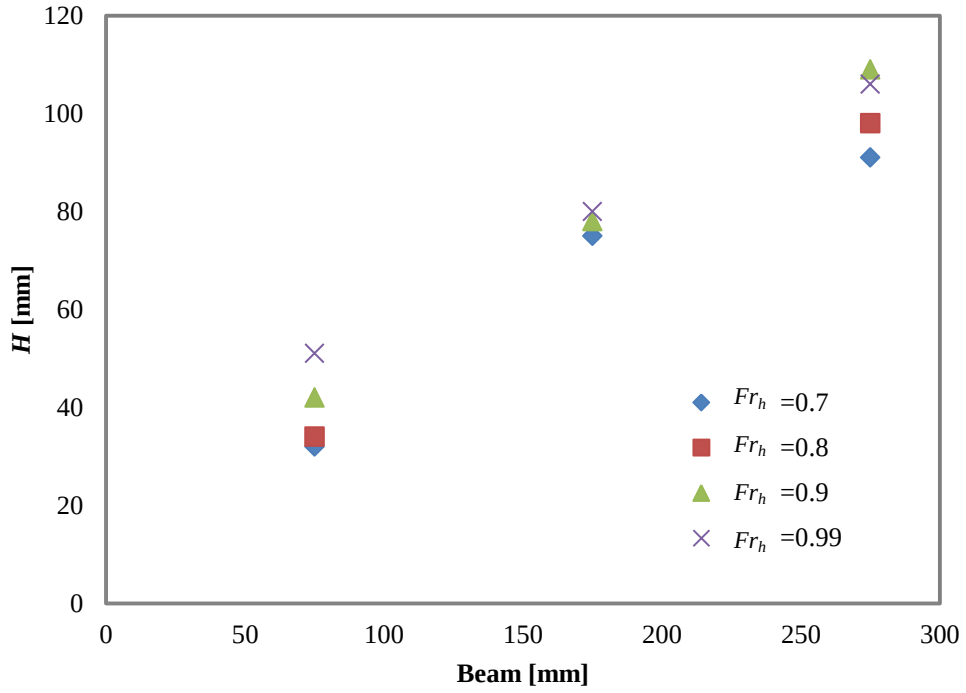

Figure 2-18: Beam effect on the generated wave height at 375 mm distance from outer wall

The channel width, beach slope and the shape of the beach were the other important investigated parameters. The various parameters for different configurations were (Figure 2-19):

- **Beach lateral start point:** The lateral distance to the start of the beach from the outer perimeter (y_{beach})
- **Beach slope:** The slope angle of the beach (s)
- **Beach start step size:** The height of the step at Beach lateral start point (z_{beach})

Different configurations were built into the MTB with variables listed below in Table 2-3. The aim of this test session was to improve the beach in terms of slope and shape to prevent the waves from steepening and breaking and to increase the wave wall length (WL) as much as possible. The wave wall length is the length of the wave crest with almost the same wave height. To analyse the effect of each of the design parameters on wave transformation, the lateral variations in wave height for each configuration were compared to a 'no beach' configuration.

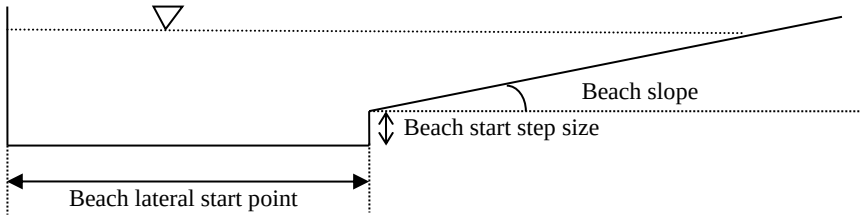

Figure 2-19: Circular channel cross-section

Table 2-3: Test Conditions

Configuration	y_{beach} (mm)	s (degrees)	z_{beach} (mm)
1	500	9.5	100
2	550	9.5	150
3	550	9.5	100
4	750	9.5	130
5	750	16.9	185
6	572	16.9	130
7	572	16.9	75
8	750	16.9	130
9	950	16.9	130
10	950	16.9	80
11	1500	16	290
12	1500	16	390
13	575	22.6	110
14	575	22.6	55
15	750	22.6	130
16	No beach		

2.2.2. Beach lateral start point

The lateral variation in H for different values of y_{beach} were compared. The aim was to maximise WL whilst maintaining H_{beach}, where H_{beach} is wave height at the start of the beach (y_{beach}). The Figure 2-21 presents the experimental test results at 375 mm (WP1) for three different conditions 6, 8 and 9 at different depth Froude numbers. The curved asymmetrical wavedozer with constant beam was used for these tests (Figure 2-20). All tests were conducted at 250mm water depth and 50 mm draught. The results showed that condition 9 (widest channel) had the highest wave height, while conditions 6 and 8 had almost equal wave height at WP1, and condition 8 had the higher wave height at further distances (Figure 2-22). It means wave breaking happens closer at condition 6. By comparing the H_{beach} verses y_{beach} for different configurations, limiting value for sufficient WL whilst maintaining H_{beach}, was 575mm < y_{beach} <950mm.

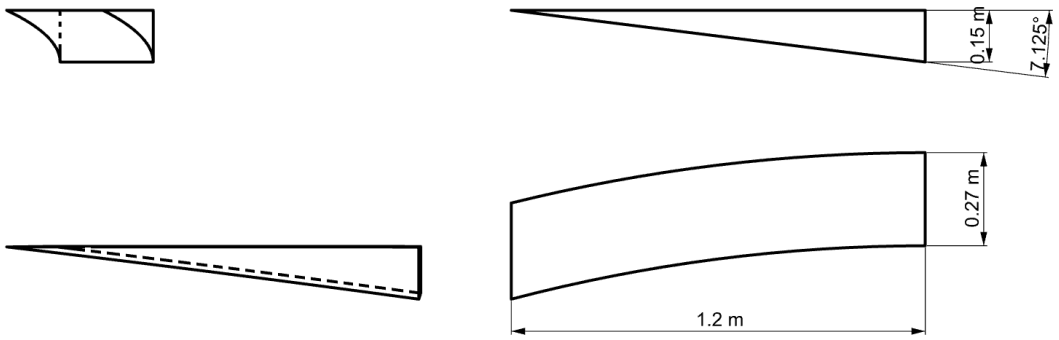

Figure 2-20: Curved asymmetrical wavedozer of B=0.275m, LWL=1.2m, AOA=7.1degrees and 0.15 m height

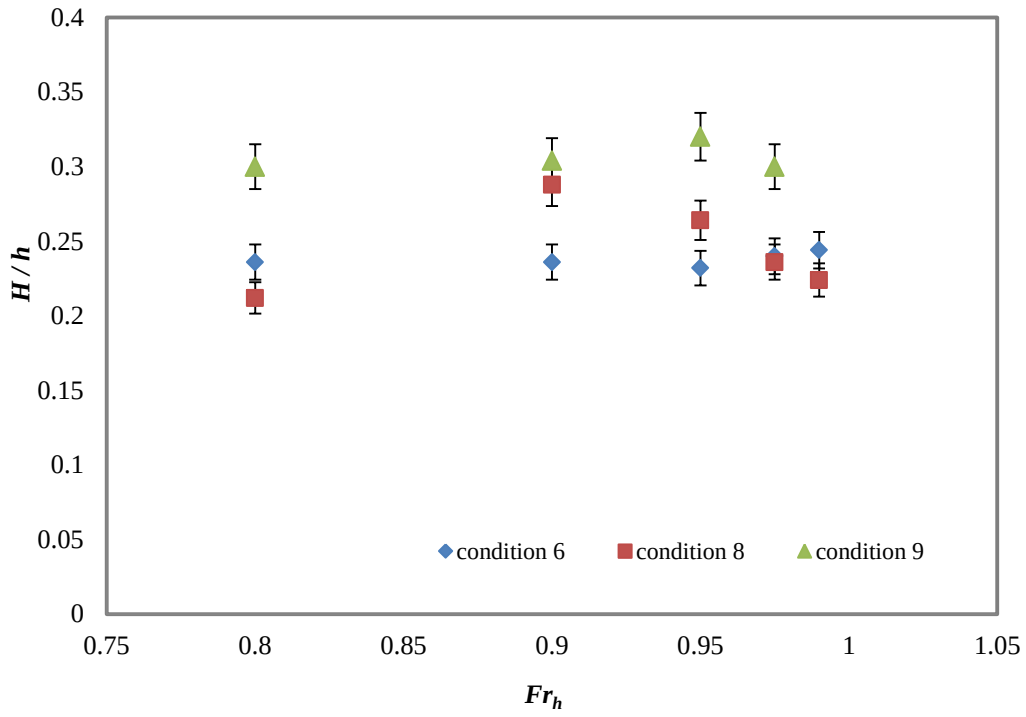

Figure 2-21: Comparison the results for three conditions 6, 8 and 9 at different depth Froude numbers at 375 mm distance from outer wall. Conditions 6,8 and 9 have different y_{beach} (575, 750 and 950 mm respectively) and same s and z_{beach} values

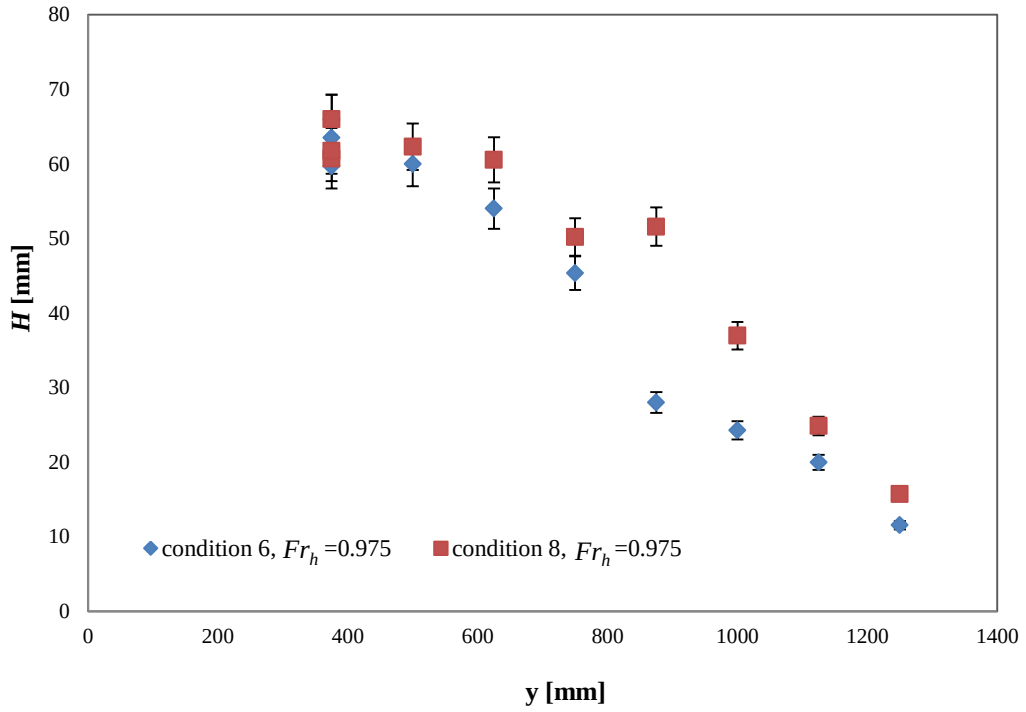

Figure 2-22:Lateral variation in H for two different conditions 6 and 8 at Fr_h=0.975. Condition 6 and 8 have different y_{beach} (575, 750 mm respectively) and same s and z_{beach} values

2.2.3. Beach slope

The effect of beach slope angle on the height of the generated waves was investigated during the experimental tests in the MTB. Conditions 4, 8 and 15 had the same beach lateral start point and beach start step size (z_{beach}=750mm and z_{beach}=130mm), while they had different slopes (Table 2-4).

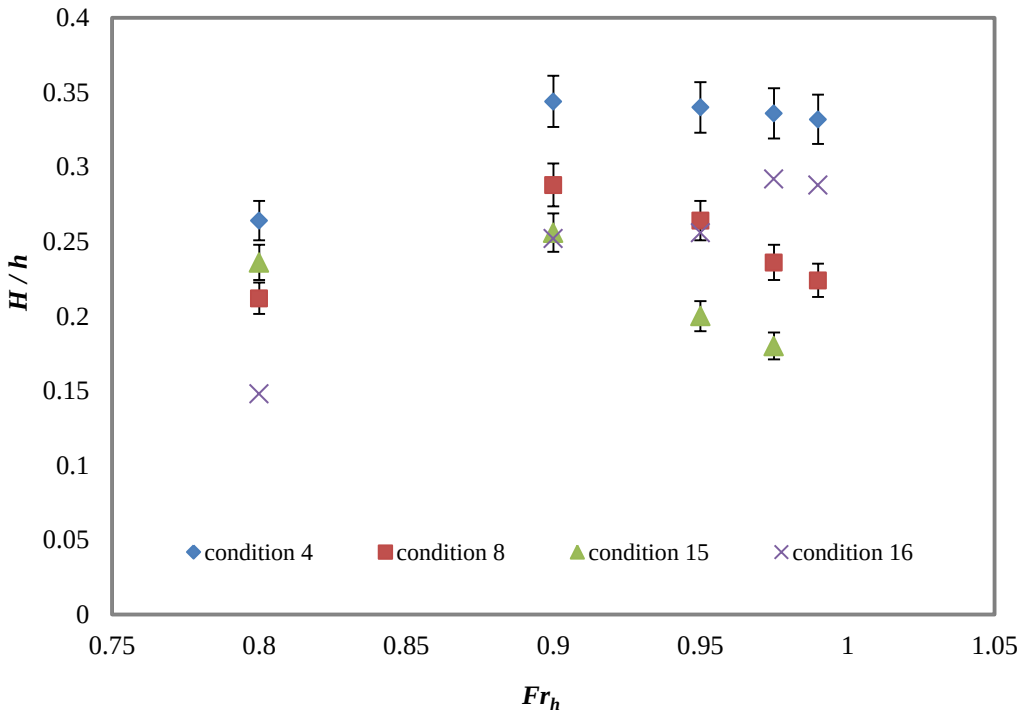

Figure 2-23: Comparing the results for different configurations with different slope angles at different depth Froude numbers and at 375 mm distance from outer wall

Figure 2-23 depicts the results for different conditions. It is clear that by increasing the slope, the wave height decreases. By comparing the results for different slope angles, *s* had a marked effect on *H* due to the formation of a soliton for *s* >9 deg.

Table 2-4: Beach Slopes

Condition	slope	slope angle (*s*) (degrees)
4	1:6	9.5
8	1:3.33	16.7
15	2:5	21.8
16 (no beach)	0	0

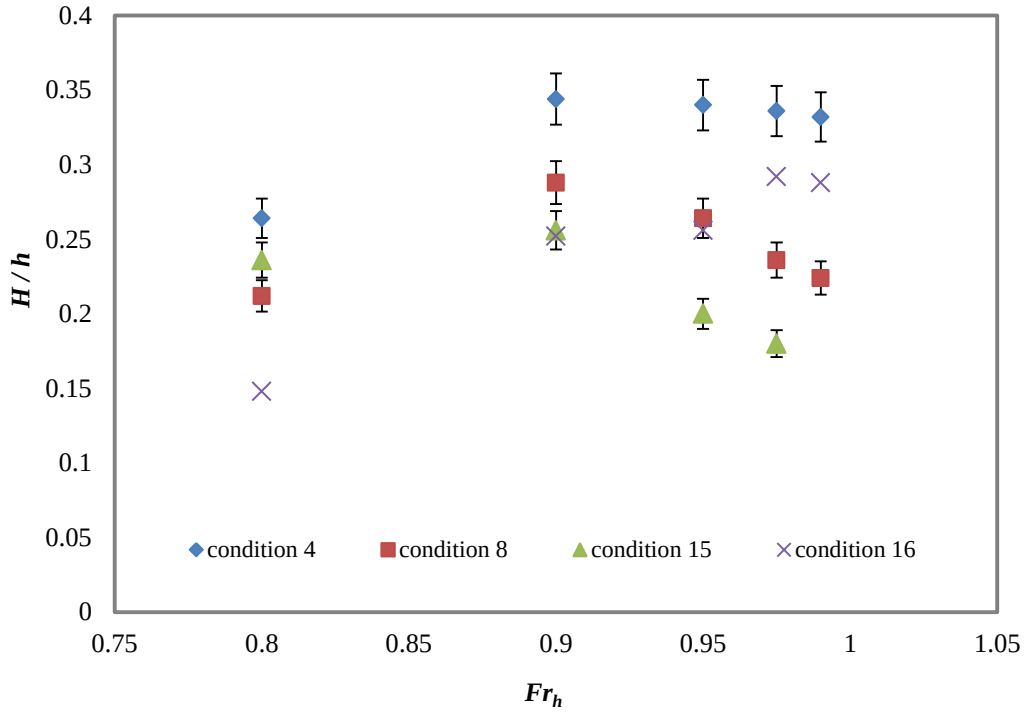

Figure 2-23: Comparing the results for different configurations with different slope angles at different depth Froude numbers and at 375 mm distance from outer wall

2.2.4. Beach start step size

The other parameter which was investigated in the test series was the effect of beach start step size on wave height. In this study, lateral variations in H for different values of h_{beach} were compared (Figure 2-24 to Figure 2-28). It is clear that h_{beach} does not have a significant effect on H, while this value has an effect on wave quality. It means that for $h_{beach} < 1.13H_{beach}$, the wave has a surging shape rather than the desired plunging shape.

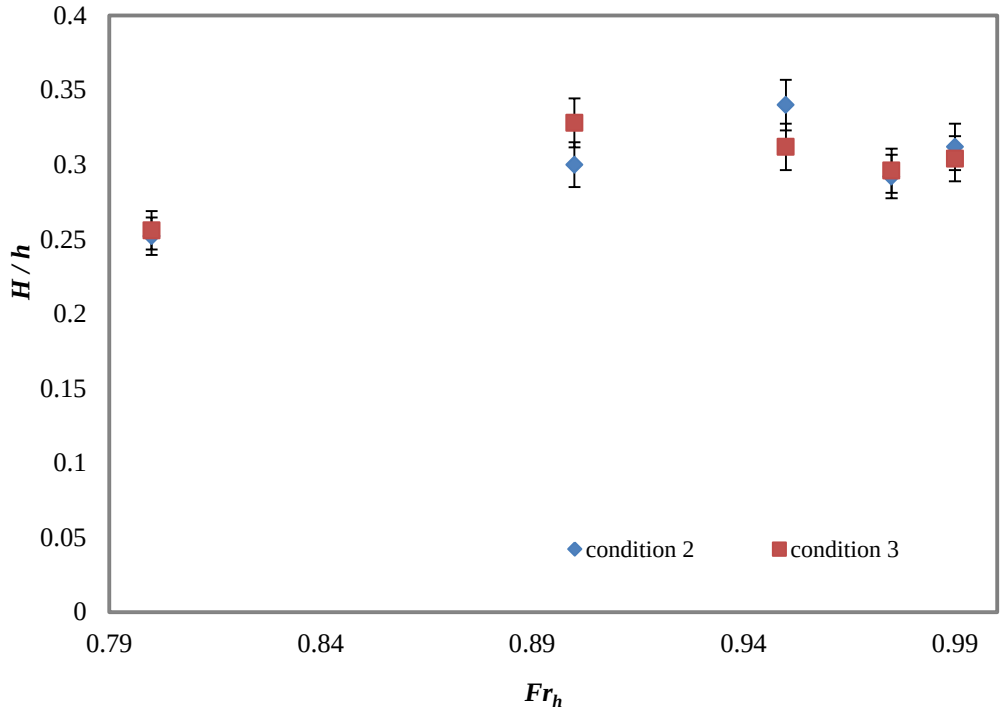

Figure 2-24: Wave height at WP1 for two different steps size in y_{beach}=550 mm and s= 9.5° in different depth Froude numbers

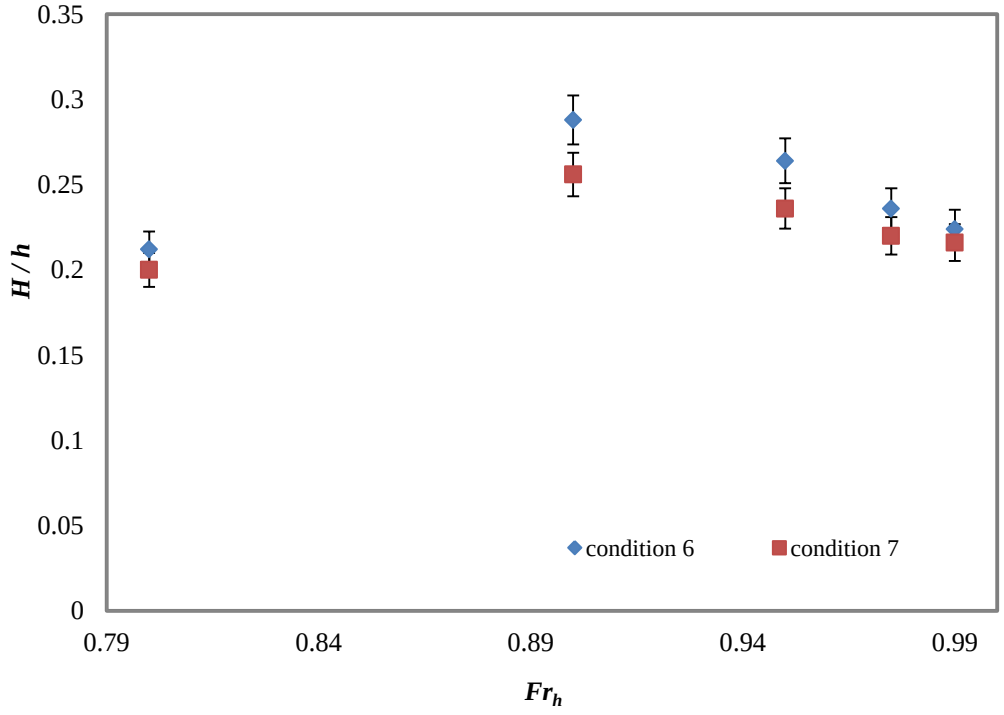

Figure 2-25: Wave height at WP1 for two different steps size in y_{beach}=572 mm and s= 16.9° in different depth Froude numbers

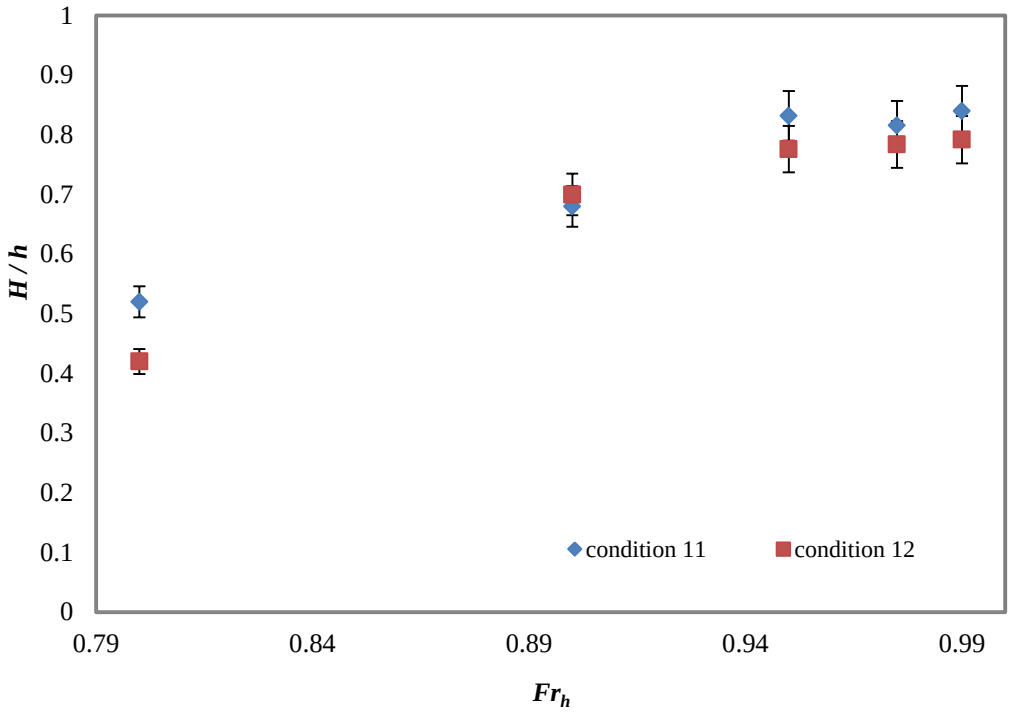

Figure 2-26: Wave height at WP1 for two different steps size in y_{beach}=1500 mm and s= 16° in different depth Froude numbers

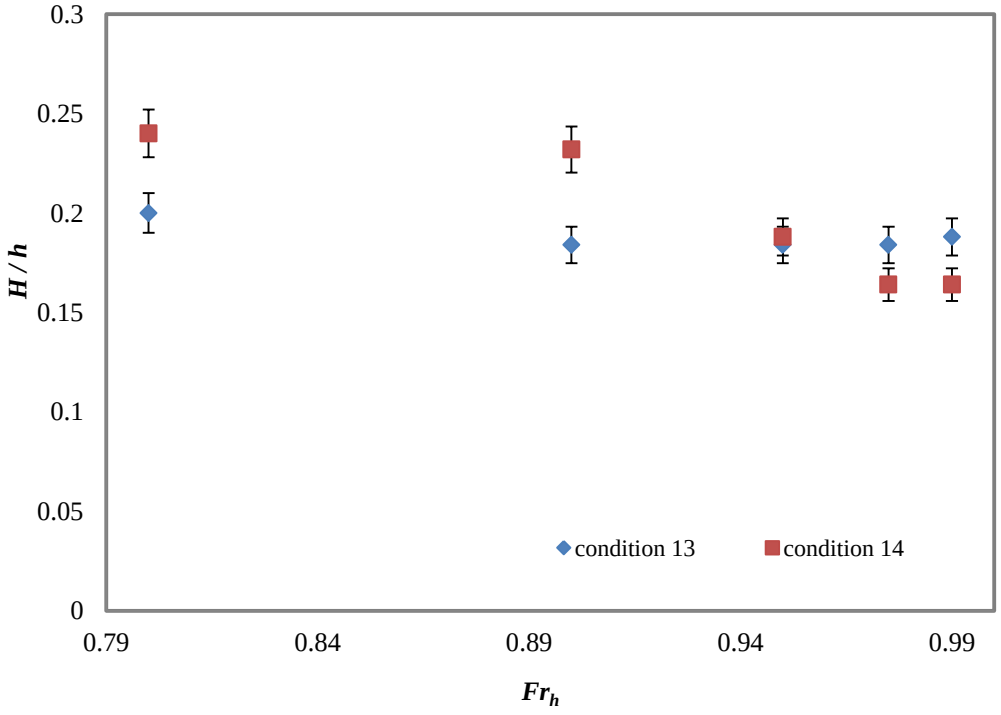

Figure 2-27: Wave height at WP1 for two different steps size in y_{beach}=575 mm and s= 22.6° in different depth Froude numbers

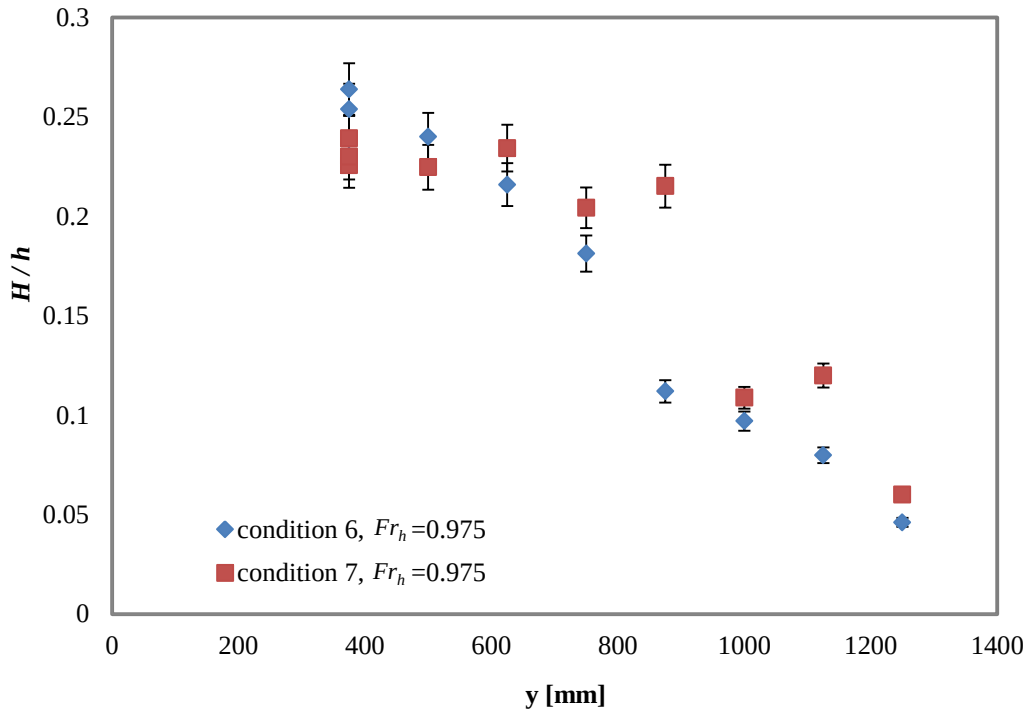

Figure 2-28: Lateral variation in *H* for two different conditions 6 and 7 at Fr_h=0.975. condition 6 and 7 have same y_{beach} and s values (575 mm and 16.9 degrees) and different z_{beach} (130 and 75 mm)

2.3. Concluding remarks

An experimental program was started at the Australian Maritime College (AMC) in 2009 to investigate wave generation limitations, including pressure source shape and channel parameters.

Towing Tank (TT) test series mostly were focused on the pressure source parameters effects on the wave generated height, while Model Test Basin test series were conducted to investigate the channel shape effects on the wave propagation.

During the towing tank tests series at 2009 by Steven Schmied was concluded that the wave generated by the parabolic pressure source was higher than the wavedozer, but they were broken across the entire width of channel for $Fr_h > 0.75$. Soliton generation causes extremely unstable wave systems, therefore speeds of $Fr_h > 1.0$ were not tested. Comparing the results for different pressure sources (parabolic and wavedozer) with same parameters shows that the pressure source type has significant effect on the wave quality.

In 2012 the towing tank test series by the author a comparison of the results with previous series was concluded that the wave heights generated at the lower water depth is higher at high speeds. For constant speed, the results are dependent on depth Froude number. Therefore, it is possible to generate higher waves for given speed by decreasing the water depth.

The Towing Tank test series was replicated by building a curved TT scaled channel in order to confirm the similarity of waves generated by a pressure source in a straight line and a circular track in Model Test Basin. It was shown that track shape does not have a significant effect on wave height. Therefore it is possible to use the straight track for future wave height investigations. It was shown that by increasing the beam, wave height increases. The channel width, beach slope and the shape of the beach were the other important investigated parameters. Different configurations with different variables were built into the MTB. The aim of this test session was to improve the beach in terms of slope and shape to prevent the waves from steepening and breaking and to increase the wave wall length (WL) as much as possible. It was shown that limiting value for sufficient WL whilst maintaining H_{beach}, was 575mm < y_{beach} <950mm. By comparing the results for different slope angles, s had a marked effect on H due to the formation of a soliton for s >9 deg. It was also shown that h_{beach} does not have a significant effect on H.

.

3. Numerical verification and validation

As mentioned in chapter one, all the previously different numerical approaches previously tested to predict wave generated parameters by different authors and with different numerical methods were unsuccessful. The most important application of this research was to prove whether numerical methods can be used to further the design of circular wave making devices. This chapter deals with verifying the numerical approach to predict the generated wave propagation. To investigate the numerical accuracy, some of the experimental test conditions were duplicated numerically and the numerical results were compared with experiments. A first step was to select simulation software capable of accurately predicting parameters.

ANSYS Fluent software [45] version 12.1 was used for this study and the results of simulations for different pressure sources and configurations were compared with experimental data to be certain that the ANSYS Fluent software was appropriate to use for further investigation.

In this chapter, after a brief presentation about Computational Fluid Dynamic (CFD), the ANSYS Fluent software and why finite volume is appropriate for this study, the numerical results and comparison with experimental data is presented. Then, the results for mesh independency and quality investigation are detailed.

3.1. Computational Fluid Dynamics

Numerical simulation is a common way for assessment of ship performance in the early design stages. The limitation of an experimental approach is a reason for employing a numerical tool. Taking into account the advances in computer hardware, the use of CFD is becoming the best choice in many cases and numerical simulation based on CFD has been the subject of a lot of hydrodynamic research in the recent past. Computational methods which can perform analyses in the early stages of design are desirable and can reduce the number of design alternatives.

In numerical simulations, the focus is on developing efficient and accurate methods. For a ship moving in water of uniform depth, linear and nonlinear theories can be applied usefully in the subcritical and the supercritical speed range [46, 47]. Thin ship theory can be used for the wave generation by a ship moving in a channel. This theory provides an alternative to higher order panel methods for estimating wave resistance when applied solely to slender hulls [48], but it is not valid for unsteady cases and transom stern flow separation which has an important effect on high speed vessels [46]. More general shallow-water approximations are obtained from Boussinesq type equations, which are valid for most arbitrarily unsteady cases. Boussinesq's equations based on a suitable reference level were used for computing ship waves in shallow water. However this method is not able to predict the 3D flow pattern around the vessel [49]. An alternative is to combine the thin ship

theory and the Boussinesq method. This hybrid approach combines a steady nonlinear panel method for the near-ship flow with a Boussinesq solver for the far-field wave propagation [46]. However, this method is only useful for steady problems. It should be noted that due to the nonlinear and unsteady nature, as well as the large domain feature of the wash problems, they can be neither solved well by the linear wave theory nor approximated efficiently by nonlinear singularity methods. Typically, the finite volume method has been used [49, 50].

The finite volume method (FVM) is a method for representing and evaluating partial differential equations in the form of algebraic equations. The finite volume method is a class of discretisation scheme that has proven highly successful in approximating the solution of a wide variety of conservation law systems. It is extensively used in fluid mechanics and many other engineering areas governed by conservative systems that can be written in integral control volume form. Some commercial CFD software uses the FVM to solve governing equations and one of the most powerful CFD software systems is Fluent [51].

3.2. Governing equations

The governing equations for computational fluid dynamics (CFD) are based on conservation of mass, momentum and energy. ANSYS Fluent uses the finite volume method (FVM) to solve the governing equations. The FVM involves discretisation and integration of governing equations over the control volume. The FVM is a numerical method for solving partial differential equations that calculates the values of the conserved variables averaged across the volume. One advantage of the FVM over finite difference methods (FDM) is that it does not require a structured mesh (although a structured mesh can also be used). Furthermore, the FVM is preferable to other methods because boundary conditions can be applied non-invasively. An additional feature is the local conservativity of the numerical fluxes, which means the numerical flux is conserved from one discretisation cell to its neighbour. Especially in fluid mechanics which the flux is important the finite volume method is quit attractive.

The basic equations for unsteady turbulent and two-phase flow are conservation of mass and momentum and turbulence. There is an approach in simulation of two-phase flow where different fluids are modeled as a single fluid obeying the same set of governing equations, with the local fluid property variation determined with a volume fraction value α.

Incompressible Navier-Stokes and continuity equations are well-known and given by the equations:

$$\frac{\partial u_i}{\partial t} + u_j \frac{\partial u_i}{\partial x_j} = -\frac{1}{\rho}\frac{\partial P}{\partial x_i} + \vartheta \frac{\partial^2 u_i}{\partial x_j \partial x_j} + g_i \tag{3-1}$$

$$\frac{\partial u_i}{\partial x_i} = 0 \tag{3-2}$$

where u_i is the velocity, P is the pressure, and ϑ is the kinematic viscosity.

In the FVM, discretization of the governing equations is considered by integration of the momentum equation over a control volume. It becomes as below:

$$\frac{d}{dt}\int_V \vec{u}\ dV + \int_A \vec{u}\,(\vec{u}.\vec{n})\,dA = \int_A \nu\vec{\nabla}\vec{u}.\vec{n}\,dA - \frac{1}{\rho}\int_A P\vec{n}\,dA + \int_V \vec{g}\,dV \tag{3-3}$$

where $\vec{u}$ is the velocity vector, v is the cell volume and A is the area around it. The first and second terms in l.h.s of Eq. 3 are unsteady acceleration and convection terms respectively. The diffusion, pressure gradient and gravity force are the terms in the r.h.s of Eq.3.

Local density ρ and viscosity ϑ of the single fluid are defined as:

$$\rho_{cell} = \alpha\rho_1 + (1-\alpha)\rho_2 \tag{3-4}$$

$$\vartheta_{cell} = \alpha\vartheta_1 + (1-\alpha)\vartheta_2$$

Subscripts 1 and 2 indicate two fluids (e.g. water and air), where α (volume fraction) is the percentage of fluid 1 (e.g. water) available in cell and defined as follows:

$$\alpha = \begin{cases} 1\ \ for\ cells\ inside\ fluid\ 1 \\ 0\ for\ cells\ inside\ fluid\ 2 \\ 0 < \alpha < 1\ for\ transitional\ area \end{cases}$$

Turbulent flow can be modelled using mean and fluctuating values for components such as velocity $u_i = \bar{u}_i + \acute{u}_i$. Substituting the mean and fluctuating value equations into the Navier-Stokes equations yields the Reynolds-averaged Navier-Stokes (RANS) equation:

$$\frac{\partial\bar{u}_i}{\partial t} + \bar{u}_j\frac{\partial\bar{u}_i}{\partial x_j} = \bar{f}_i - \frac{1}{\rho}\frac{\partial\bar{P}}{\partial x_i} + \vartheta\frac{\partial^2\bar{u}_i}{\partial x_j\partial x_j} - \frac{\partial\overline{\acute{u}_\iota\acute{u}_J}}{\partial x_j} \tag{3-5}$$

where f_i is a vector representing external forces. The non-linear term $\overline{\acute{u}_\iota\acute{u}_J}$ known as the Reynolds stress is the difference between the laminar and turbulent flow equations.

The $k-\varepsilon$ model is a semi-empirical two-equation turbulence model based on an exact solution for the turbulent kinetic energy (k) and a model of the dissipation rate (ε). To model the Reynolds stress in the RANS equations, the $k-\varepsilon$ model uses the Boussinesq approximation to relate the Reynolds stresses to the mean velocity gradient, see [52]. Generally the $k-\varepsilon$ model works better far from walls and $k-\omega$ model is better near walls. Shear-Stress transport (SST) turbulence modelling combines the $k-\varepsilon$ and $k-\omega$ with a weight factor which causes the SST model to perform like the $k-\omega$ model near the wall and $k-\varepsilon$ model far from the wall. Meanwhile, since Y^+ should be less than 1 for using $k-\omega$ model, the finer mesh is needed near the wall for $k-\omega$ and SST turbulence models. Since the

accuracy of the wave parameter at the breaking point is more important than near the pressure source, the $k-\varepsilon$ turbulence model was chosen for this study.

3.2.1. Discretisation methodology and solver

In this study, the governing equations were the three-dimensional Reynolds Averaged Navier-Stokes equations for incompressible flows, and the $k-\varepsilon$ turbulence model. They were solved using the FVM in ANSYS Fluent. The volume of fluid approach, which is a pressure based (segregated) solver, was used with a time dependent and explicit time discretisation scheme to solve the equations. The SIMPLE algorithm was used for pressure-velocity coupling. The SIMPLE algorithm is a semi-implicit method for pressure-linked equations and it is a segregated algorithm. The SIMPLE algorithm was used to solve the momentum equation first, then to solve for pressure, and later to correct the discretised solutions. This algorithm can offer a reduced convergence time due to the smaller memory requirement over the coupled algorithm. The PRESTO scheme was used to interpolate the pressure on the cell faces. This scheme uses the discrete continuity equation to calculate the pressure field on a mesh that is geometrically shifted so that the new cell centres are where the faces of the ordinary mesh are placed. The PRESTO scheme is recommended for VOF simulations [53]. The Least Squares Cell Based scheme was used for gradient discretization and momentum was discretized with second order upwind approach. The standard wall function was utilised for $k-\varepsilon$ turbulence modelling and first order upwind approach was utilised to discretize the turbulent kinetic energy. In this work, to discretise the convective term in the equation for transport of the volume fraction, High Resolution Interface Capturing scheme (HRIC) was used. In addition, first order implicit scheme was used for transient formulation. Simulations were accomplished using moving reference frames (MRF) with Fluent ANSYS providing these for both translating and rotating systems.

For simulations using the VOF multiphase model, upwind schemes are generally unsuitable for interface tracking because of their overly diffusive nature. Central differencing schemes, while generally able to retain the sharpness of the interface, are unbounded and often give physically unrealistic results. In order to overcome these deficiencies, ANSYS FLUENT uses a modified version of the High Resolution Interface Capturing (HRIC) scheme, which is a composite of the normalized variable diagram (NVD) scheme consisting of a non-linear blend of upwind and downwind differencing [54].

First, the normalized cell value of volume fraction, $\tilde{\emptyset}_c$, is computed and is used to find the normalized face value, $\tilde{\emptyset}_f$, as follows:

$$\tilde{\emptyset}_c = \frac{\tilde{\emptyset}_D - \tilde{\emptyset}_U}{\tilde{\emptyset}_A - \tilde{\emptyset}_U} \tag{3-6}$$

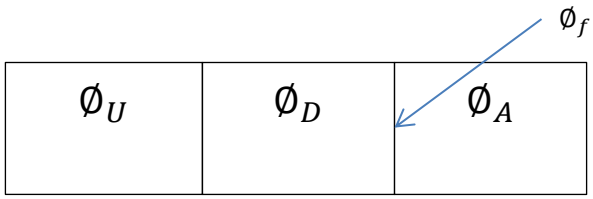

Figure 3-1: Cell Representation for Modified HRIC Scheme

where A is the acceptor cell, D is the donor cell, and U is the upwind cell, and

$$\tilde{\emptyset}_f = \begin{cases} \tilde{\emptyset}_c & \tilde{\emptyset}_c < 0 \; or \; \tilde{\emptyset}_c > 1 \\ 2\tilde{\emptyset}_c & 0 \le \tilde{\emptyset}_c \le 0.5 \\ 1 & 0.5 \le \tilde{\emptyset}_c \le 1 \end{cases} \tag{3-7}$$

Here, if the upwind cell is not available (for example, unstructured mesh), an extrapolated value is used for $\emptyset_U$. Directly using this value of $\tilde{\emptyset}_f$ causes wrinkles in the interface, if the flow is parallel to the interface. So, ANSYS FLUENT switches to the ULTIMATE QUICKEST scheme (the one-dimensional bounded version of the QUICK scheme) based on the angle between the face normal and interface normal:

$$\emptyset_f^{\tilde{U}O} = \begin{cases} \tilde{\emptyset}_c & \tilde{\emptyset}_c < 0 \; or \; \tilde{\emptyset}_c > 1 \\ MIN\left(\tilde{\emptyset}_f, \dfrac{6\tilde{\emptyset}_c + 3}{8}\right) \end{cases} \tag{3-8}$$

This leads to a corrected version of the face volume fraction, $\tilde{\emptyset}^*{}_f$:

$$\tilde{\emptyset}^*{}_f = \tilde{\emptyset}_f\sqrt{\cos\theta} + (1 - \sqrt{\cos\theta}) \;\; \emptyset_f^{\tilde{U}O} \tag{3-9}$$

where

$$\cos\theta = \frac{\nabla\emptyset . \overline{d}}{|\nabla\emptyset||\overline{d}|}$$

and $\overline{d}$ is a vector connecting cell centres adjacent to the face f .

The face volume fraction is now obtained from the normalized value computed above as follows:

$$\tilde{\emptyset}_f = \tilde{\emptyset}^*{}_f(\emptyset_A - \emptyset_U) + \emptyset_U \tag{3-10}$$

The modified HRIC scheme provides improved accuracy for VOF calculations when compared to QUICK and second-order schemes, and is less computationally expensive than the Geo-Reconstruct scheme.

3.3. Benchmarks

To validate the numerical method's ability to investigate the generated wave propagation, the experimental test data was used as a benchmark. The simulations were conducted in the same conditions as the experiment and finally, through the comparison of computed and measured results, applicability of the numerical method was examined. These details are explained below. As benchmarks, parabolic and wavedozer pressure sources in straight track and the wavedozer in a circular track were simulated. This section presents the numerical ability in terms of predicting the wave parameters, propagation and forces. For a circular track simulation the mesh domain should move and the flow should be at rest and so it is not possible to set an inlet flow velocity. The Moving Reference Frame (MRF) approach was utilised for both straight and curved tracks, with the setting for both conditions kept as constant as possible. Therefore for both straight and circular tracks the mesh domains move with constant speed and the absolute flow inlet velocity set to zero. A translating moving reference frame was used for the straight track and rotating system for curved track simulations.

3.3.1. Straight track

As mentioned previously, in order to investigate the pressure source shape effects on generated waves, some experimental tests were conducted at the AMC towing tank. Two different body shapes; parabolic and wedge (wavedozer), with different dimensions were used. Based on the results, it was determined that the quality of waves generated by the wavedozer was better than those generated by the parabolic pressure source. It was therefore decided to use the wavedozer for further investigation.

Parabolic pressure source

The Table 3-1 shows the parabolic pressure source dimensions. The model and channel parameters are exactly same as the tested model and towing tank. The parabolic test was simulated in 500mm water depth. In all simulations, the heave and trim were fixed at the same value as used in the experiments. As the flow has a plane of symmetry about the centre plane, to decrease the processing time, half of the domain was used. No-slip boundary condition (BC) was selected for all walls. Inlet velocity BC for inlet, and out flow BC for outlet were chosen. The upstream length of the domain was 3m (7.5 LWL), and 8m (20 LWL) was used for downstream. Figure 3-2 shows the domain of the simulation.

Table 3-1:Parabolic Pressure Source and Channel Characteristics

Length of model (mm)	700
Beam of model (mm)	300
Height of model (mm)	500
Draught (mm)	100
Channel width (mm)	3500
Depth of water (mm)	500

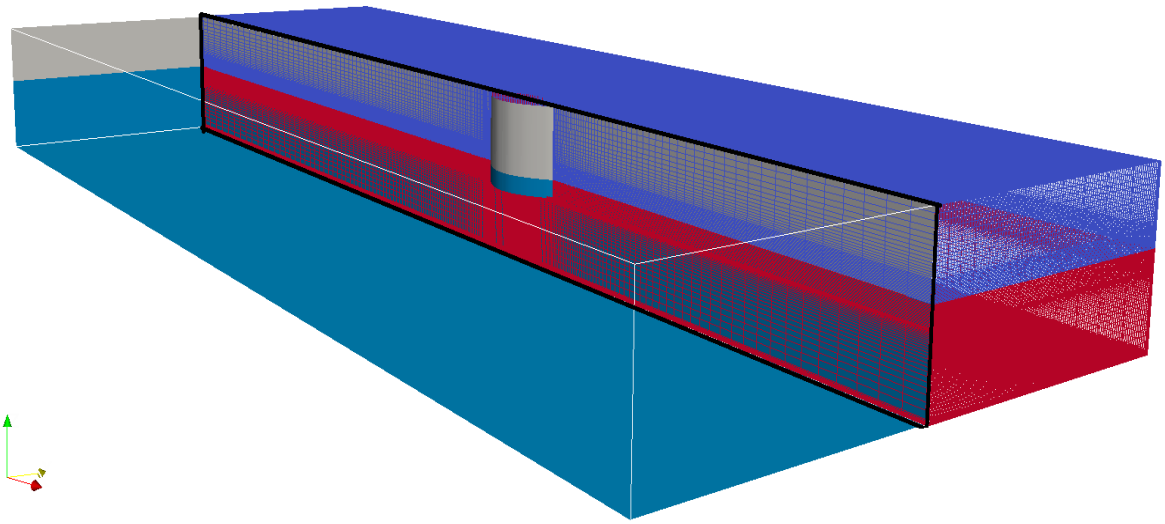

Figure 3-2: Computational domain for the parabolic pressure source

Figure 3-3 illustrates the wave time history for the numerical and experimental tests for Fr_h=0.9 at 750 mm lateral distance from the model centreline. It is clear that the simulation results agree with the experimental data with respect to wave height and frequency, while the uncertainty of the experimental results should be considered. In the towing tank tests, it was concluded that although the waves generated by the parabolic pressure source were higher than those generated by the wavedozer, they were always broken across the entire width of the channel for Fr_h >0.75. The numerical simulation was able to predict bow wave breaking qualitatively the same as the experimental tests. The free surface evolution for the numerical and experimental test is compared in Figure 3-4.

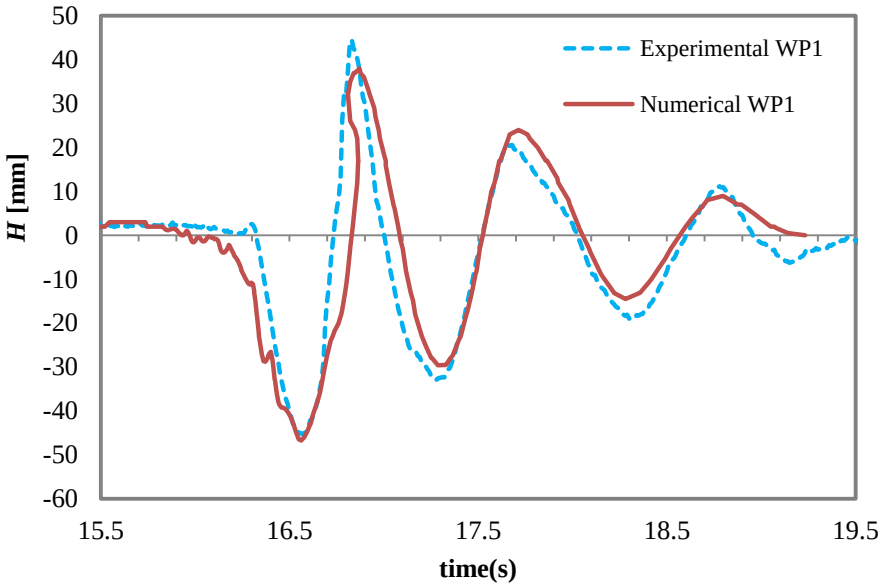

Figure 3-3: Wave probe results at 750mm lateral distance from centre-line (WP1)

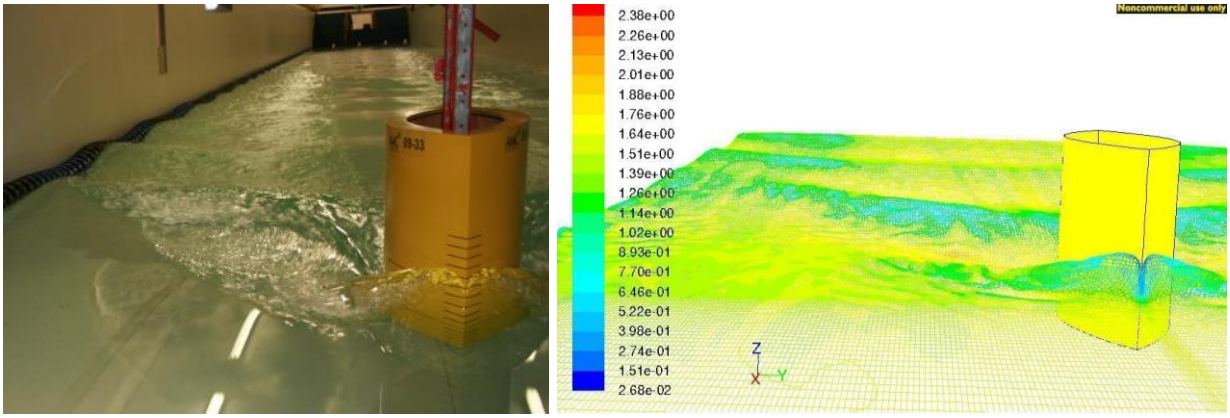

Figure 3-4: Free surface at Fr_h = 0.9

Wavedozer

A wavedozer is a wedge shaped pressure source with a constant beam which is used as wave maker. During the experimental tests in the towing tank it was observed that minimal to no breaking occurred for waves generated by the wavedozer for $Fr_h < 0.95$. Therefore, the wavedozer was selected as a suitable pressure source and further investigations were conducted. The wavedozer was simulated in two different water depths, 500 mm (as shallow water condition) and 1500 mm (as deepwater condition).

Shallow water

In the second step, wavedozer simulations at different speeds were undertaken in shallow water conditions, in a water depth of 500 mm. Table 3-2 shows the wavedozer and channel characteristics.

The boundary conditions and domain dimensions for the wavedozer simulations were same as for the parabolic pressure source. The wave patterns generated by the wavedozer were simulated at Fr_h values of 0.5, 0.75, 0.9 and 1.2.

Table 3-2: Wavedozer and Channel Characteristics

Length of model (mm)	1500
Beam of model (mm)	300
Angle of attack (deg.)	14
Draught (mm)	100
Channel width (mm)	3500
Water depth (mm)	500

The numerical wave height results are compared to the experimental data in Figure 3-5. In this figure, wave height (*H*) is defined as the trough to crest height of the first significant waves and *h* is equal to water depth (500 mm). In addition, the figure presents the results of wave height at 750mm lateral distance from model centreline. It can be concluded that numerical simulation can predict the trend of wave height as a function of speed.

Deepwater

As mentioned in Chapter 2, to measure the drag, vertical forces and water depth effect, the same wavedozer (Table 3-2) was tested in 1500mm water depth. To predict better wave height at further lateral distances, the downstream length was increased to 14.5m (33.75 LWL). The simulations were conducted at a wide range of velocities, from Fr_h=0.7 to Fr_h=0.99. Figure 3-6 to Figure 3-17 show wave height time histories for numerical and experimental tests for different lateral distances.

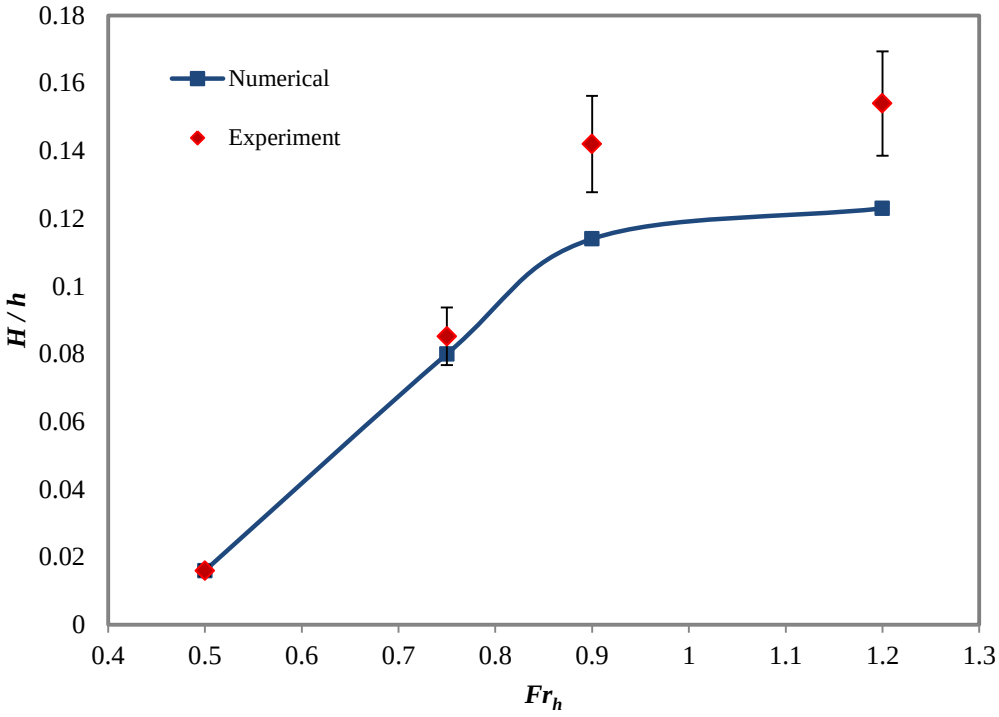

Figure 3-5: Wave height at different depth Froude number at 750mm lateral distance from centre-line

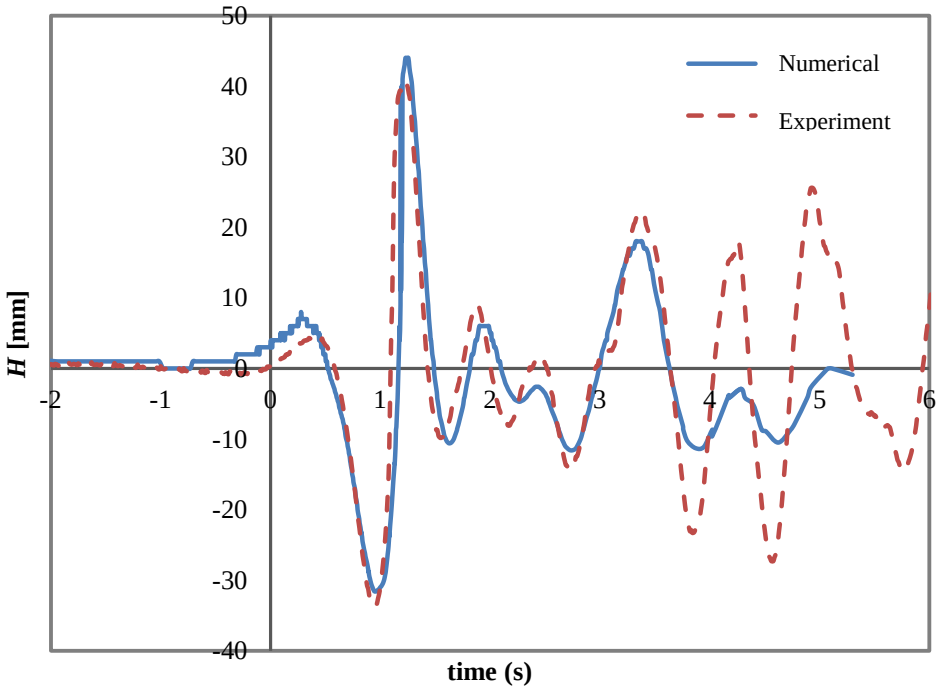

Figure 3-6: Wave height time history for Fr_h=0.7 at 0.75m lateral distance from centre-line (WP1)

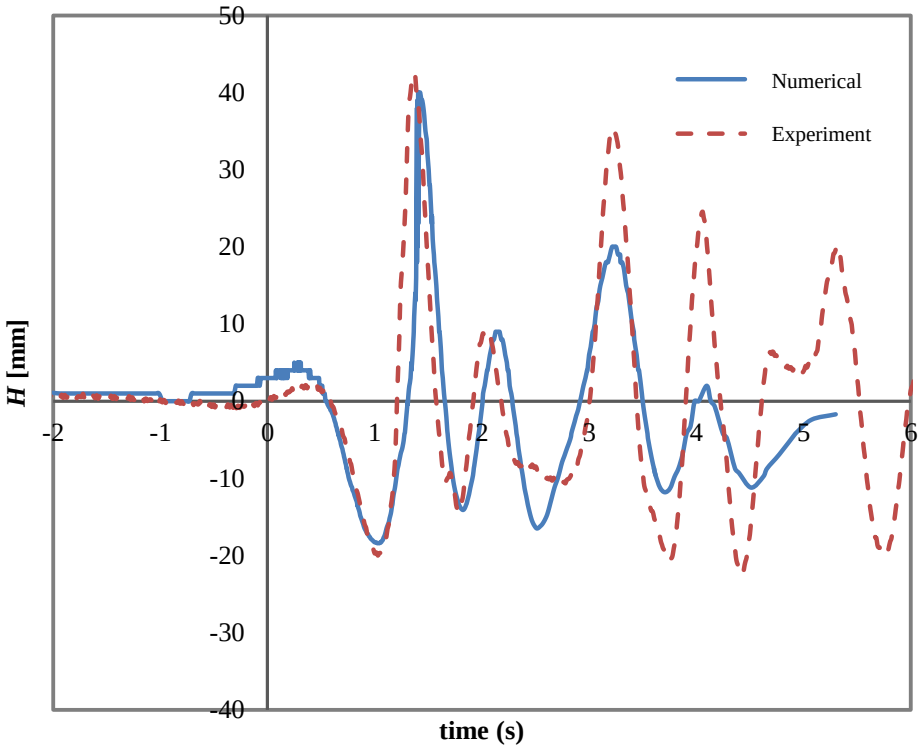

Figure 3-7: Wave height time history for Fr_h=0.7 at 1.0m lateral distance from centre-line (WP2)

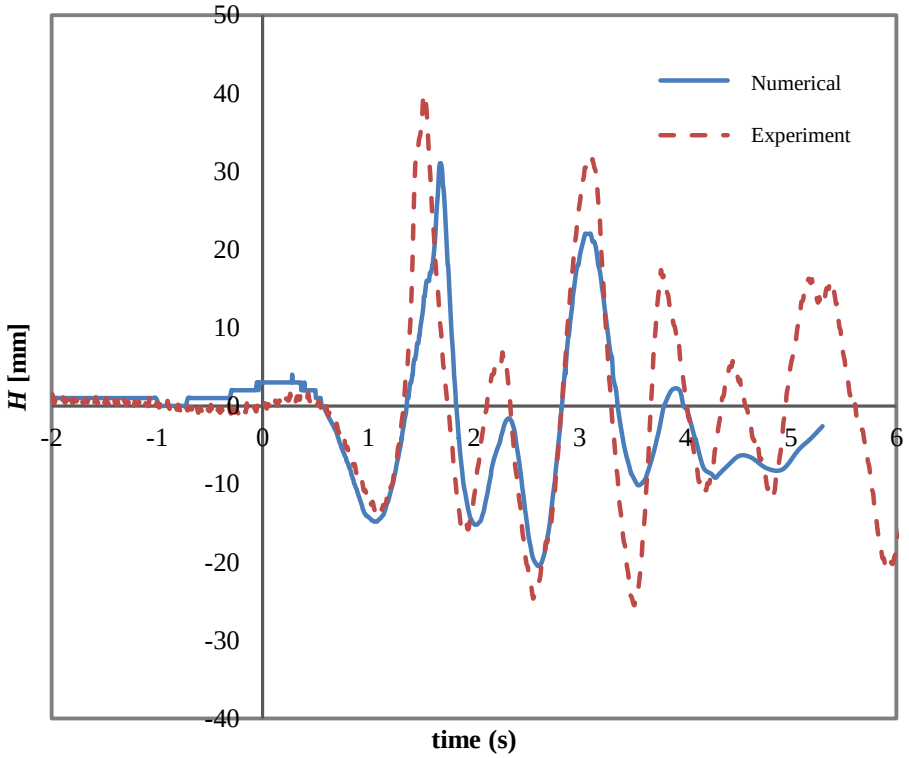

Figure 3-8: Wave height time history for Fr_h=0.7 at 1.25m lateral distance (WP3)

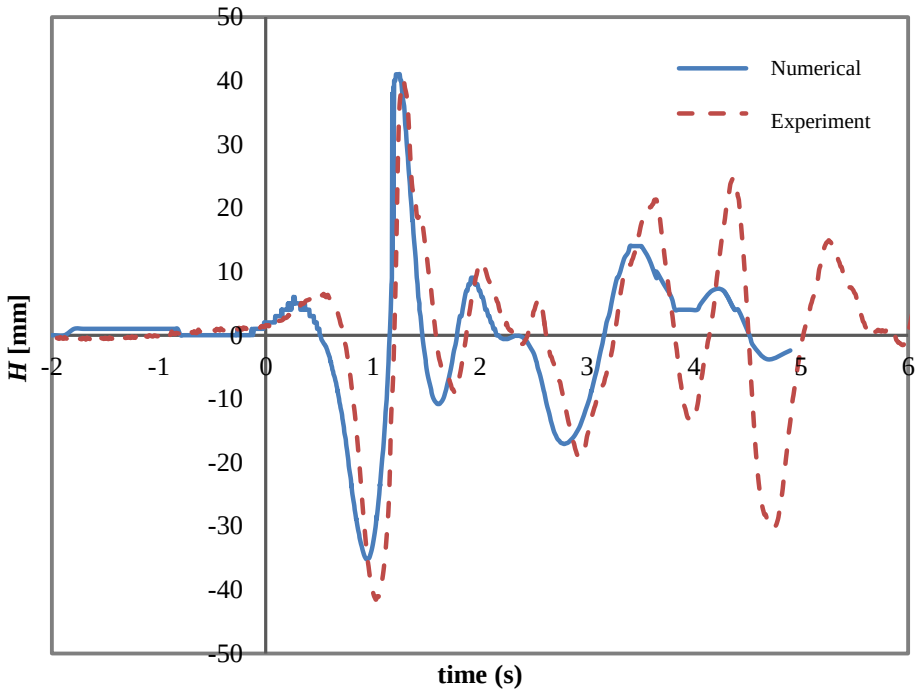

Figure 3-9: Wave height time history for Fr_h=0.75 at 0.75m lateral distance from centre-line (WP1)

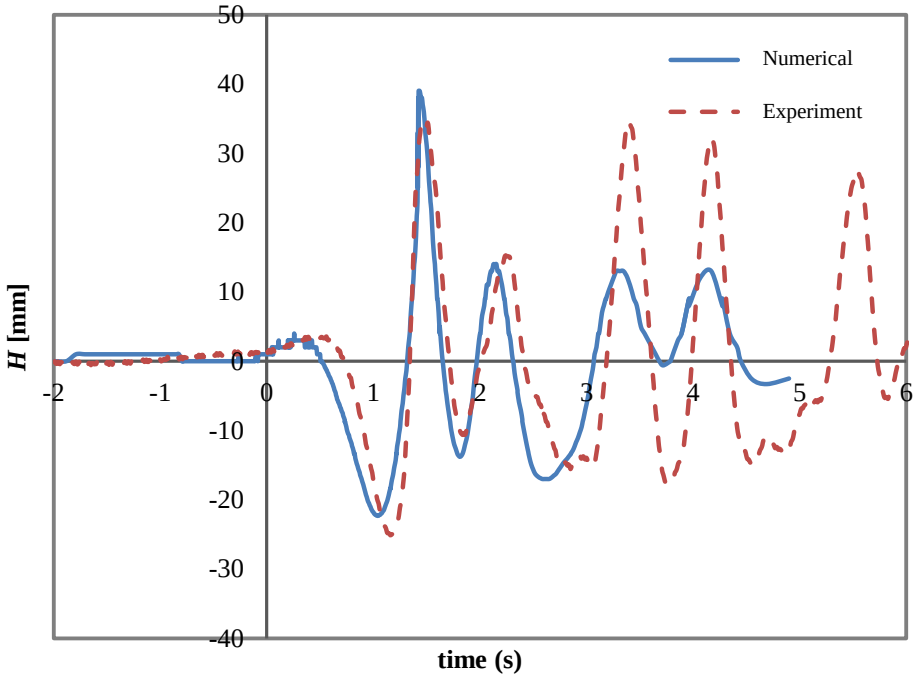

Figure 3-10: Wave height time history for Fr_h=0.75 at 1.0m lateral distance from centre-line (WP2)

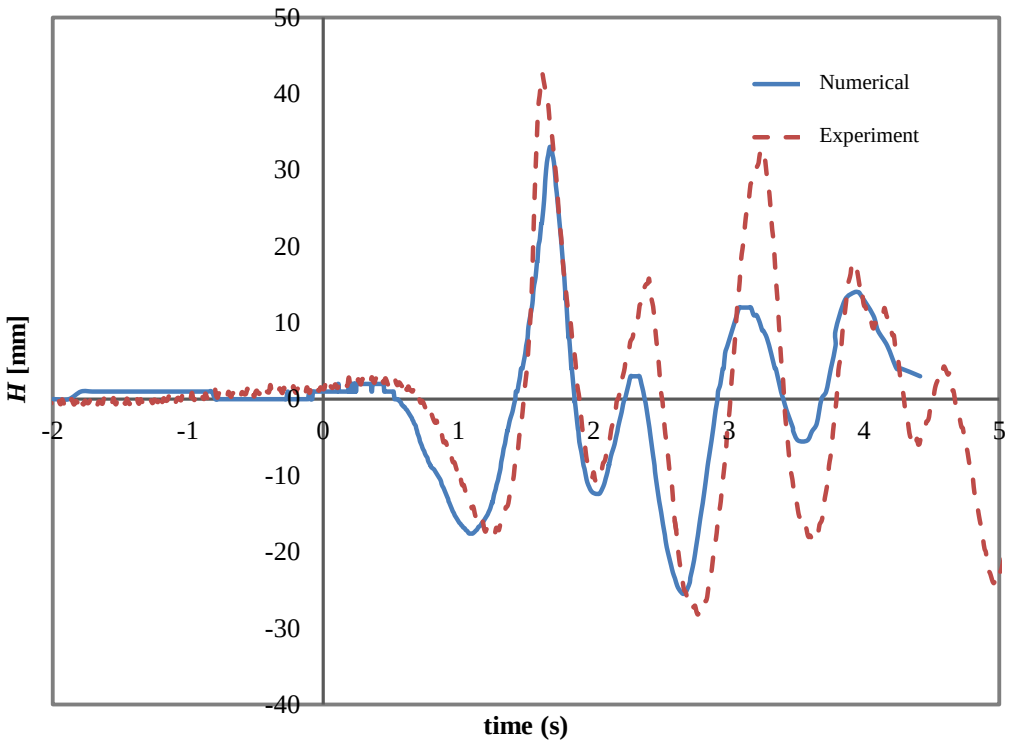

Figure 3-11: Wave height time history for Fr_h=0.75 at 1.25m lateral distance from centre-line (WP3)

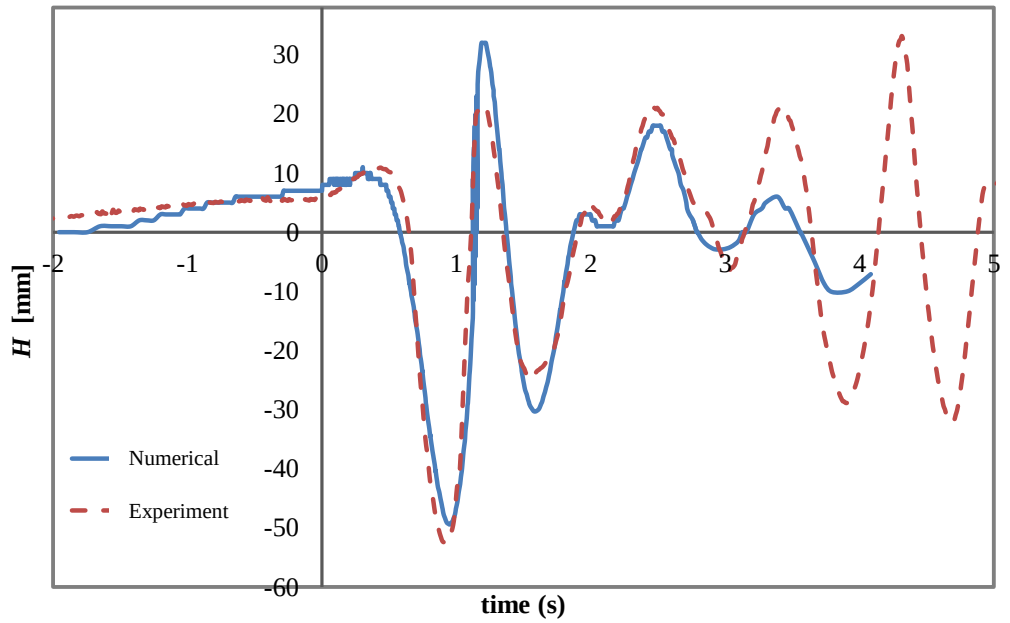

Figure 3-12: Wave height time history for Fr_h=0.9 at 0.75m lateral distance (WP1)

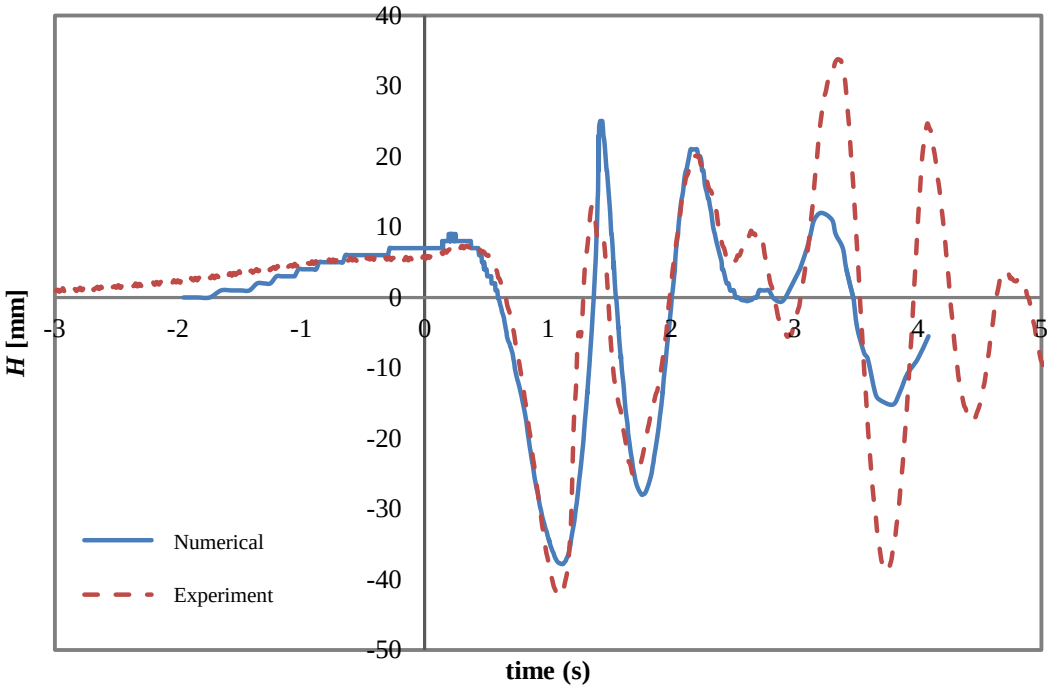

Figure 3-13: Wave height time history for Fr_h=0.9 at 1.0m lateral distance from centre-line (WP2)

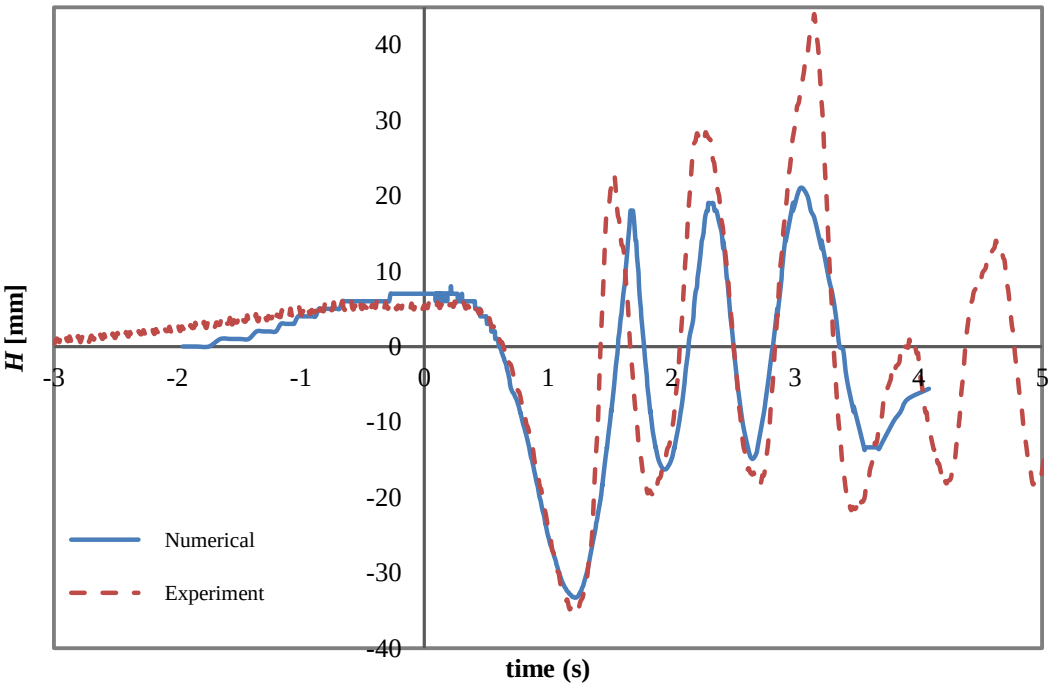

Figure 3-14: Wave height time history for Fr_h=0.9 at 1.25m lateral distance from centre-line (WP3)

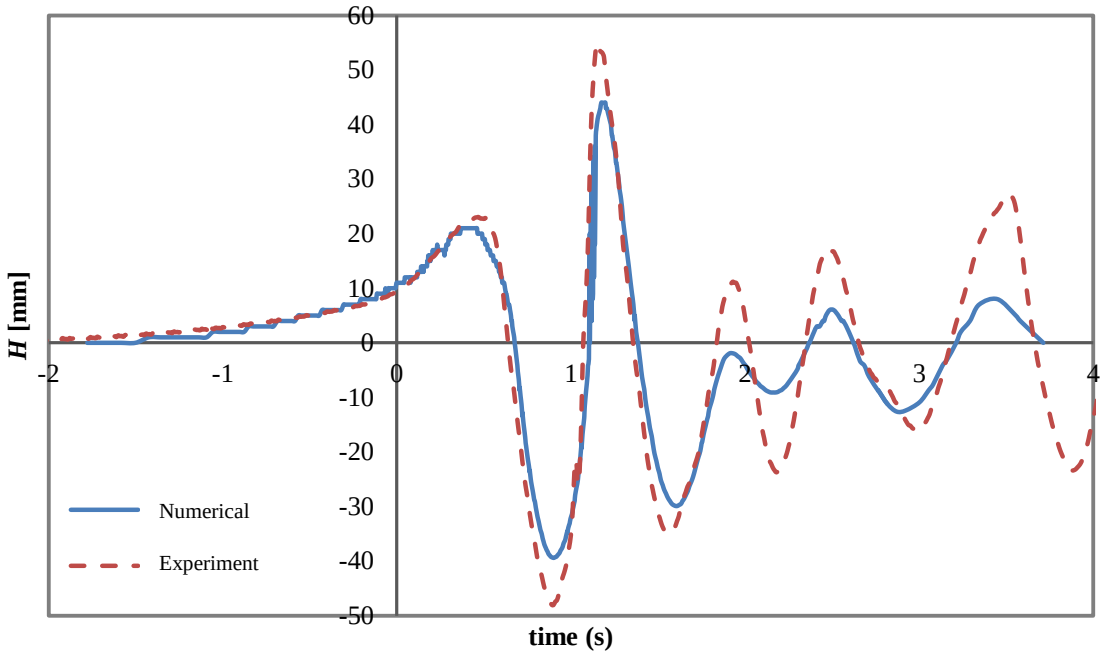

Figure 3-15: Wave height time history for Fr_h=0.99 at 0.75m lateral distance from centre-line (WP1)

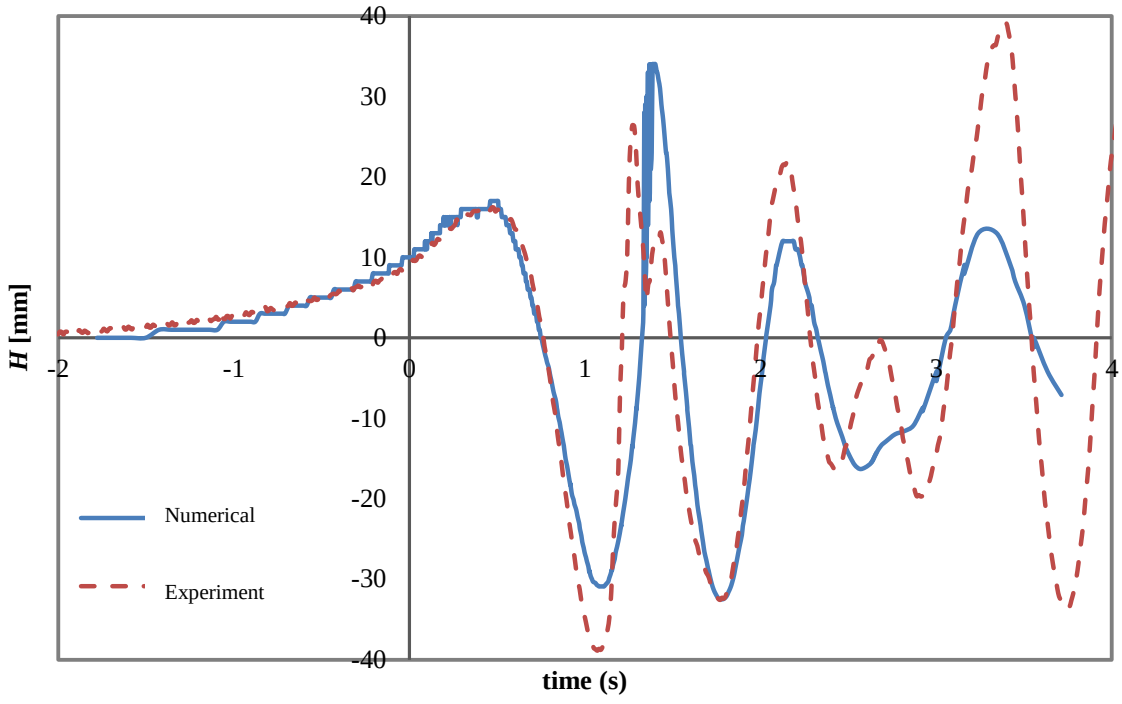

Figure 3-16: Wave height time history for Fr_h=0.99 at 1.0m lateral distance from centre-line (WP2)

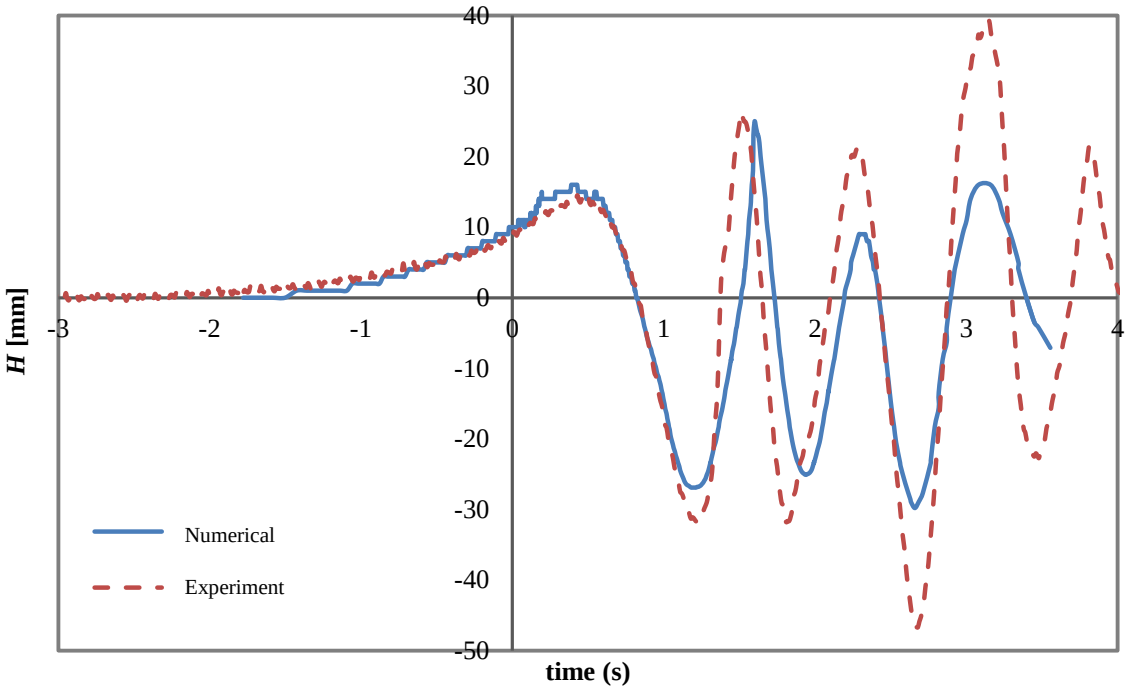

Figure 3-17: Wave height time history for Fr_h=0.99 at 1.25m lateral distance from centre-line (WP3)

Based on the above figures, it is clear that the numerical approach can be used to predict wave height and frequency in a straight track in agreement with the experimental data. This level of accuracy is acceptable for numerical results. Mesh refinement, number of iterations per time step, Courant number and discretisation methods can improve the level of accuracy. According to the design purpose, the first largest wave behind the pressure source was chosen as the desired surfable wave. From the analysis of the results from the experiments, a maximum two waves behind the pressure sources were considered as surfable waves [38]. Since the first wave is important, the simulation run was cut off as soon as the first wave reached a steady state and it was investigated that continuing the simulation does not affect the first wave. As mentioned before the heave and trim of model were fixed and tests were conducted in deepwater, therefore it was possible to generate steady state wave. The simulation started from the calm water situation and at zero speed. The first wave height results at different lateral distances during the simulation time were considered and when no-change was detected in these first wave parameters the simulation was considered as being at a steady state and the run was stopped. To capture more accurate waves at a greater distance, the simulation time must be extended and the mesh size at that area must be refined. Figure 3-18 to 3-20 illustrate the first wave height for different lateral distances numerically and experimentally.

Forces

The numerical drag and vertical forces were validated by comparing the numerical and experimental results. The numerically predicted drag and vertical forces at 1500mm water depth for different Fr_h were compared with the experimental data in Figure 3-21and Figure 3-22. As is shown in the figures, the difference between the numerical results and the experiments is less than 5%. Therefore the numerical approach can be used to predict the forces with good accuracy. Table 3-3 presents the viscous and pressure drags for two Fr_h 0.9 and 0.99. It was shown that about 96% of total drag is related to pressure drag. The water was completely separated from the wavedozer sides and transom and only underneath of the model remained wet. Thus the viscous drag of wavedozer is a very small portion of total drag.

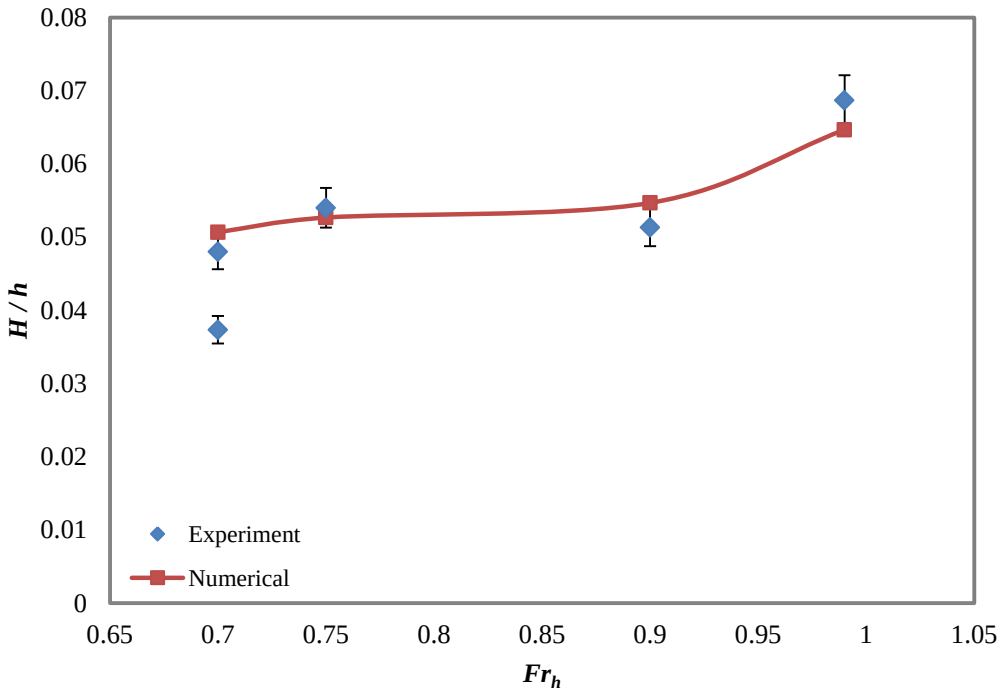

Figure 3-18: The first wave height for different depth Froude numbers at 0.75m lateral distance from centre-line (WP1)

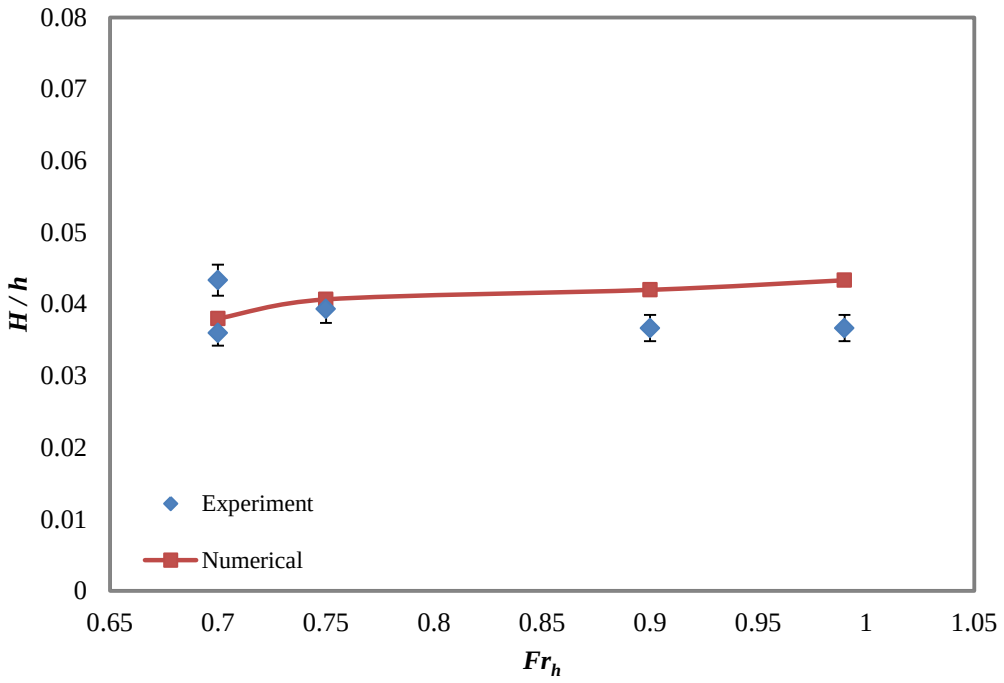

Figure 3-19: The first wave height for different depth Froude numbers at 1.0m lateral distance from centre-line (WP2)

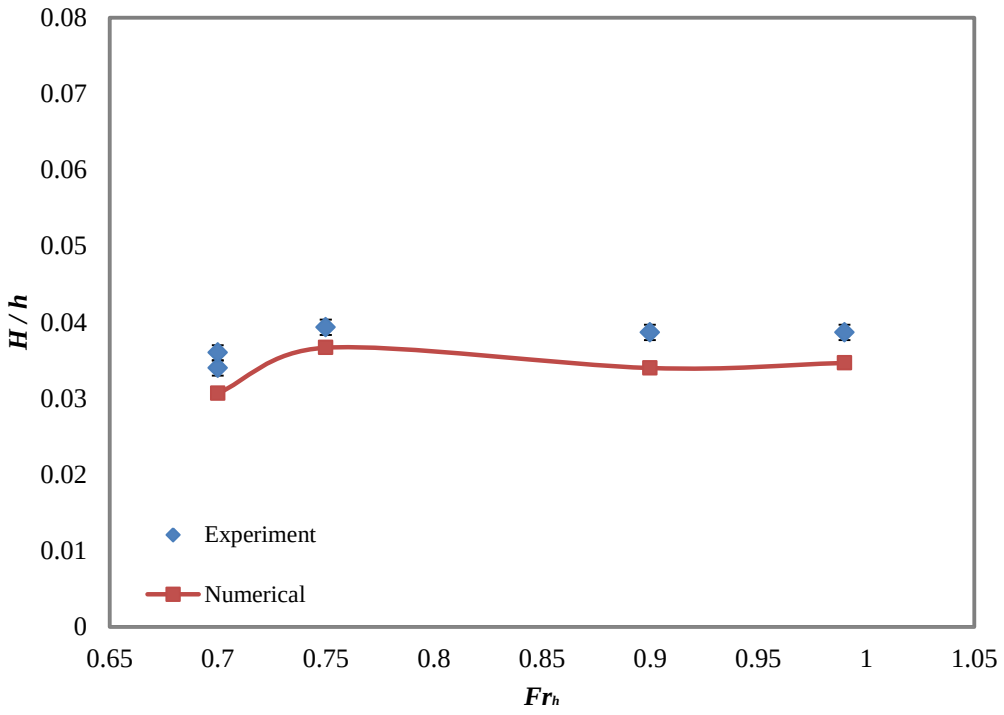

Figure 3-20: The first wave height for different depth Froude numbers at 1.25m lateral distance from centre-line (WP3)

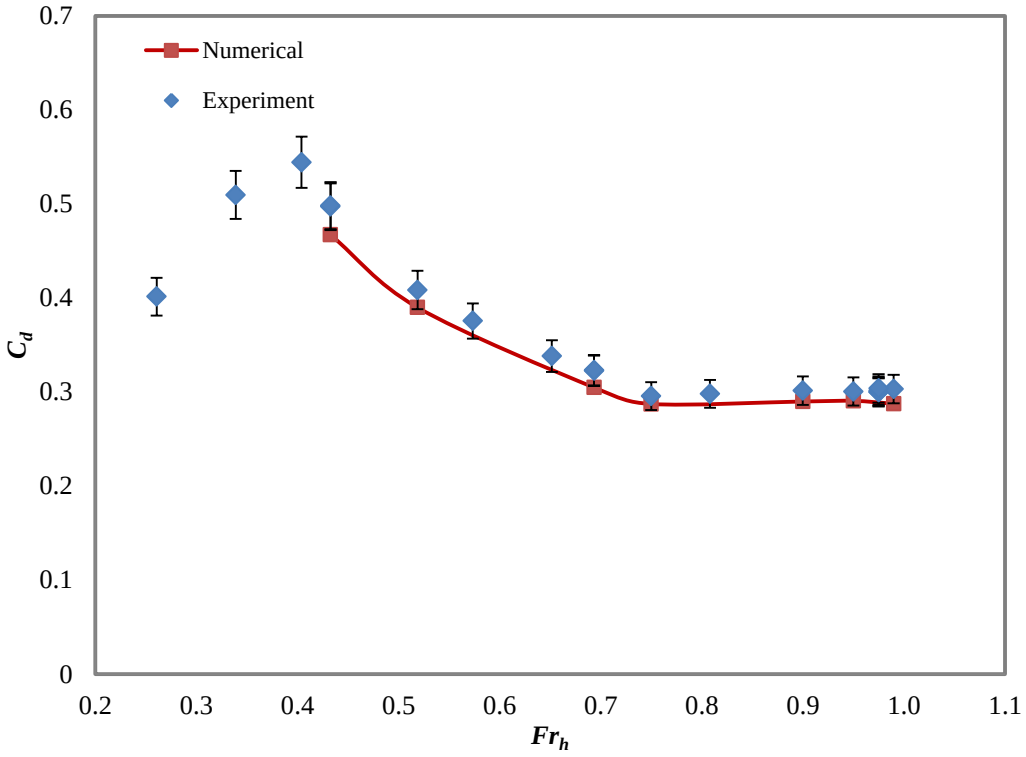

Figure 3-21: Comparison of experiment and numerical drag coefficients for different Fr_h at 1500mm water depth

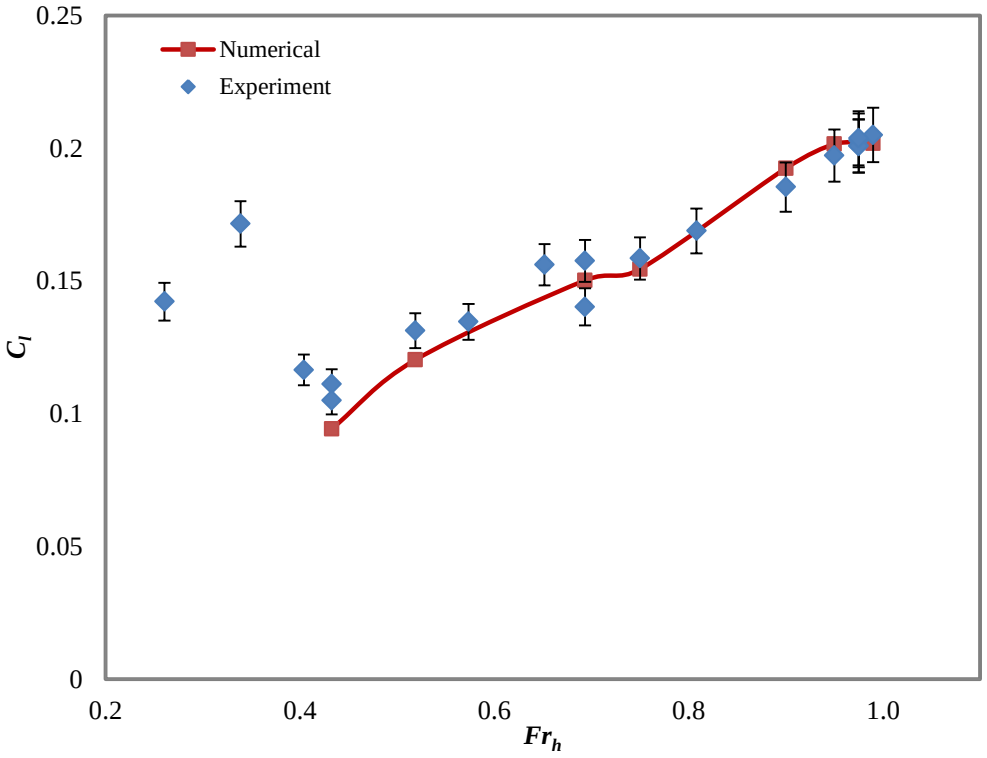

Figure 3-22: Comparison of experiment and numerical lift coefficients for different Fr_h at 1500mm water depth

Table 3-3: Viscous and Pressure Drags for Two Different Fr_h

Fr_h	Pressure drag [N]	Viscous drag [N]	Total drag [N]	Viscous drag/Total drag
0.9	49.48	2.24	51.72	0.04
0.99	59.71	2.81	62.52	0.04

In addition, the drag forces of parabolic and wavedozer pressure sources at 500 mm water depth compared together. Figure 3-23 shows the drag forces for parabolic and wavedozer pressure sources at different depth Froude numbers. It can be seen the drag forces for parabolic pressure sources at all investigated depth Froude numbers are much bigger than wavedozer drags. Figure 3-24 presents the percentage of viscous drag at different depth Froude numbers for parabolic and wavedozer pressure sources. The portion of viscous for parabolic pressure source is more than twice of the wavedozer's. Therefore the required power to run the wavedozer is less than the parabolic pressure source. As a conclusion, the wavedozer is more efficient not just regarding to the wave generated quality, but also in terms of energy consumption.

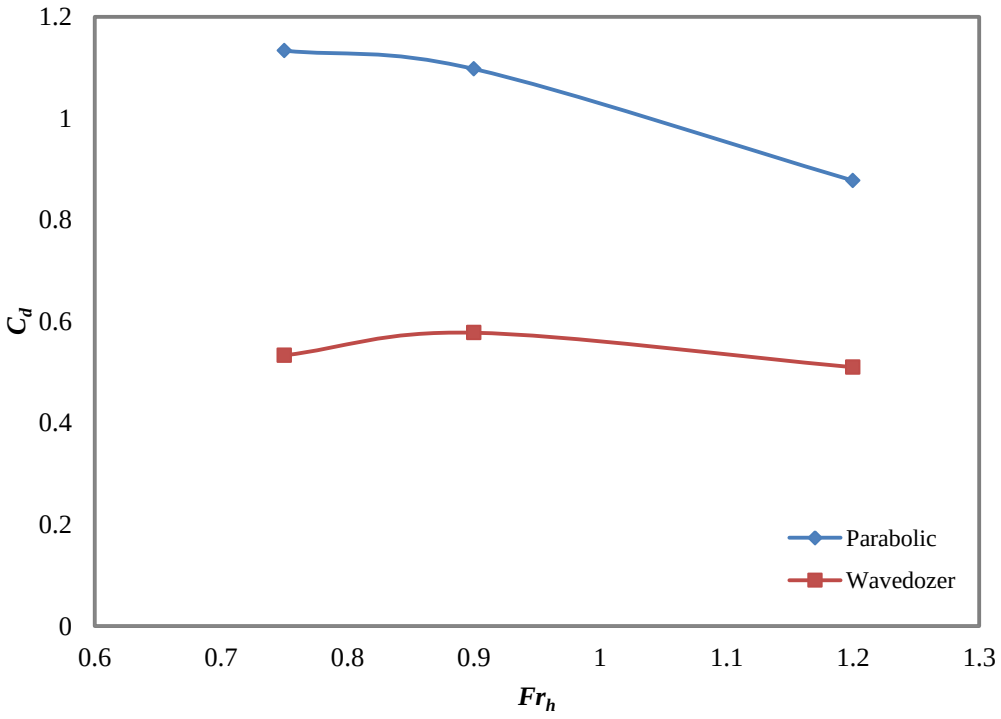

Figure 3-23: The drag forces for parabolic and wavedozer pressure sources at different depth Froude numbers at 500mm water depth

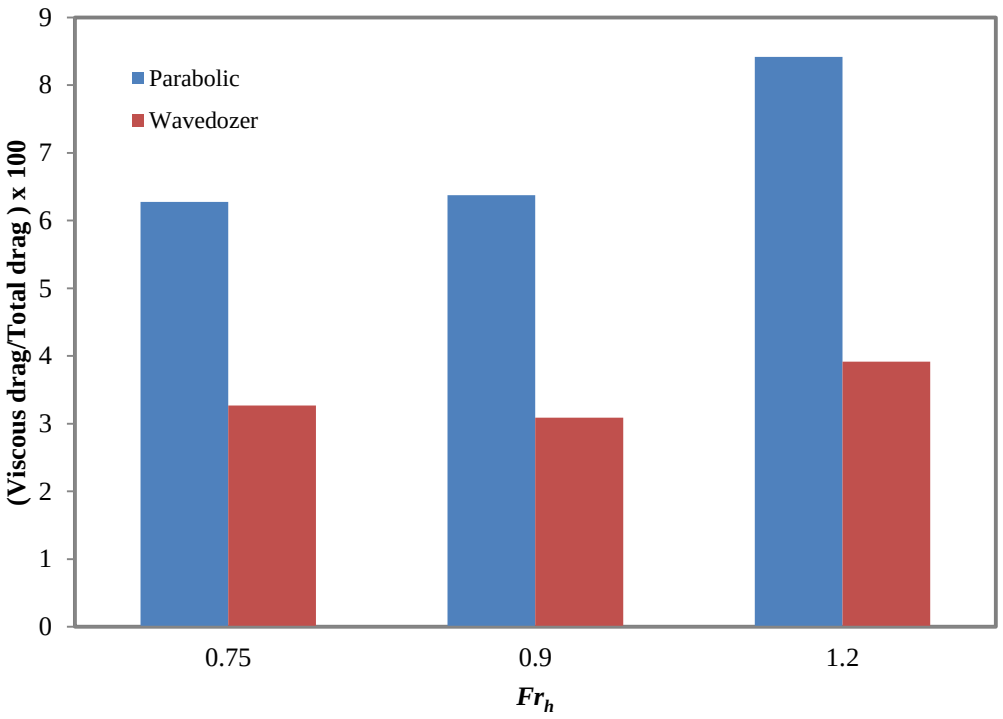

Figure 3-24: Comparing the viscous forces at different depth Froude numbers for parabolic and wavedozer pressure sources at 500mm water depth

3.3.2. Curved track

After validating the ability of the numerical method to predict the generated wave parameters and forces in a straight track, numerical simulations were conducted to investigate its ability to predict wave parameters in a curved track. An experimental condition was modelled numerically at different Fr_h in a curved track with parallel walls.

Circle track with parallel wall

To determine the effects of a curved track on the wave heights generated by the wavedozer, the towing tank cross-section was modelled at half scale as a curved track. The circular experimental tests had been previously undertaken in the AMC Model Test Basin [39]. The outer wall radius was 5m and the width of the channel was 888mm. For the simulation, 110 degrees of this circle were modelled. Table 3-4 gives the wavedozer parameters for this curved track. The wave height comparison based on numerical predictions and the experimental results is shown in Figure 3-25. As can be seen, the numerical predictions agree very well with experimental test data. In particular, it can be seen that the numerical method can predict that the wave height is less for Fr_h>0.9 as shown in the experimental data. Some free surface pictures captured in the experimental tests and simulation results are given in Figure 3-26 and Figure 3-27.

Table 3-4: Wavedozer Characteristics in Curved Track

Length (mm)	602
Beam (mm)	275
Draught (mm)	50
Angle of attack (degree)	14
Depth (mm)	500

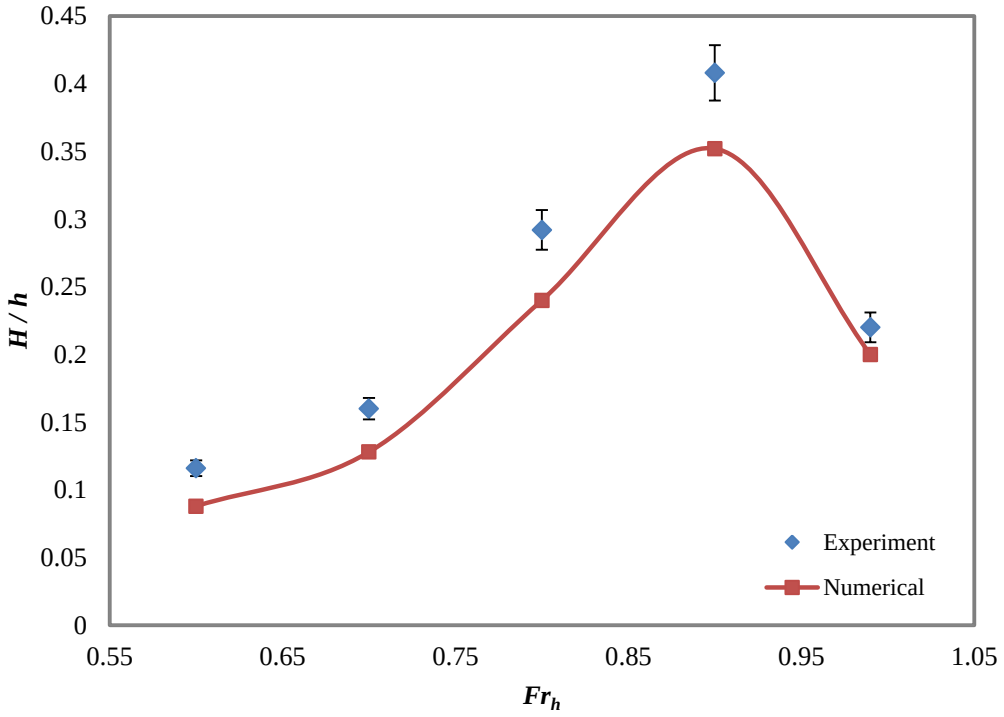

Figure 3-25: Wave height as a function of depth Froude number for experimental results and numerical predictions at 365mm lateral distance from centre-line

Figure 3-26: Free surface elevation (the experiment)

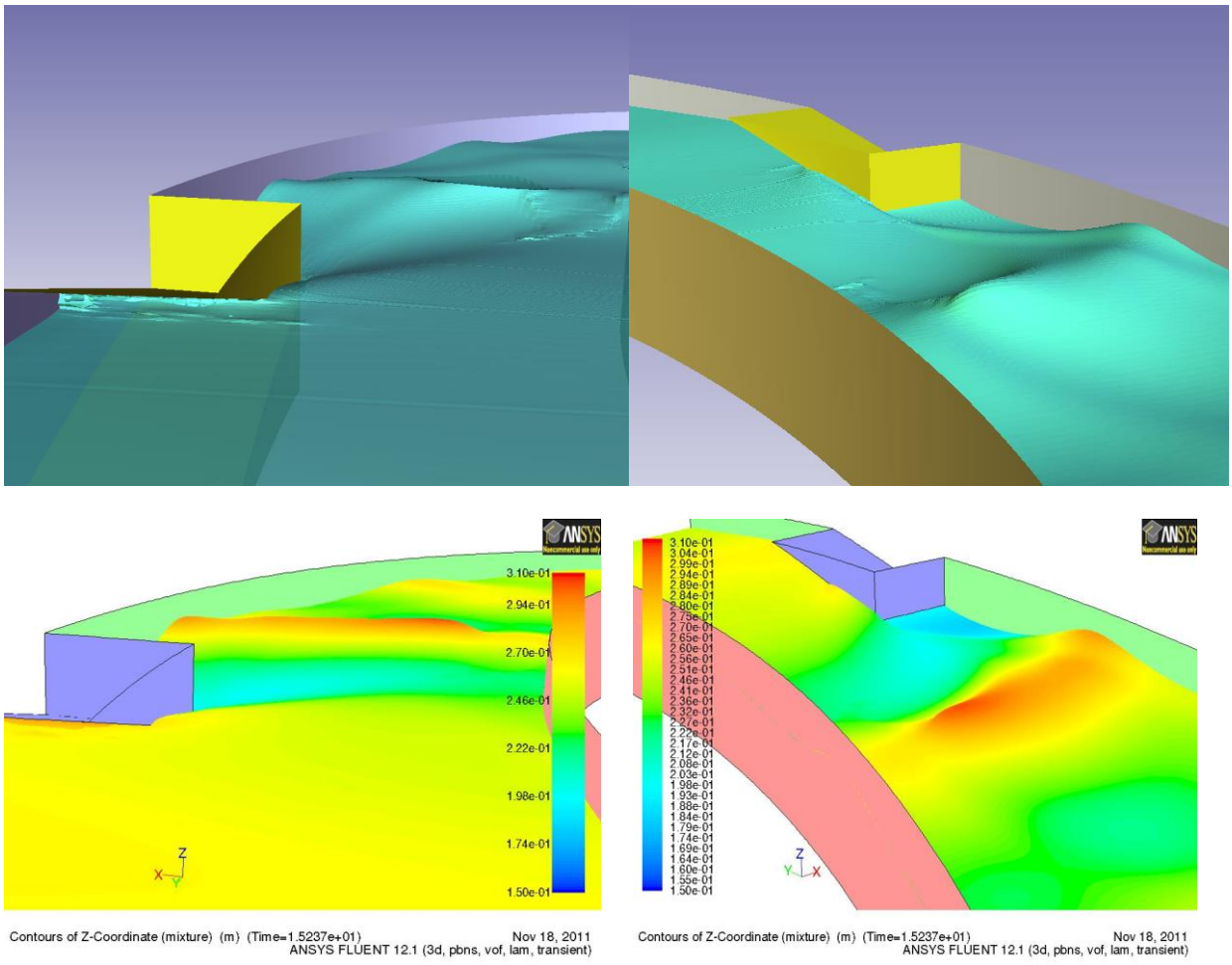

Figure 3-27: Free surface elevation (the numerical)

3.4. Grid Independence

In this context, "grid-independent" results means results which are sufficiently independent from grid size, such that the truncation error can be ignored in a numerical simulation. Truncation error is one of the sources of error in numerical simulations. This error is generated by truncating an infinite sum and approximating it by a finite sum. To discretise a PDE using a Taylor series, the first few terms of the series are used and other terms are considered as truncation error. This is considered by the discretisation method used in numerical software.

For this study, the Richardson Extrapolation approach [55] was used to quantify the results of a numerical method in terms of its grid-independence. The idea is to use a low order formula for which the expression of the truncation error is well known. Then results with higher order accuracy can be derived from the low order formula.

Richardson Extrapolation Formula:

If it is assumed that discretisation of the transport equations is of second order then the grid-independent solution (GIS) is approximately equal to the calculated value (ϕ) plus a value proportional to β^2 (eq. (3-11)), where β is step size (grid size). Expressed mathematically:

$$\mathrm{GIS} = (\phi)_h + c(\beta^2) \tag{3-11}$$

By refining the grid size, to half of previous size, the true value can be calculated based on eq. (3-12):

$$\mathrm{GIS} = (\phi)_{\frac{h}{2}} + c(\frac{\beta^2}{4}) \tag{3-12}$$

By finding the difference of eq. (3-6) and eq. (3-7), the Richardson extrapolation formula can be calculated (eq. (3-13)):

$$\mathrm{GIS} = (\phi)_{\frac{h}{2}} + \frac{((\phi)_{\frac{h}{2}} - (\phi)_h)}{3} \tag{3-13}$$

The common formula (for second order discretization) is (eq. (3-14)):

$$\mathrm{GIS} = f_1 + \frac{f_1 - f_2}{r^2 - 1} \tag{3-14}$$

where f_1 is the result for the finer mesh, f_2 is the result for the coarse mesh and r is the grid refinement ratio.

The grid independency was conducted for shallow water (500 mm water depth) wavedozer simulations in the straight track. For grid independency, four mesh domains with different numbers of

cells were simulated. Table 3-5 shows the number of cells in different meshes. The number of cells in the fine mesh is 8 times greater than the average mesh. This means the number of nodes in each direction is two times more than in the average mesh. The number of cells in coarse mesh (1) is almost one-eighth of the average mesh, which means the number of nodes in each direction is half the number of those in the average mesh, and so on. Figure 3-28 shows the wave height for different depth Froude number at 750 mm lateral distance. It is clear that the average mesh domain is the ideal, because by increasing the number of cells to the finer mesh domain, the change in the results was insignificant. In addition, the domain with coarse mesh (2) is not appropriate as a decrease in wave height is evident for a shift in depth Froude number where the finer meshes and the experiments all indicate that the opposite is true. By using the results from coarse mesh (1) and average mesh domain, grid-independent solutions were calculated by using the Richardson extrapolation formula second order. As it can be seen, this result is the same as what was obtained by using the fine mesh domain.

Table 3-5: The Number of Cells for Different Domains

Domain name	**number of cells**	**ratio**
Fine	23243760	8
Average	2905470	1
Coarse (1)	376800	0.129686
Coarse (2)	46288	0.015931

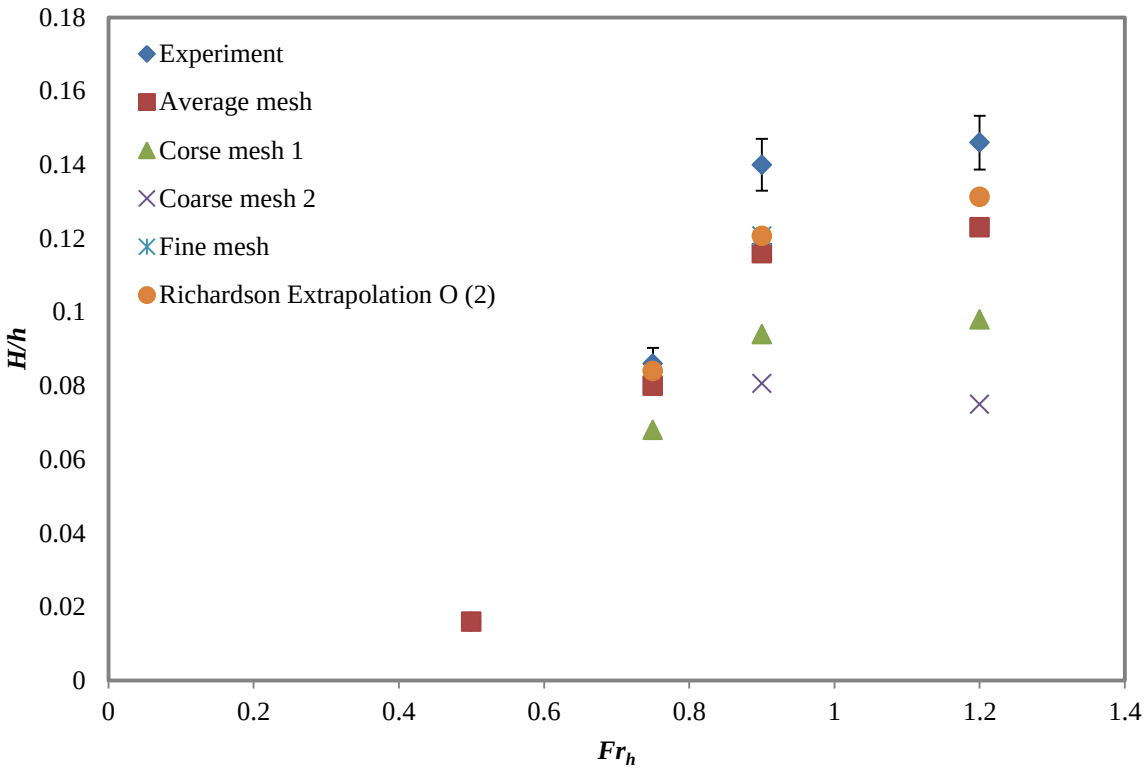

Figure 3-28: Wave height predicted by different number of cells at 750 mm lateral distance from centre-line (WP1)

3.4.1. Observed order of accuracy

When the exact solution is not known (which is generally the case for solution verification), three numerical solutions on different meshes are required in order to calculate the observed order of accuracy. Consider a *p*th-order accurate scheme with numerical solutions on a fine mesh (β_1), a medium mesh (β_2), and a coarse mesh (β_3). For the case of a constant grid refinement factor:

$$r = \frac{\beta_2}{\beta_1} = \frac{\beta_3}{\beta_2} \tag{3-15}$$

We can thus write

$$\beta_1 = \beta, \beta_2 = r\beta, \beta_3 = r^2\beta \tag{3-16}$$

Where r is the grid refinement ratio. The three descritisation error equations can be written as:

$$GIS = f_1 + c\beta^p + O(\beta^{p+1}) \tag{3-17}$$

$$GIS = f_2 + c(r\beta)^p + O([r\beta]^{p+1})$$

$$GIS = f_3 + c(r^2\beta)^p + O([r^2\beta]^{p+1})$$

Neglecting the higher-order terms, these three equations can be used to solve for the observed order of accuracy *p* to give

$$p = \frac{\ln(\frac{f_3 - f_2}{f_2 - f_1})}{\ln(r)} \quad (3\text{-}18)$$

Note that here the observed order of accuracy is calculated and does not need to be assumed (as with the Richardson extrapolation).

This approach was used to calculated the order of accuracy based on three available results at Fr_h=0.9.

Table 3-6 presents the results and order of accuracy.

Table 3-6: Observed order of accuracy

Domain name	*H/h*
Fine	0.121
Average	0.116
Coarse (1)	0.094
Order of accuracy	2.2

3.5. Mesh quality

Regardless of the variety of CFD approaches, e.g. discretisation methodologies and solvers, the quality of the grids used has a significant effect on the final results. To predict the flow parameters, the density of cells in a computational grid needs to be fine, while the high number of cells requires much more simulation time, memory requirement and computational cost. Therefore there is a need to 'trade-off' between accuracy and computational effort. The proper geometrical mesh quality is essential to reduce discretisation and computational errors.

Most mesh quality metrics are geometric in nature; considering shape, size, angles, aspect ratio, and skewness of the mesh elements. Additional considerations include variations between mesh elements, such as cell-to-cell and face-to-face ratios. Improper geometric mesh quality may have considerable influence on the propagation of numerical errors and can result in an imprecise solution [56].

Historically, mesh quality analyses were first performed for finite-difference and finite-element methods. It is not straightforward to translate those approaches to finite-volume method (FVM) that represent state-of-the-art CFD computations [57]. There is no doubt that certain mesh characteristics critically affect the accuracy of CFD solutions and gradients. For finite-difference approaches, most mesh quality methods aim to establish connections between mesh and truncation error [58, 59]. The truncation error analysis is often applied to FVM schemes as well. The standard finite-element estimates use Sobolev norms that simultaneously estimate errors in the solution and its derivatives.

These estimates might be too conservative because recent finite-volume computations indicate that accurate solutions can be obtained in spite of poor gradient accuracy [60, 61].

Different physics and different solvers have different mesh quality requirements. ANSYS Fluent software requires a high quality mesh to avoid numerical diffusion. Several metrics are involved in order to meet the required mesh quality. Skewness, aspect ratio and cell size change are most important mesh parameters to be considered. In worst case scenarios and depending on the solver used (density based or pressure based) ANSYS Fluent can tolerate poor mesh quality. However some applications may require higher mesh quality, resolution and good mesh distribution. The location of poor quality elements determine their effect [62].

- Aspect Ratio

  Aspect for generic triangles and quads is a function of the ratio of longest side to the shortest side of the reconstructed quadrangles. The ideal aspect ratio for an equilateral triangle or a square is 1. Figure 3-29 shows ideal and high aspect ratio for a quadrilateral and triangle cell.

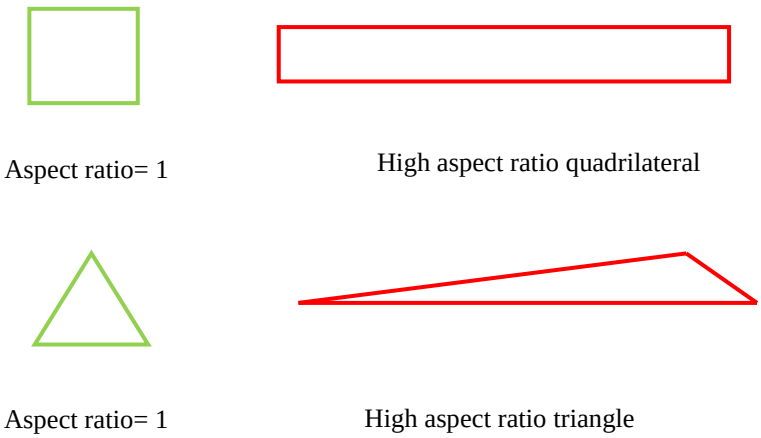

Figure 3-29:Aspect ratio

- Skewness

There are two methods for determining skewness. One is based on equilateral volume deviation (eq. 3-19) and the other is based on the deviation from a normalized angle deviation (eq. 3-20).

$$Skewness = \frac{\text{optimal cell size} - \text{cell size}}{\text{optimal cell size}} \tag{3-19}$$

$$Skewness = \max\left[\frac{\theta_{\max} - \theta_e}{180 - \theta_e}, \frac{\theta_e - \theta_{\min}}{\theta_e}\right] \tag{3-20}$$

where θ_e is the equiangular face/cell (60 for tetrahedral and triangle, and 90 for quadrilateral and hexahedral). In Equation 10, a skewness value of 0 means perfect and 1 indicates the worst skewness.

- Cell size change

This is the mesh expansion factor, or the ratio of largest to smallest element volumes surrounding a node. The cell size change must be between 1 and 2, i.e. cell must be no more than two times bigger than the smallest neighbouring cell.

Geometrical mesh quality is important from some different points of view, including:

— Source of discretisation error

- large mesh expansion introduces errors in storage and source approximations
- non-orthogonality introduces errors in flux approximations

— Difficulties solving linearized equations

- large aspect ratios require use of more significant digits (i.e. use of double precision solver)

The influence of grid quality on free surface deformations behind the wavedozer was investigated. Various grid domains with different mesh quality were generated and the numerical results compared with the experimental results. For this study, the condition of wavedozer in 1.5 m water depth was simulated. The computational domain was constructed to be 6m (15 LWL) upstream and 13.5m (33.75 LWL) downstream of the model. The domain length was long enough to have no significant effect on the first wave propagation. As before, the flow had a plane of symmetry about the centre plane, and to reduce the processing time only half of the domain was used. The velocity inlet and outflow conditions were used to specify the inlet and outlet boundary conditions. A symmetry plane was used along the centre plane, and the remaining boundary surfaces along the exterior of the domain were set to wall conditions. Figure 3-30 shows the exterior of the domain. The width of the domain was the same as that of the towing tank, as described in the previous sections.

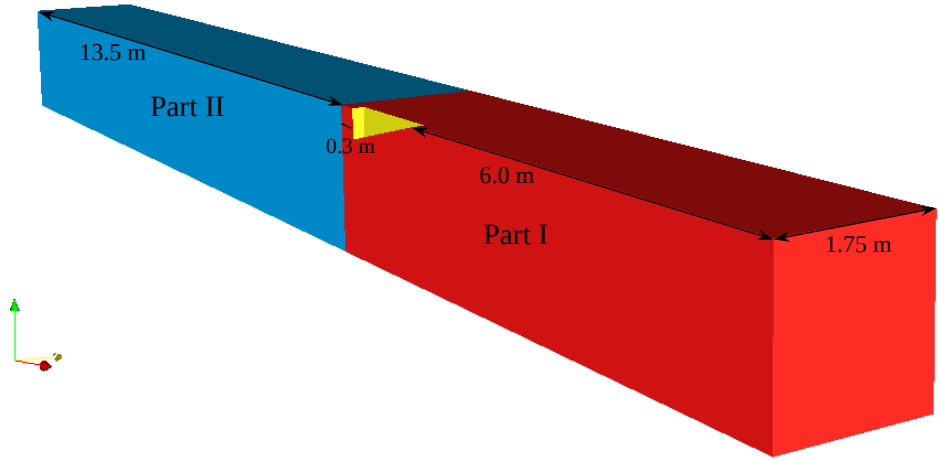

Figure 3-30: Computational grid domain

To study the effects of mesh quality on wave propagation, the exterior computational grid domain dimensions were kept constant. In addition, the cell parameters for the upstream domain part (Part I as shown in Figure 3-30) were kept constant in all of the computational domains, while the cell parameters in the downstream part (Part II) were changed. The changing area started from 0.3m (0.75 LWL) aft of the transom to the termination of the domain. The reason for changing only the rear portion was to maintain the same accuracy in order to predict pressure around the pressure source. The study only investigated the effect of mesh quality on numerical diffusion relating to wave propagation. These simulations allowed a comparison of the results in terms of mesh quality with the same wave generating pressure for all conditions. The cell dimensions in the longitudinal (x) and the vertical (z) directions were changed, but there was no change in the lateral (y) direction. It should be noted that the neighbouring cells of Part I and Part II in the computational domain had the same size in all of the mesh domains. In addition, all cells in Part II were hexahedral cells and were all orthogonal, therefore the skewness is zero for all cells in Part II. For this study eight mesh domains with different cell qualities were generated. The different mesh characteristics for two depth Froude numbers; 0.9 and 0.99 are presented in Appendix A.

The first simulation was conducted using a mesh domain (M1), which had high aspect ratio cells in Part II. This mesh was not able to accurately predict wave height (Figure 3-31)

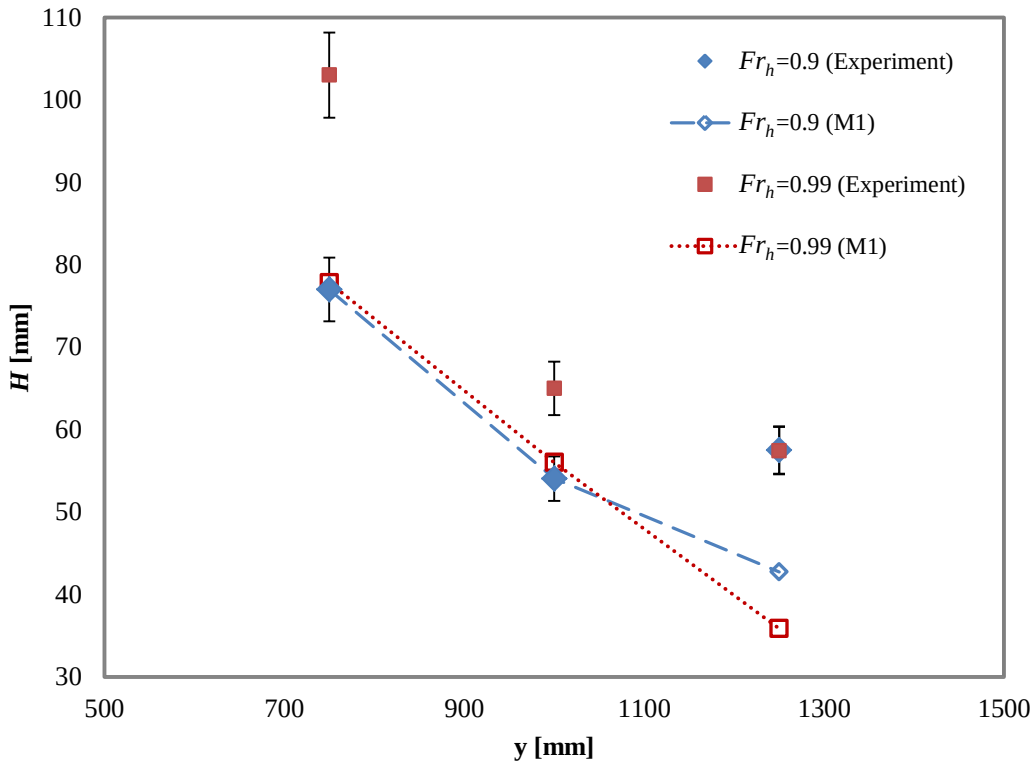

Figure 3-31: comparison of wave height of numerical, using high aspect ratio mesh domain M1, and experimental results at varying lateral distances, the horizontal axes presents the distance from from centre-line

The number of cells per wave length at different lateral distances for different depth Froude numbers was less than 22 cells. The number of cells per wave height at different lateral distances was more than 10 (see Appendix A), except for Fr_h=0.9 at WP1 which was 8. The average aspect ratio of cells for different depth Froude numbers 0.9 and 0.99 was more than 15 at different lateral distances.

A second mesh (M2) was generated. The number of cells in the x direction was increased and, as a result, the average aspect ratio was decreased. This means that compared with the previous mesh (M1), the average number of cells per wave length was increased from about 20 to 80 and the aspect ratio was decreased to less than 7 (Appendix A). The size of the cells in the z direction was kept the same as for M1. The wave height prediction was improved, as shown in Figure 3-32. Hence further depth Froude numbers, 0.7 and 0.75, were modelled using this mesh. The drag and vertical force comparisons with the experimental data are presented in Figure 3-21 and Figure 3-22. The level of predicted forces accuracy confirms that the mesh around the pressure source is able to predict flow characteristics and that the cell size in Part I is fine enough. The results for M2 were acceptable across a range of depth Froude numbers.

In the next change, the number of cells in x direction was increased from 80 (M2) to 120 (M3), which caused a decrease in the average aspect ratio to less than 5. Again, the cells size in the z direction remained the same as before (Appendix A). There was no significant improvement in the wave height predictions compared to the M2 results (Figure 3-33).

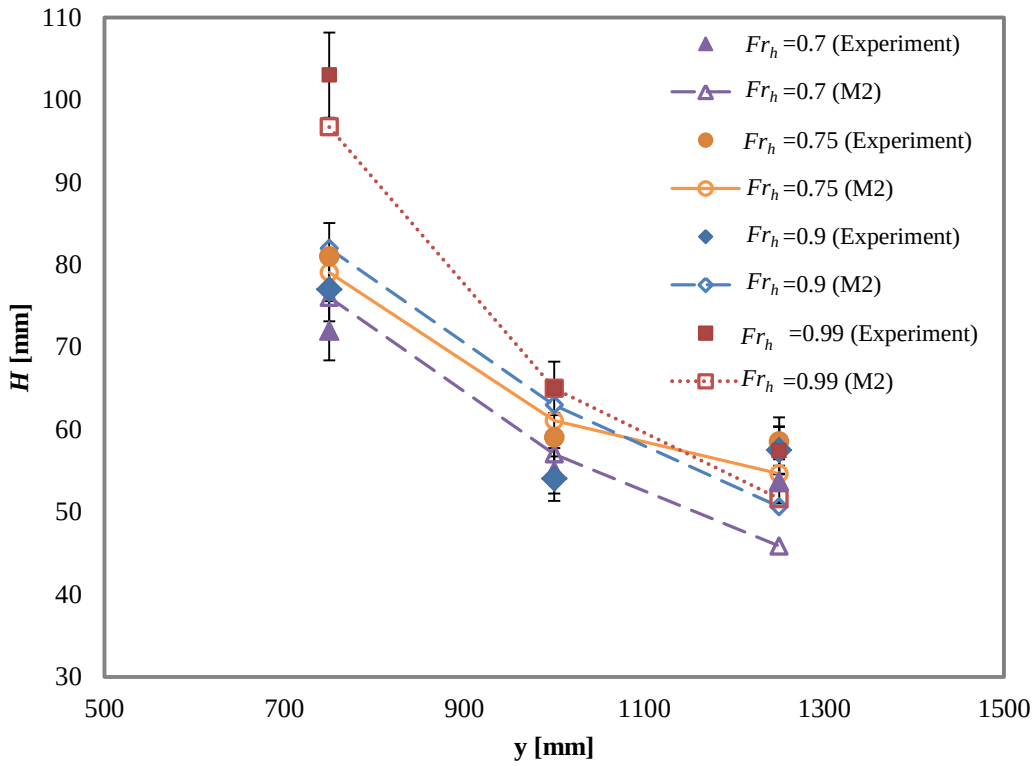

Figure 3-32: Comparison of wave height of numerical, with mesh domain M2, and experimental results at varying lateral distances for different depth Froude numbers, the horizontal axes presents the distance from from centre-line

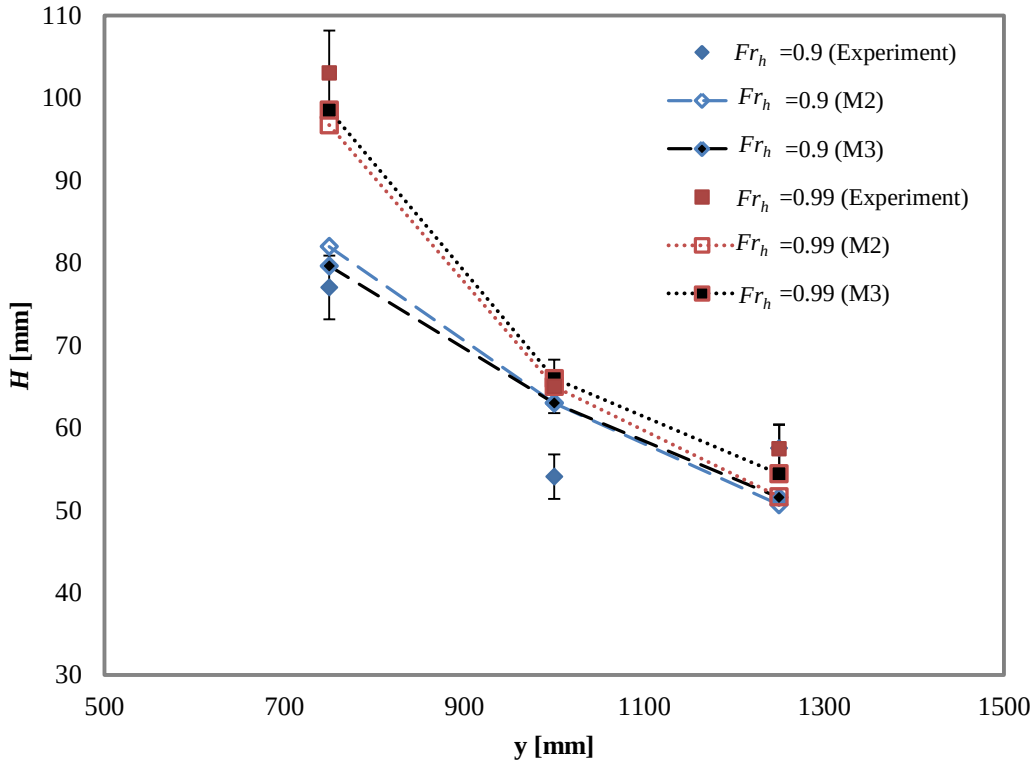

Figure 3-33: Comparison of wave height of numerical, with mesh domain M2, M3 and experimental results at varying lateral distances for different depth Froude numbers, the horizontal axes presents the distance from from centre-line

By increasing the number of cells in the x direction, two parameters (aspect ratio and the number of cells per wave length) were changed. The next investigation focused on whether the improvement in the prediction of the wave height was due to the aspect ratio modification or the change in the number of cells per wave length. A new mesh was generated (M4), wherein the number of cells per wave length was kept the same as for the previous mesh (M3), i.e. 120, but the cell height was decreased by changing the expansion ratio, thus causing the aspect ratio to increase. This meant that the total number of cells in M3 and M4 were the same, but the density of cells around the free-surface in M4 was more than that of M3. The results are presented in Figure 3-34. The average aspect ratio for this mesh (M4) was less than 10 and the number of cells per wave height was more than 20 at all lateral distances (Appendix A).

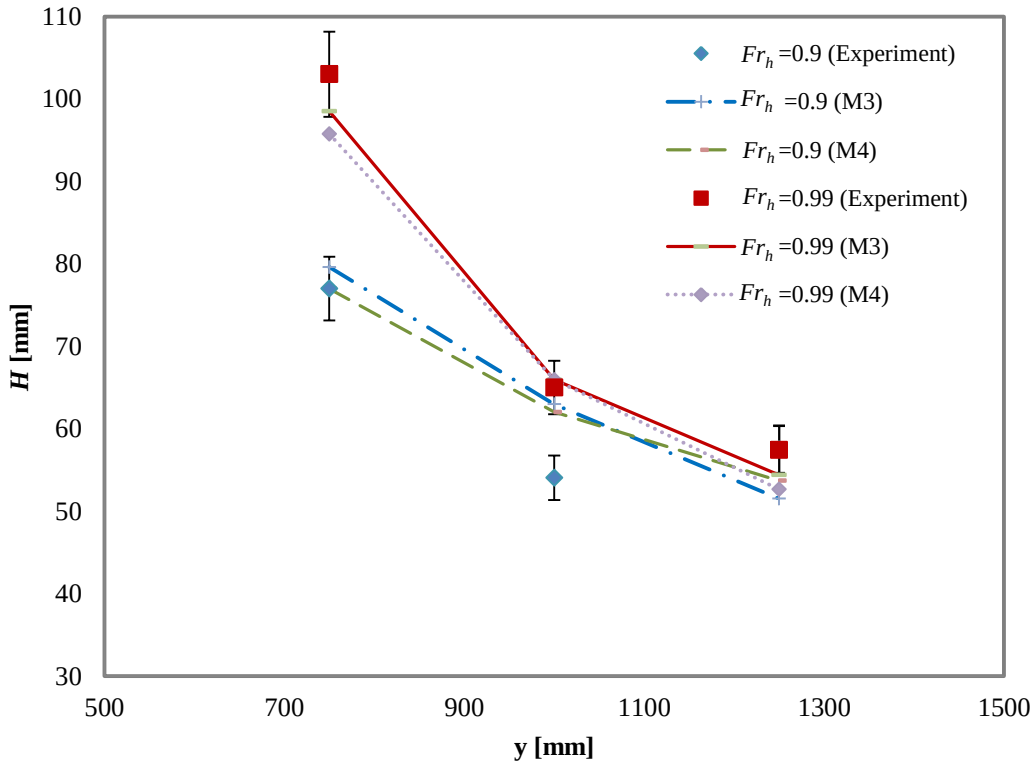

Figure 3-34: Comparison of wave height of numerical results with mesh domain M3 and M4 at varying lateral distances for different depth Froude numbers, the horizontal axes presents the distance from from centre-line

Since this mesh did not result in a significant change in wave height predictions, the cells in the z direction were condensed further to increase the aspect ratio. In the fifth mesh (M5) the average aspect ratio was about 15, while the number of cells per wave height and wave length were more than 40 and 110 respectively in M5 (Appendix A), and the accuracy of predictions reduced dramatically Figure 3-35.

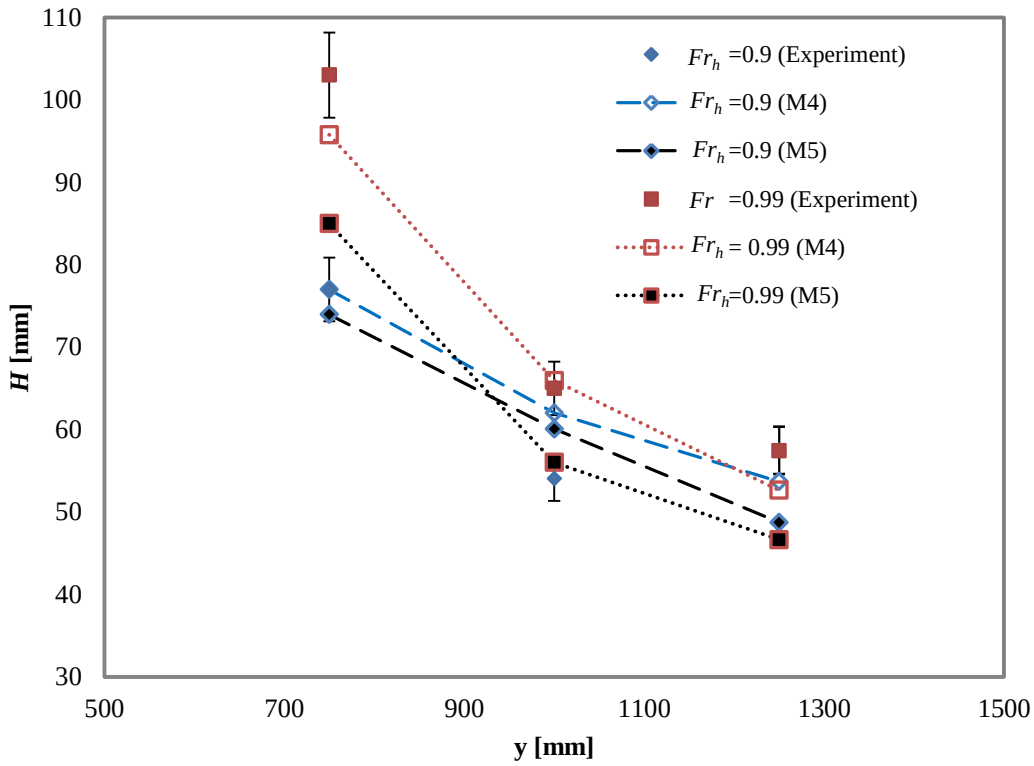

Figure 3-35: Comparison of wave height of numerical, with mesh domain M4, M5 and experimental results at varying lateral distances for different depth Froude numbers, the horizontal axes presents the distance from from centre-line

In short, the total number of cells in mesh domains M3, M4 and M5 were similar and the changes in accuracy resulted from changing the ratio and interval size between the cells. By comparing the results from the last three mesh domains, it can be concluded that the aspect ratio is a significantly more important parameter than the number of cells per wave length.

To reduce computation time, the number of cells must be reduced. In the next stage two new mesh domains were generated (M6 and M7). In M6 the size of cells in the x direction was the same as M2 at about 80 cells per wave length, and the number of cells per wave height was reduced to less than 10 at different lateral distances (Appendix A). Generally the wave height predicted by mesh domain M6 was higher than that predicted using M2 in the far field domain (Figure 3-36).

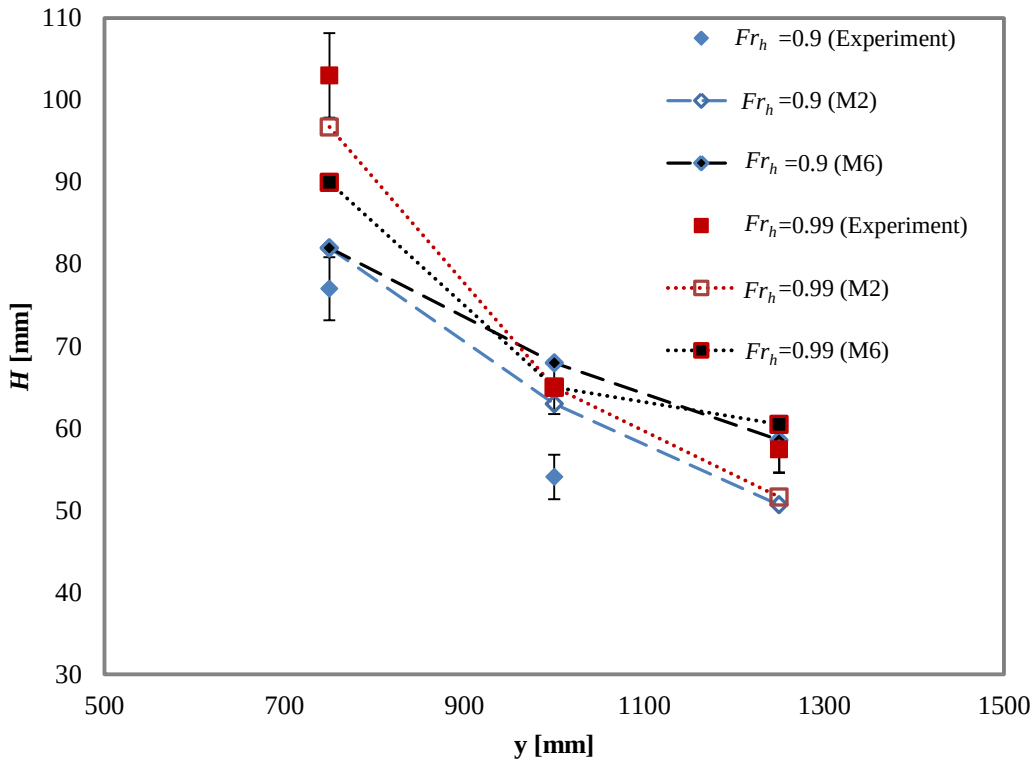

Figure 3-36: Wave height for varying depth Froude number for mesh domains M2, M6 experimental results at varying lateral distances for different depth Froude numbers, the horizontal axes presents the distance from from centre-line

In mesh domain M7, the number of cells in the x direction was the same as in mesh domain M3 and in the z direction was the same as in mesh domain M6. The average aspect ratio for this mesh domain was less than 3 (Appendix A). The wave height did not change significantly compared to M6. Figure 3-37 presents the results for M6 and M7.

In the next change, the number of cells in the x direction was reduced to about 50 cells per wave length (M8), while the number of cells in the Z direction was kept the same as M7. The aspect ratio increased to about 5 (Appendix A). The results for M8 are shown in Figure 3-38.This mesh was not able to predict the wave height accurately.

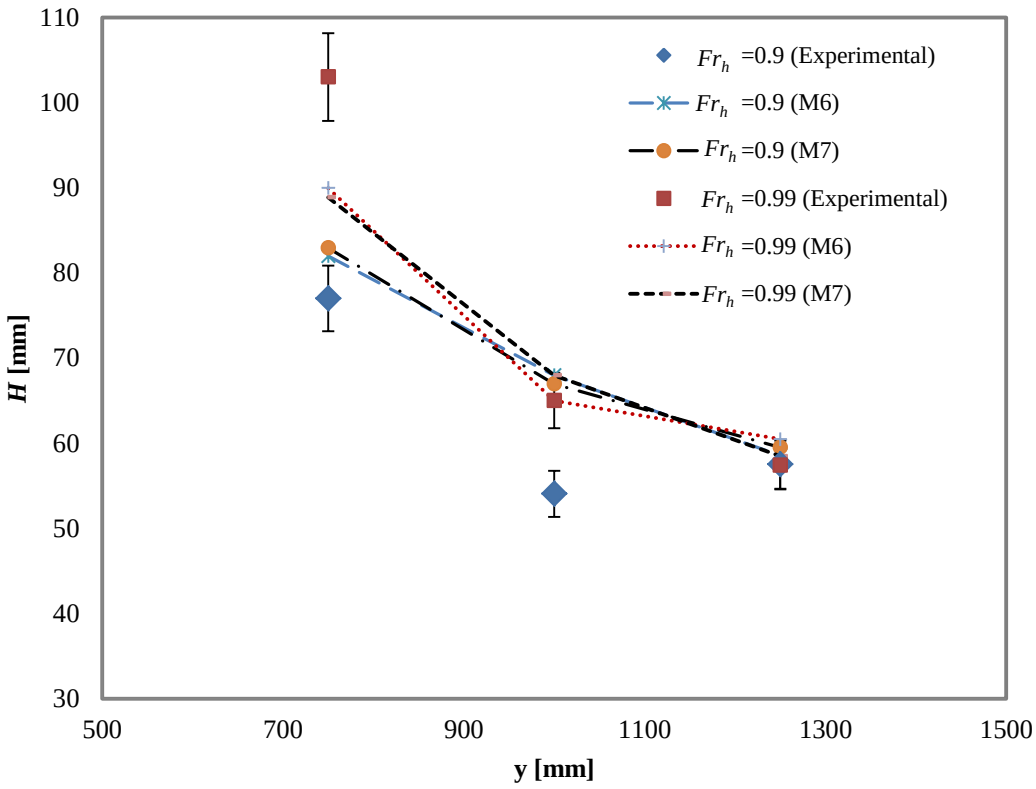

Figure 3-37: Wave height for varying depth Froude number with mesh domains M6 and M7 at varying lateral distances for different depth Froude numbers, the horizontal axes presents the distance from from centre-line

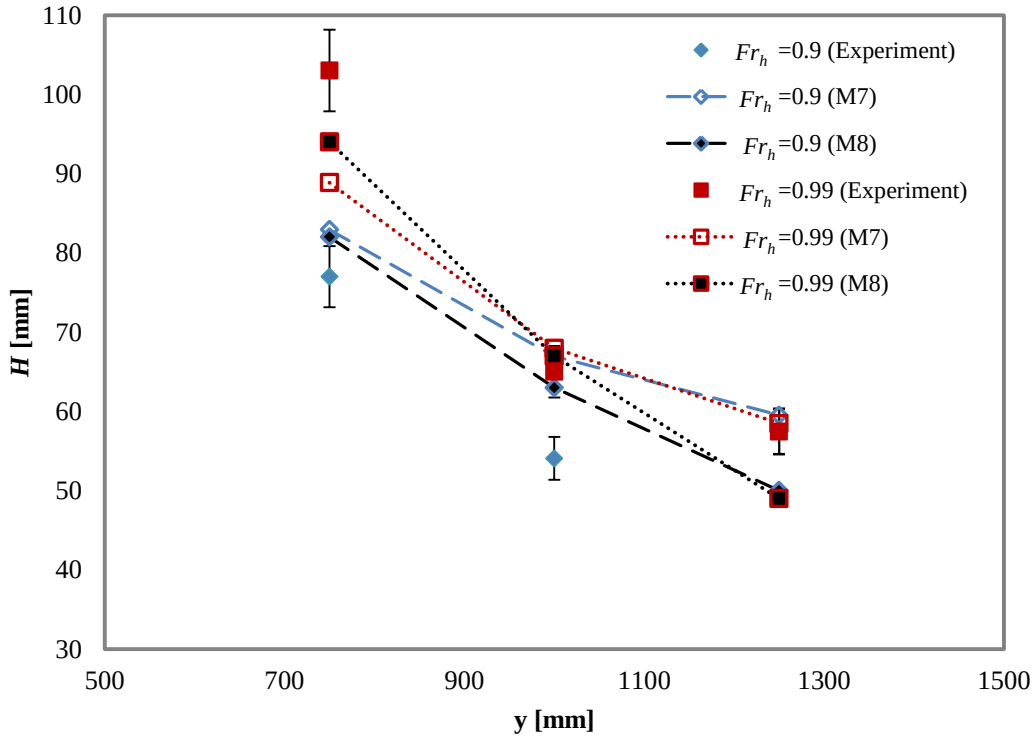

Figure 3-38: Wave height for varying depth Froude number with mesh domains M7, M8 and the experimental data at varying lateral distances for different depth Froude numbers, the horizontal axes presents the distance from from centre-line

It is possible to examine the number of cells per wave height by comparing the results for M3, M4, M5 and M7 (Figure 3-39 and Figure 3-40). These four mesh domains have the same number of cells in the x direction. It is clear that the predicted results using M7, with less than 10 cells per wave height for both depth Froude numbers, are better than results for M5, with more than 40 cells per wave height.

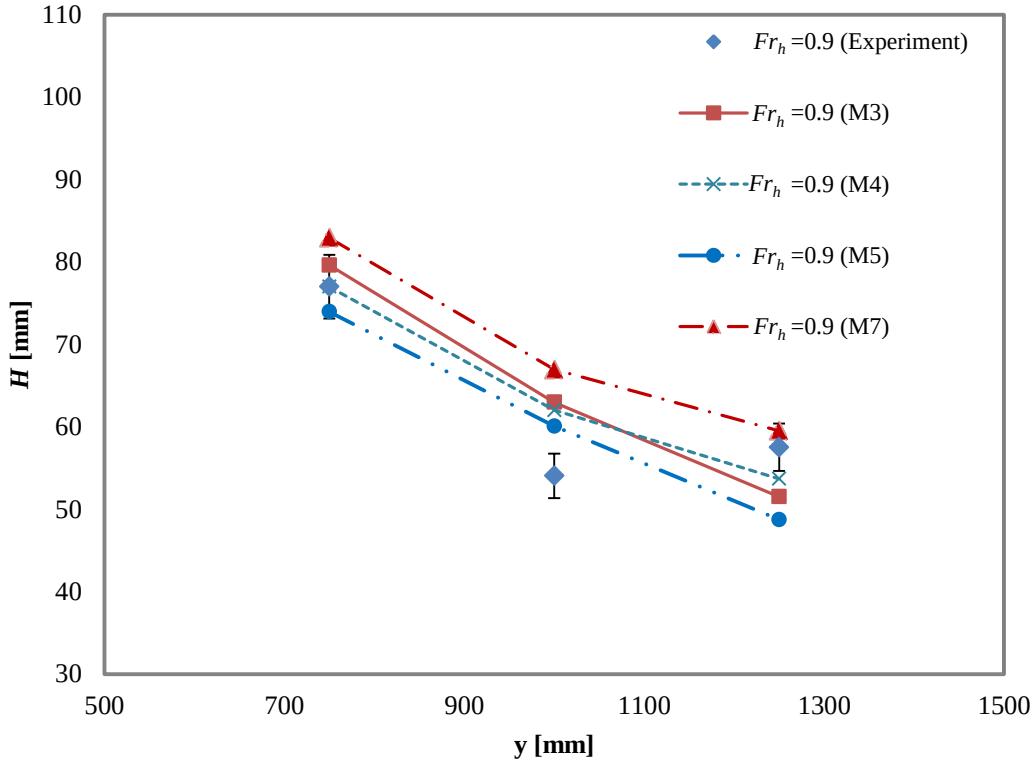

Figure 3-39: Wave height for depth Froude number 0.9 with mesh domains M3, M4, M5, M7 and the experimental data at varying lateral distances for different depth Froude numbers, the horizontal axes presents the distance from from centre-line

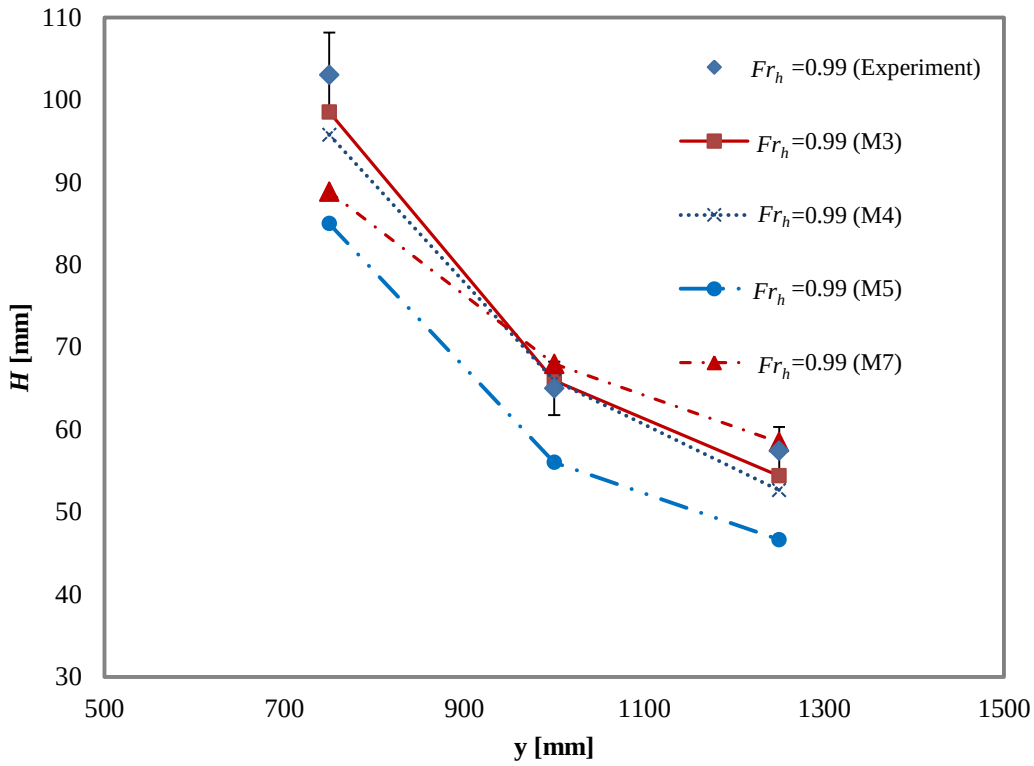

Figure 3-40: Wave height for depth Froude number 0.99 with mesh domains M3, M4, M5, M7 and the experimental data at varying lateral distances for different depth Froude numbers, the horizontal axes presents the distance from from centre-line

In conclusion, this study confirmed that mesh quality has a major effect on wave propagation prediction. According to numerical results and experimental data, the aspect ratio is a significantly more important parameter than the number of cells per wave length. An aspect ratio of about 7 is required to predict wave height. The results show that 10 cells per wave height are sufficient for wave height prediction and increasing this value does not mean that the predicted wave height will be improved. Therefore, it is possible to optimise the number of required cells (and reduce the simulation time) and capture accurate results, by considering these two numbers (aspect ratio about 7 and number of cells per wave height about 10)

In the next step, simulation by the wavedozer in shallow water (500mm water depth) was undertaken by using improved aspect ratio and the results were compared with previous simulation results (section3.4). Two different mesh domains were generated. The domain dimensions and boundary conditions were the same as those mentioned in section 3.3. The results of the new meshes are compared with previous results in Figure 3-41 (section 3.4).

Table 3-7: The Number of Cells in New Meshes

	Number of cells
New average mesh	6,883,620
New coarse mesh	872,560

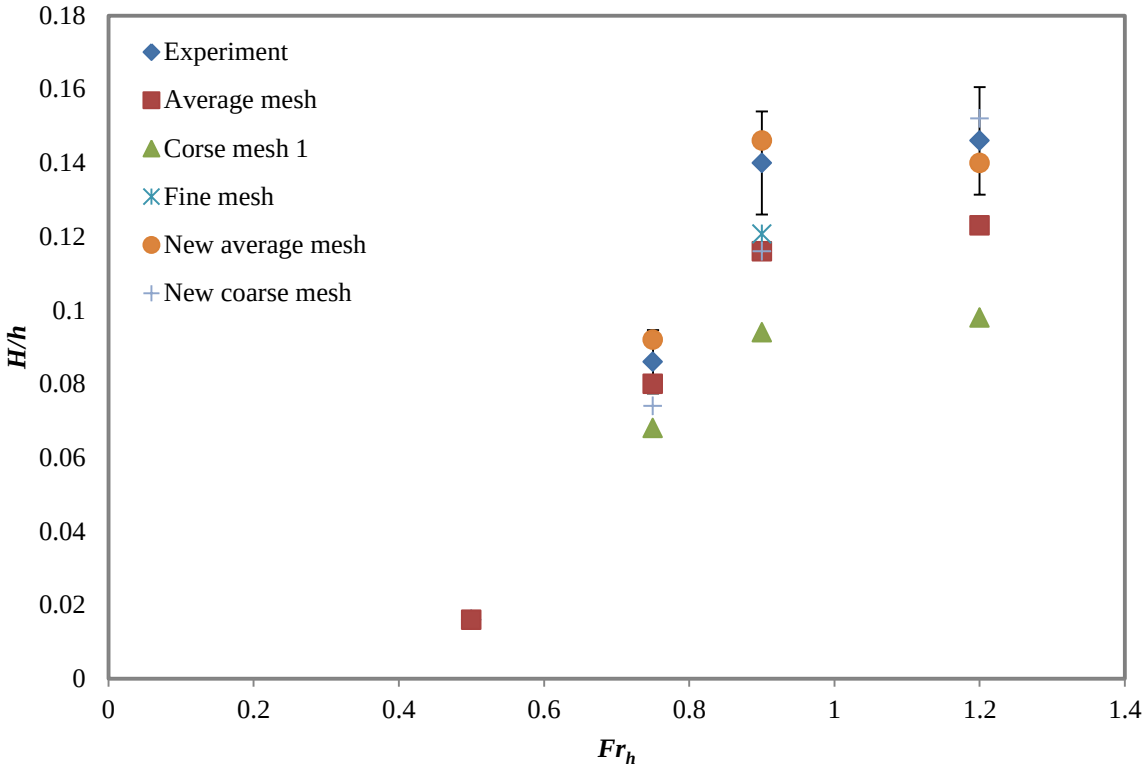

Figure 3-41: Wave height predicted by different mesh domains with different aspect ratio and number of cells at 750mm lateral distance, the horizontal axes presents the distance from from centre-line

The predicted wave heights with the new mesh domains were much more accurate than those obtained with the previous meshes. The prediction of wave height using the coarse mesh (873 000 cells) was more accurate than with the average mesh (>2.9 million cells). The fine mesh domain (>23 million cells) can predict the wave height just a little bit better than new coarse mesh, while the number of cells in the fine mesh domain was more than 26 times of the number of cells in new coarse mesh domain. In addition, the new average mesh domain was able to predict wave height in a range of speeds very accurate (better than the fine mesh domain), while the number of cells in new average mesh domain is one-third of the fine mesh domain. This represents a significant increase in computational efficiency, where efficiency is defined as the accuracy obtained per computational resource used.

3.6. Concluding remarks

This chapter considered the validation of numerical simulations. Some numerical simulations have been conducted and compared with the experimental data. To verify the ability of the numerical method to predict generated waves by a moving body, different pressure sources and configurations were modelled.

Firstly, two different pressure sources were modelled in shallow water condition. The numerical results agreed with the experimental results. Then, the effects of water depth were investigated. Comparison of the numerical and experimental results showed that the numerical method can be used to capture the effect of water depth on wave height.

In the next step, curved track simulations were conducted. The numerical results were in good agreement with experiments in the curved track. From these comparisons it was concluded that the numerical approach was able to predict the forces and wave parameters for the investigated depth Froude numbers.

Finally, an investigation was concluded into the grid independency and mesh quality effects on the numerical results. In order to improve the computational efficiency, different mesh domains were generated with varying mesh parameters. Comparison of the numerical predictions with the experimental data confirmed that mesh quality has a significant effect on wave height prediction. Based on the numerical results, an average aspect ratio of about 7 is required to predict wave height. In terms of the number of cells per wave height, the results show that 10 cells are sufficient to predict wave height and increasing this value does not mean that the predicted wave height will be improved. Initial simulations were repeated with new meshes which were generated according to these values. The results showed a great improvement in the accuracy of wave height prediction. It was concluded that cell parameters are much more significant than the number of cells in the computational domain.

4. Output parameters for judging pool design

This chapter deals with the output parameters that can be used to evaluate the pool design. The experimental investigation of parameters affecting wave formation was described in chapter 2, and it was shown that a numerical approach can predict wave propagation accurately and efficiently in chapter 3. Given this, further numerical investigations were conducted and the results are presented here. These simulations were concluded at full scale. Previous investigations showed that a curved track does not have a significant effect on wave height (2.2), and therefore these simulations were conducted in a straight track. Different channel shapes were modelled to investigate the wave breaking location, breaking intensity and peel angle. A wavedozer was used as the pressure source to generate the wave, and then by changing the channel shape and bathymetry, the aforementioned parameters were investigated.

4.1. Wave breaking location

A wavedozer was used as a pressure source, and Table 4-1 presents the wavedozer parameters. Firstly, a channel with the parameters shown in Figure 4-1 was modelled in different depth Froude numbers by changing velocity. For this simulation, 144.5m of channel length with a downstream domain of 84m was modelled. Approximately 17 million cells were used to mesh the domain based on mesh density studies conducted earlier as in Chapter 3. Figure 4-2 presents the wave height at different lateral distances for various depth Froude numbers. The no fill markers in Figure 4-2 show the start of wave breaking at different depth Froude numbers. It can be seen that for all Fr_h, the wave starts to break around 14.0m lateral distance except for $Fr_h = 0.8$. The wave breaking point at $Fr_h = 0.8$ is close to pressure source and wave at $Fr_h = 0.9$ has two breaking points.

Table 4-1: Full Scale Wavedozer Characteristics

Angle of attack (deg)	7
Beam (m)	4.0
Draught (m)	0.75
Water depth (m)	3.75

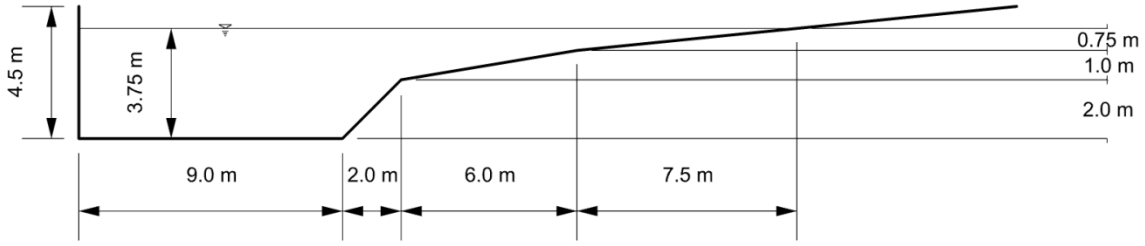

Figure 4-1: Channel 1

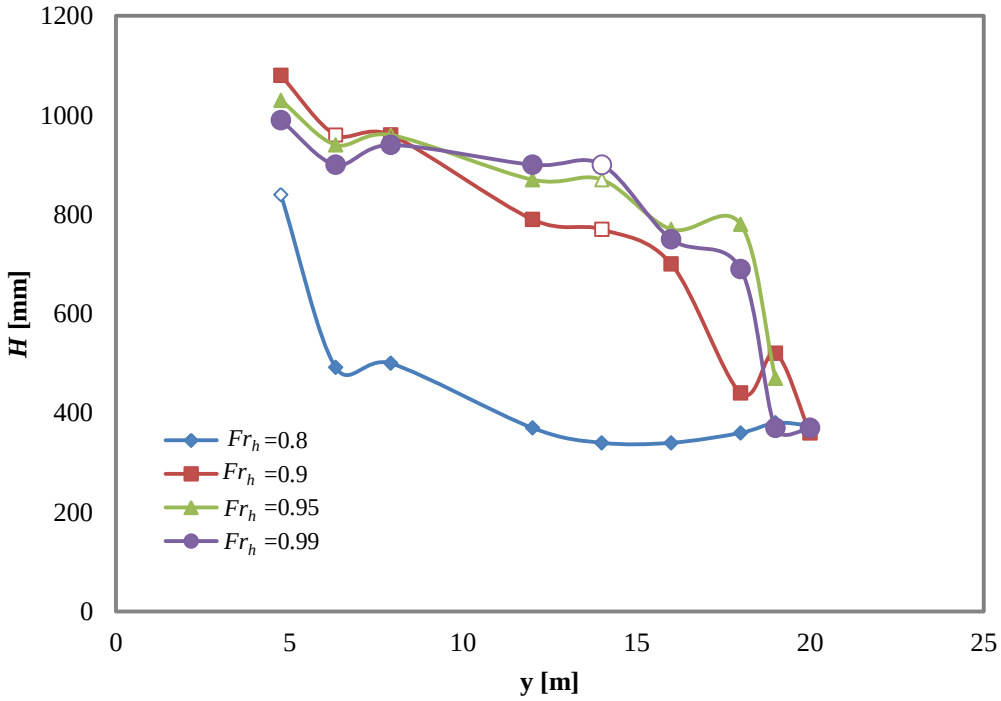

Figure 4-2: Wave height at different lateral distances for various depth Froude numbers

Since nearly all of the waves break at around 14.0m lateral distance, it was thought to be possible to move the breaking point by changing the bathymetry after 13.5m lateral distance (0.5m before the breaking point) and making it plateau: Figure 4-3. According to Mead et al. horizontal plane has very little effect on the waves[4]. Moving the breaking point further away from the wavedozer could result in an increased wave wall length. The length of a smooth, unbroken wave crest was defined as the usable 'wall length', increasing this value would significantly increase the desirability for surfing. This configuration was simulated at two Fr_h, 0.8 and 0.99. Figure 4-4 and Figure 4-5 compare the results for the two channel configurations: Channel 1 and Channel 2. The breaking point for Channel 2 configuration occurred at the same position as in Channel 1 for both the simulated values of Fr_h. It was concluded that changing the bathymetry after 13.5m lateral distance does not have any effect on the breaking point.

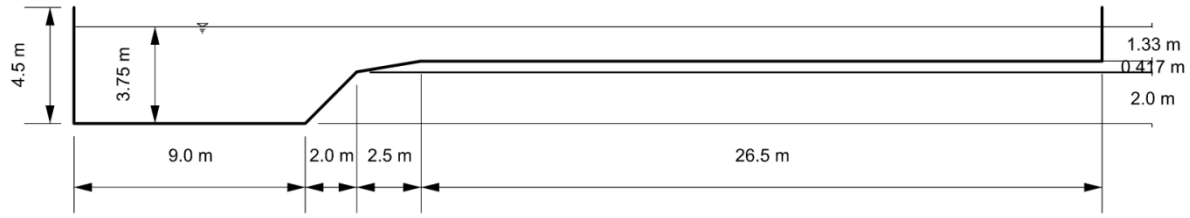

Figure 4-3: Channel 2

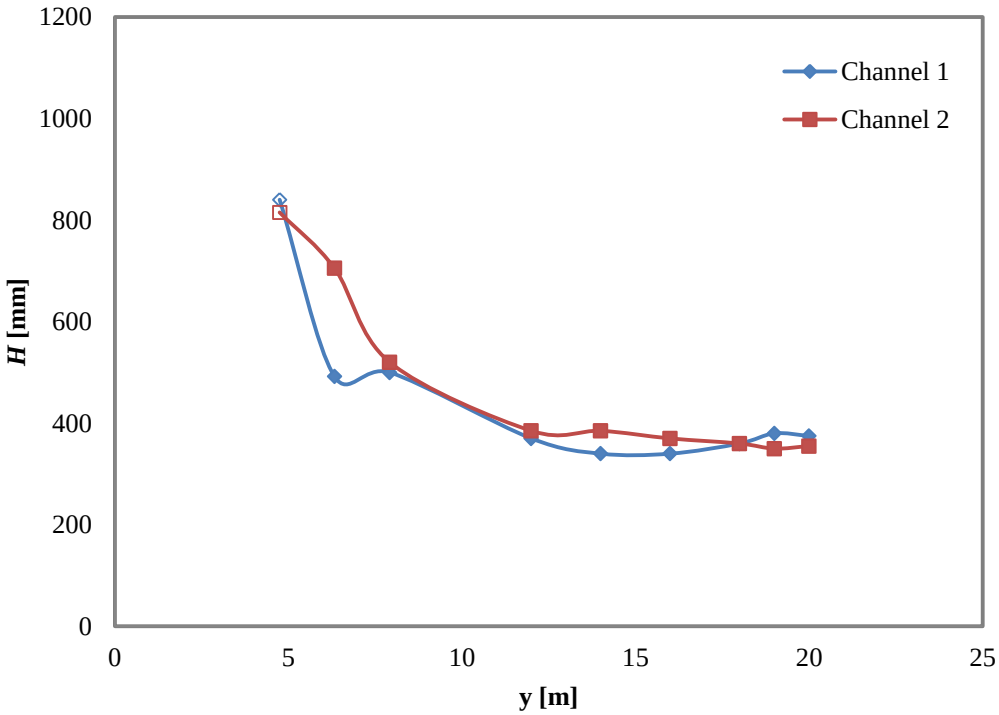

Figure 4-4: Comparison the results for two different channel configurations; channel 1 and channel 2, at Fr_h = 0.8

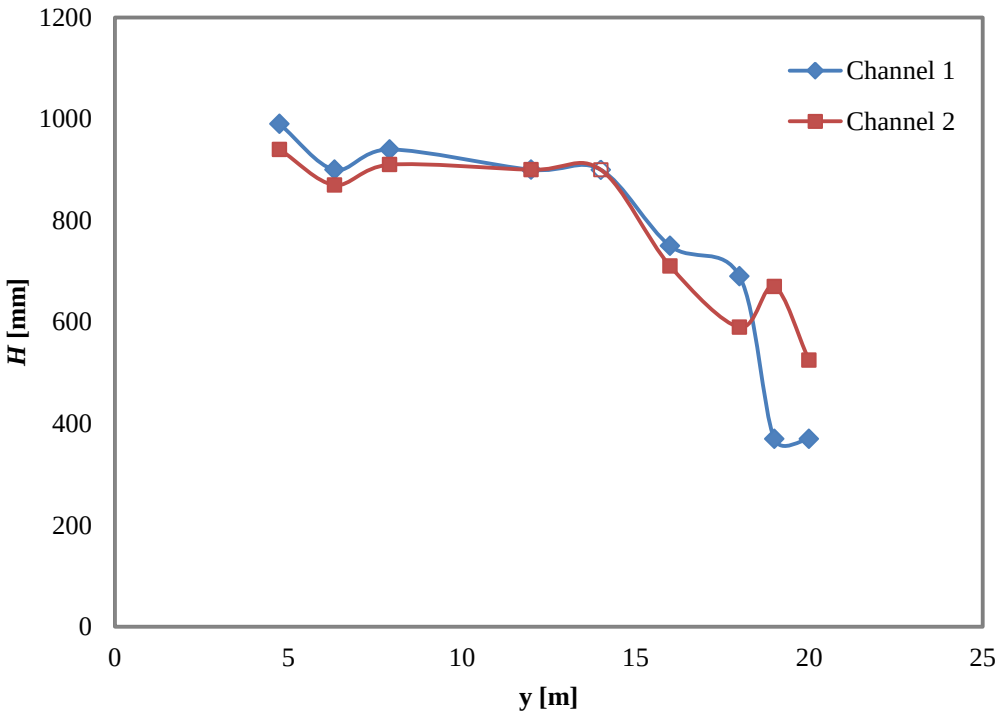

Figure 4-5: Comparison the results for two different channel configurations; channel 1 and channel 2, at Fr_h = 0.99

Since changing the bathymetry for that area did not improve the results in Channel 2 compared to Channel 1, it was though that there is a lag between changing the bathymetry and its effect on the wave parameters. It was assumed that the wave completely developed prior to 13.5m lateral distance and changing the bathymetry only half a meter before breaking point (14.0m) does not have any influence. Therefore, it was decided to move this bathymetry change point closer to the pressure source, i.e. 11.0 m from the wall in Channel 3: Figure 4-6. This configuration was simulated at $\mathrm{Fr_h} = 0.99$. Figure 4-7 presents the results for each of the three channel configurations at $Fr_h = 0.99$. It is clear that changing the bathymetry did not have any effect on the breaking point nor on the wave height before breaking. In addition, it can be seen that the wave wall lengths are the same for all the three channel configurations. A wide, steep wall is required to provide surfers with sufficient vertical and lateral space to perform standard manoeuvres. The wave wall length for these three channels is approximately 6m, which is from 7.9m to 14.0m lateral distance.

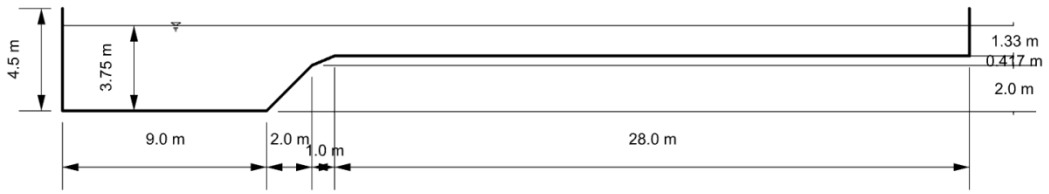

Figure 4-6: Channel 3

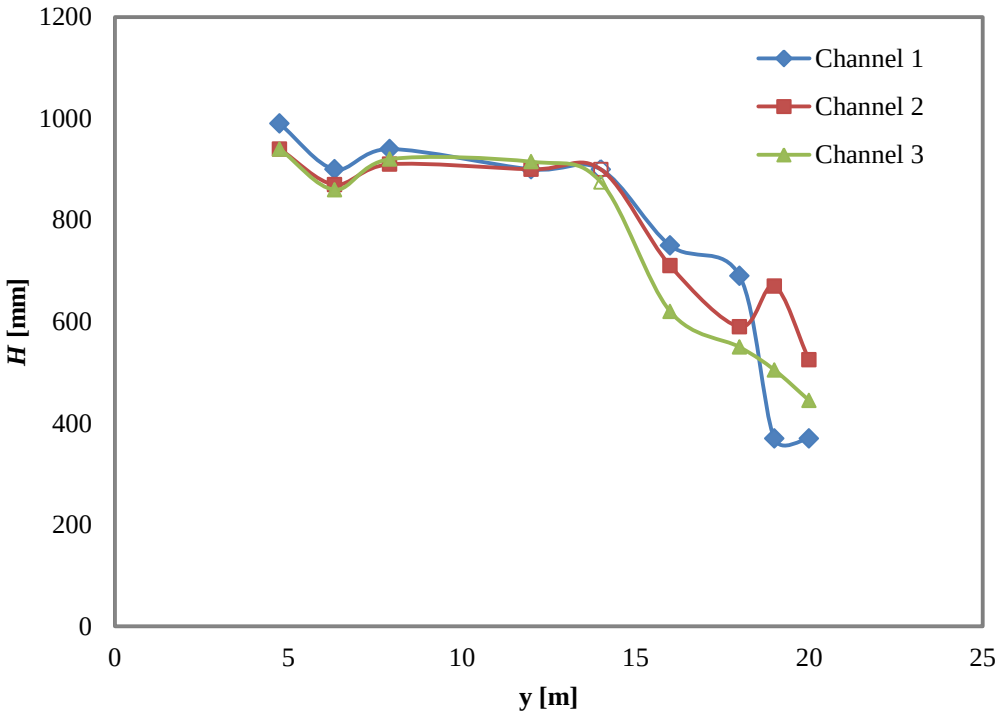

Figure 4-7: Simulation results of wave height for different lateral distances for three channel configurations at Fr_h=0.99.

In the next configuration, the slope of the bathymetry was kept identical to Channel 1, but the width of the deep part of the channel was increased to 12m (Figure 4-8). Comparing the results of Channel 4 with previous results showed that increasing the width of the deep part of the channel causes the wave breaking point to move further (closer to the beach): Figure 4-9. Figure 4-10 to Figure 4-13 show the breaking point locations for different Fr_h.

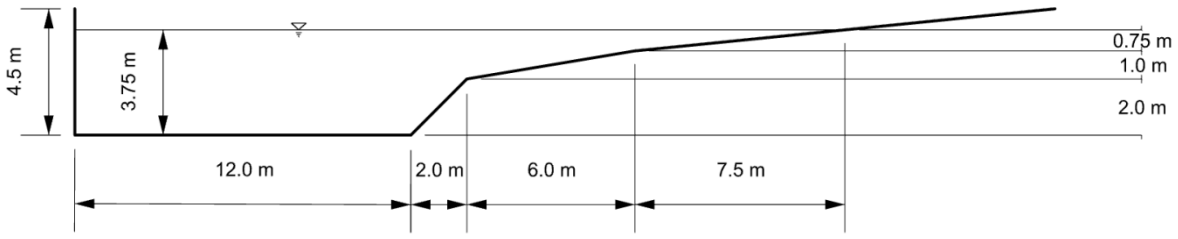

Figure 4-8: Channel 4

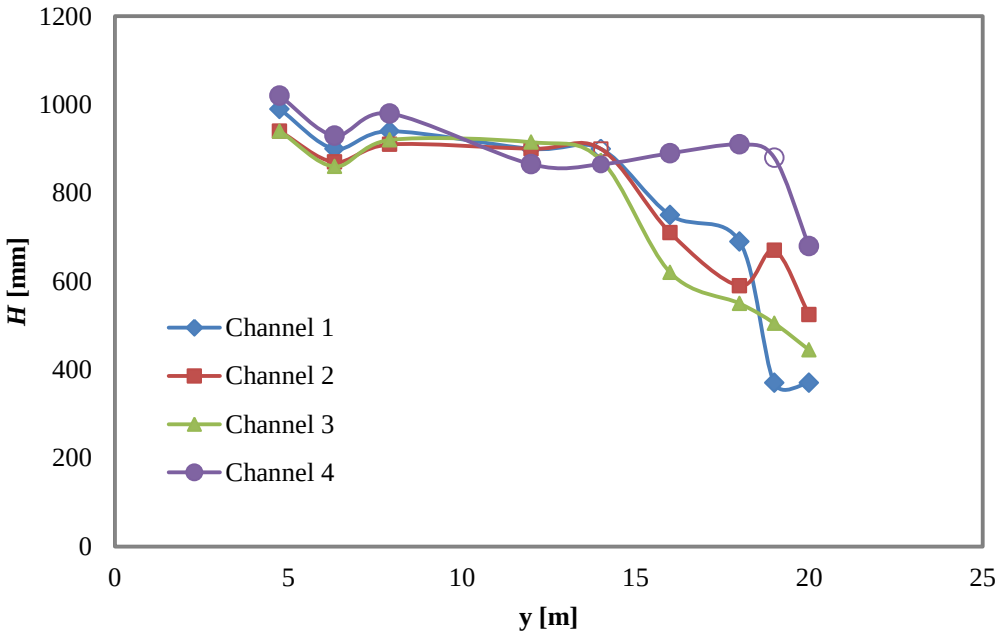

Figure 4-9: Simulation results of wave height for different lateral distances for four channel configurations at Fr_h =0.99

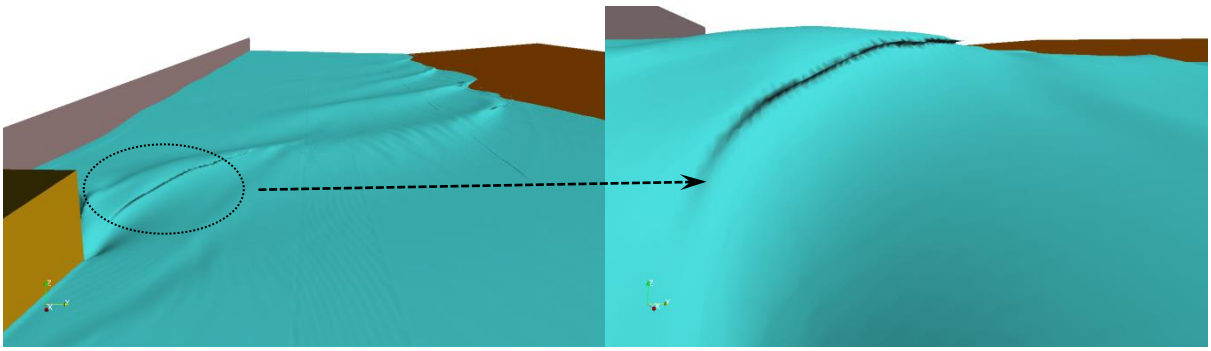

Figure 4-10: Free surface elevation for Channel 1 at Fr_h=0.8 at the same time instant but different views

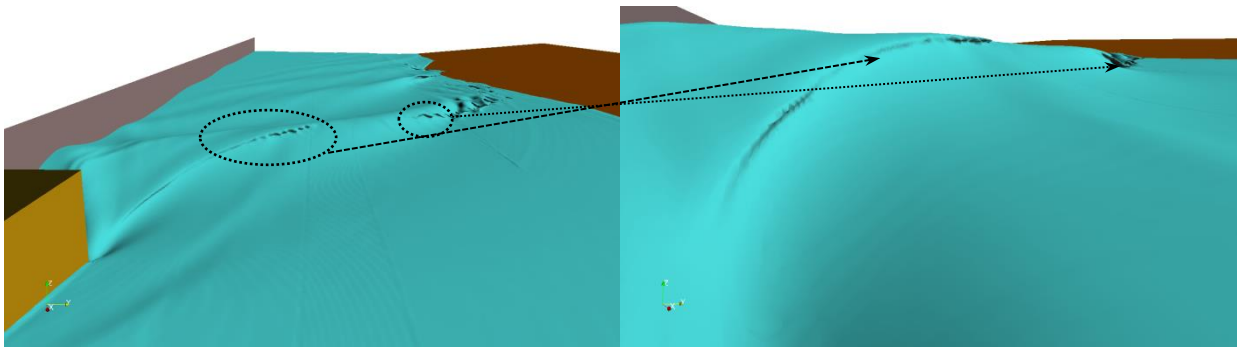

Figure 4-11: Free surface elevation for Channel 1 at Fr_h=0.9 at the same time instant but different views

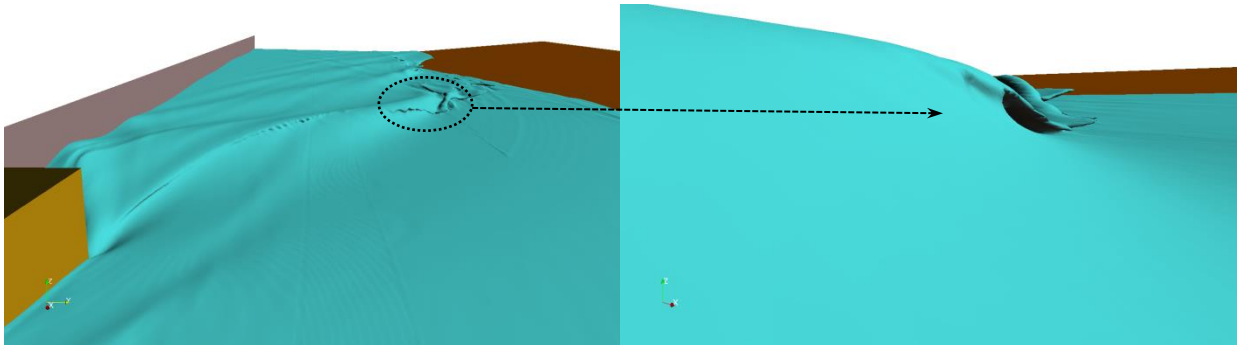

Figure 4-12: Free surface elevation for Channel 1 at Fr_h=0.95 at the same time instant but different views

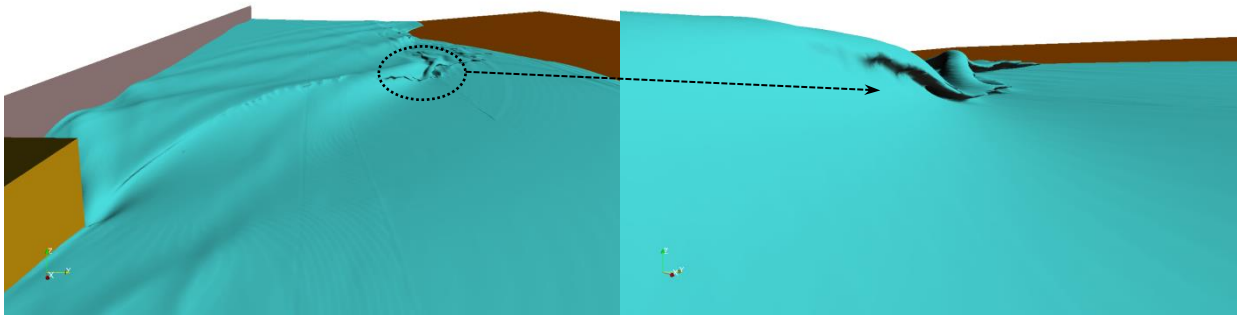

Figure 4-13: Free surface elevation for Channel 1 at Fr_h=0.999 at the same time instant but different views

By comparing the results for all channel configurations, two important conclusions can be made. Firstly, in terms of construction costs and commercial considerations, Channel 1 is the most successful, because it is possible to generate a wave with the same height as the other channels while this channel is the narrowest, thus needing the least materials and would have the lowest construction cost. Secondly, in terms of surfing, since the breaking point in Channel 4 happens further from pressure source than other channels, the surfable wave width is larger than other waves and this will enhance surfers' manoeuvrability and the ride quality.

4.2. Wave breaking intensity

It is well known that a wave will break in different shapes depending on the beach slope, wave height and the wavelength perpendicular to the beach slope. The types of breaker shapes were defined by Galvin [63] and are illustrated in Figure 4-14:

a. **Spilling waves** occur if the wave crest becomes unstable and flows down the front face of the wave producing a foamy water surface. Surfers call this a 'soft' or 'weak' wave.
b. **Plunging waves** occur if the crest curls over the front face and falls into the base of the wave; surfers call this a 'barrelling' or 'tubing' wave.

c. **Collapsing waves** occur if the crest remains unbroken and the front face of the wave steepens and then falls, producing an irregular turbulent water surface. Surfers often encounter this at reef breaks when the tide is too low and the reef is not submerged enough to produce surfable waves.

d. **Surging waves** occur if the crest remains unbroken and the front face of the wave advances up the beach with minor breaking. This type of wave is unsurfable.

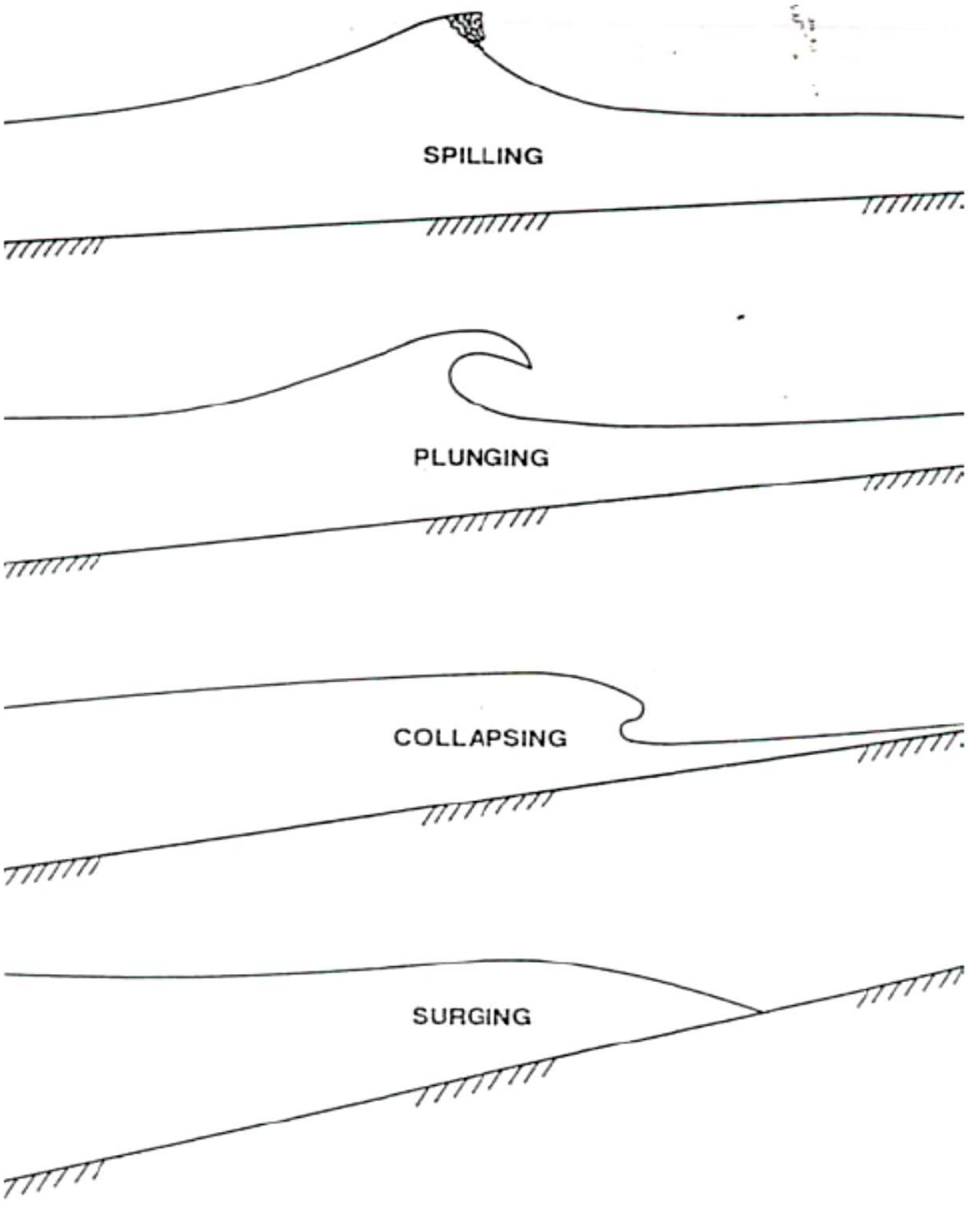

Figure 4-14: Breaker type classification [25]

Of the four breaker types, spilling or plunging waves are required for surfing, with plunging wave being better [64]. Collapsing and surging breakers occur at the water's edge or where very steep seabed gradients come close to the water's surface. Such waves cannot be surfed because they lack a steep smooth face and/or they break at the water's edge. Indeed, surfing requires a steep unbroken

wave face to create board speed for performing manoeuvres. In particular, good surfing waves break in a ‘peeling’ manner, where the breaking region of the wave translates laterally across the wave crest [65]. It is the region close to the breaking crest of the peeling wave, sometimes known as the ‘pocket’ (Figure 4-15) has the steepest face and therefore offers the most speed for surfing. While both spilling and plunging waves are utilised for surfing, the face of a spilling wave is relatively gently sloping and therefore provides low board speed in comparison to the steeper-faced plunging wave. As a consequence, spilling waves are not preferred for surfing, except by beginners in the early stages of learning. Of the four categories of breakers (spilling, plunging, collapsing and surging), it is plunging waves that are highly sought by surfers. The steep face of a plunging wave provides the high speed needed to perform manoeuvres, not unlike that required for skiing. In addition, the open vortex of the plunging wave provides the opportunity to perform surfing’s ultimate manoeuvre, the tube ride, where the surfer rides under the breaking jet of the wave: Figure 4-16.

Figure 4-15: The pocket, the steep wave face close to the peeling crest of the wave offers the most speed for surfing [66]

Figure 4-16: The tube ride, a surfer riding under the jet of a breaking wave [67]

Several factors affect the category that waves fall into when breaking (spilling, plunging, collapsing or surging), such as wave height and period, wind strength and direction. However, the bathymetry has most influence on the shape of breaking waves. The transition of breaker shape, from spilling through to surging, is mainly a result of increasing the seabed gradient. On low gradient seabeds, waves break with a spilling form. As seabed gradients increase, breaker form tends towards plunging, and finally to collapsing or surging waves on very steep gradients.

There are some existing methods that can be used to describe wave breaking characteristics such as Irribarren number [68]. Irribarren number is defined as:

$$\xi = \frac{\tan(s)}{\sqrt{H_{beach}/\lambda_s}}$$

where s is the beach slope, H_{beach} is wave height at the start of the beach and λ_s is the wavelength perpendicular to the beach slope. The range of values for ξ for the different wave breaker types, is detailed in Table 4-2. However, while these methods give an indication of breaker intensity, studies of surfing wave shape have found that they do not accurately differentiate the transition between breaker categories [25].

Table 4-2: Breaker Type and Irribarren Number ξ [29]

Breaker type	**Irribarren number** ξ
Spilling	$\xi < 0.4$
Plunging	$0.4 \leq \xi \leq 2.0$
Surging / collapsing	$\xi > 2.0$

The cubic curve method is a method for predicting the shape of a plunging surfing wave [30] based on vortex length (l), vortex width (w), vortex breaking angle (θ) and wave height (Figure 4-17). The 'vortex ratio' (tube length to width: Figure 4-17) is a measure of the 'roundness' of the tube. As the ratio of vortex length to width approaches 1, the tube shape becomes more circular and breaking is more intense. Table 4-3 presents the surfing wave breaking classification based on vortex ratio.

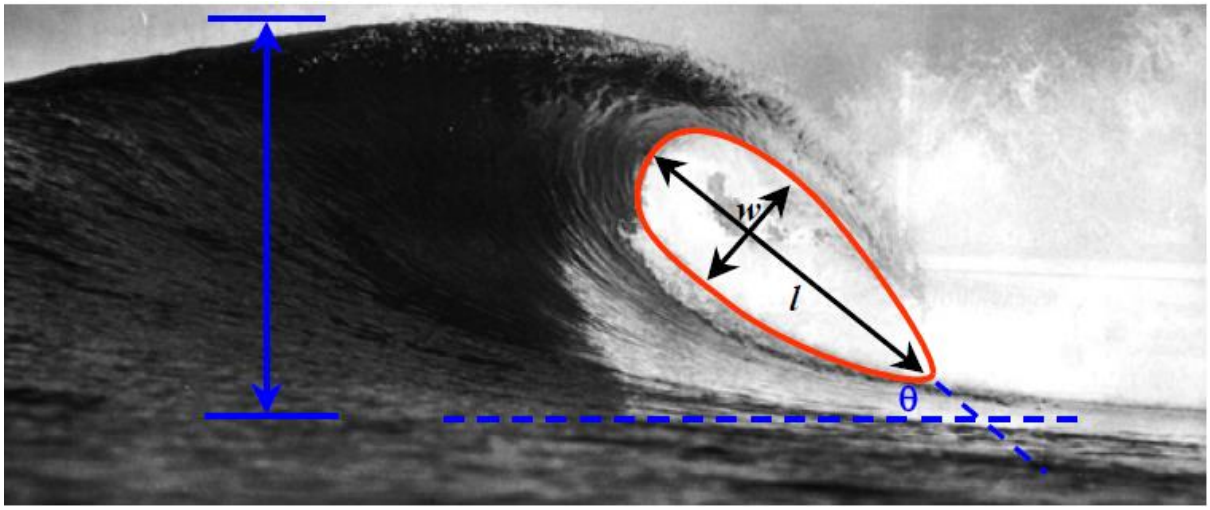

Figure 4-17: Curve fitting method [30]

Table 4-3: Classification Schedule of Surfing Wave Breaking Intensity [4]

Intensity	Extreme	Very High	High	Medium/high	Medium
Vortex Ratio	1.6-1.9	1.91-2.2	2.21-2.5	2.51-2.8	2.81-3.1
Descriptive Terms	Square, spitting	Very hollow	Pitching, hollow.	Some tube sections	Steep faced, but rarely tubing
Example Break	Pipeline, Shark Island	Backdoor, Padang Padang	Kirra Point, Off-The-Wall	Bells Beach, Bingin	Manu Bay, Whangamata
Example Break Wave Profile		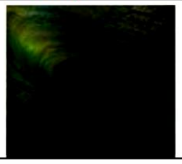			

Due to the following reasons, the Irribarren number cannot be used to predict wave breaking intensity. Simulation results for Channel 2 and Channel 3 indicate that it is possible to have the breaking point where the beach slope is zero, while according to definition, the Irribarren number would be zero when the bathymetry is flat (tan(s) is equal to zero). Therefore the breaking type is spilling. In addition, the Irribarren number was defined for waves with crests perpendicular to the beach, while

the waves generated by moving pressure sources have an angle relative to the beach. Therefore, it is proposed that it is inappropriate to use the Irribarren number to quantify the wave breaking intensity in this study.

Since all the channels studied were able to generate plunging breaking waves, the cubic curved method was used to classify wave breaking intensity. To identify the vortex ratio for different channel shapes, the numerical results were postprocessed by generating a plane at the distance where the wave plunged. Figure 4-18 to Figure 4-21 present the plunging shape of the wave for different channels at $Fr_h = 0.99$ for different lateral distances and Table 4-4 shows the measured vortex ratio for different channels. It is clear that the breaking shapes for the different channels are different. As a general conclusion, the beach slope shape has an effect on the breaking intensity but no significant effect on the breaking point. Channel 1 has the lowest vortex ratio and Channel 4 has the highest. It means Channel 1 has highest intensity and Channel 4 has lowest.

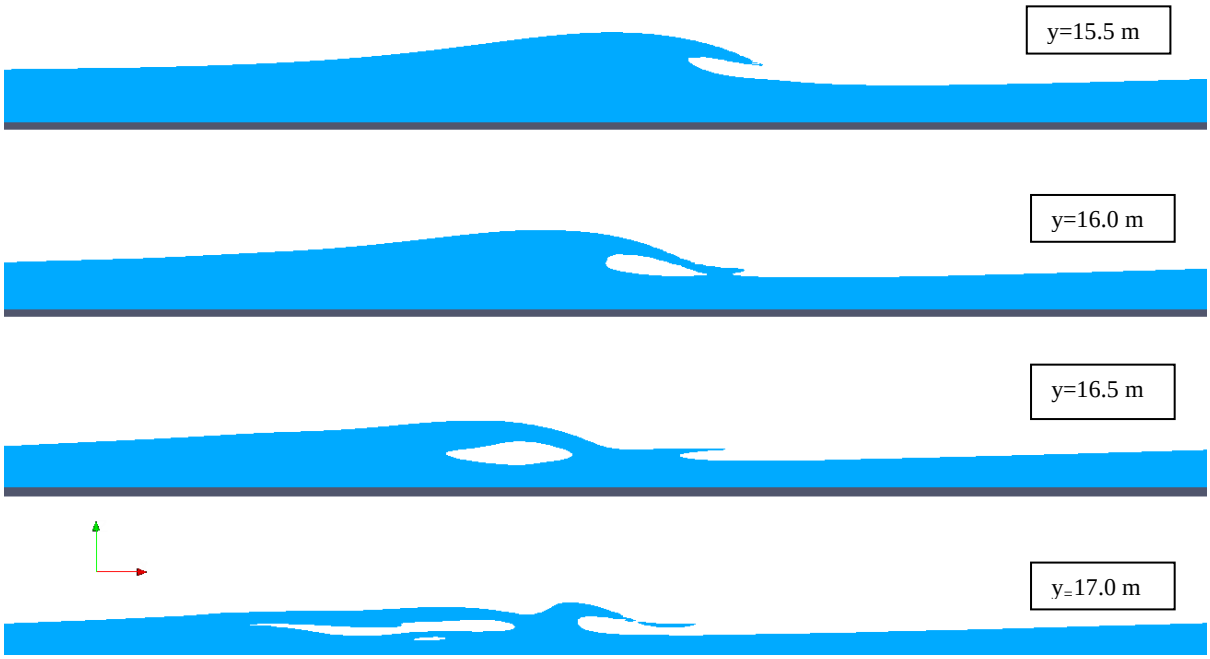

Figure 4-18: Plunging shape of the wave for channel 1 at Fr_h=0.99 at different lateral distances

Figure 4-19: Plunging shape of the wave for channel 2 at Fr_h=0.99 at different lateral distances

Figure 4-20: Plunging shape of the wave for channel 3 at Fr_h=0.99 at different lateral distances

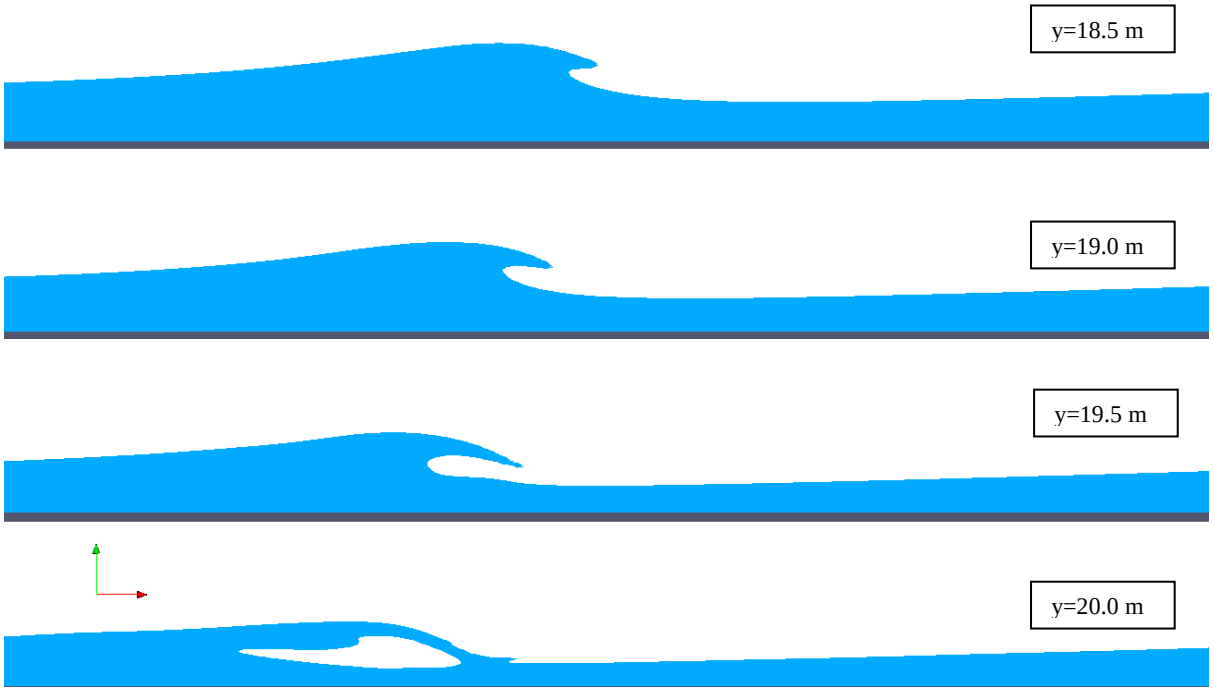

Figure 4-21: Plunging shape of the wave for channel 4 at Fr_h=0.99 at different lateral distances

Table 4-4: Vortex Ratio for Different Channel at Fr_h=0.99

	Vortex ratio
Channel 1	3.8
Channel 2	5
Channel 3	4.2
Channel 4	5.5

4.3. Peel angle

Peel angle is a term used to describe the speed that a surfer needs to travel successfully across the face of a wave [25]. The peel angle is defined as the angle between the trail of the broken white water and the crest of the unbroken part of the wave as it propagates shoreward (Figure 4-22). Peel angles range between 0° and 90°, with small peel angles resulting in fast surfing waves and large angles in slow surfing waves.

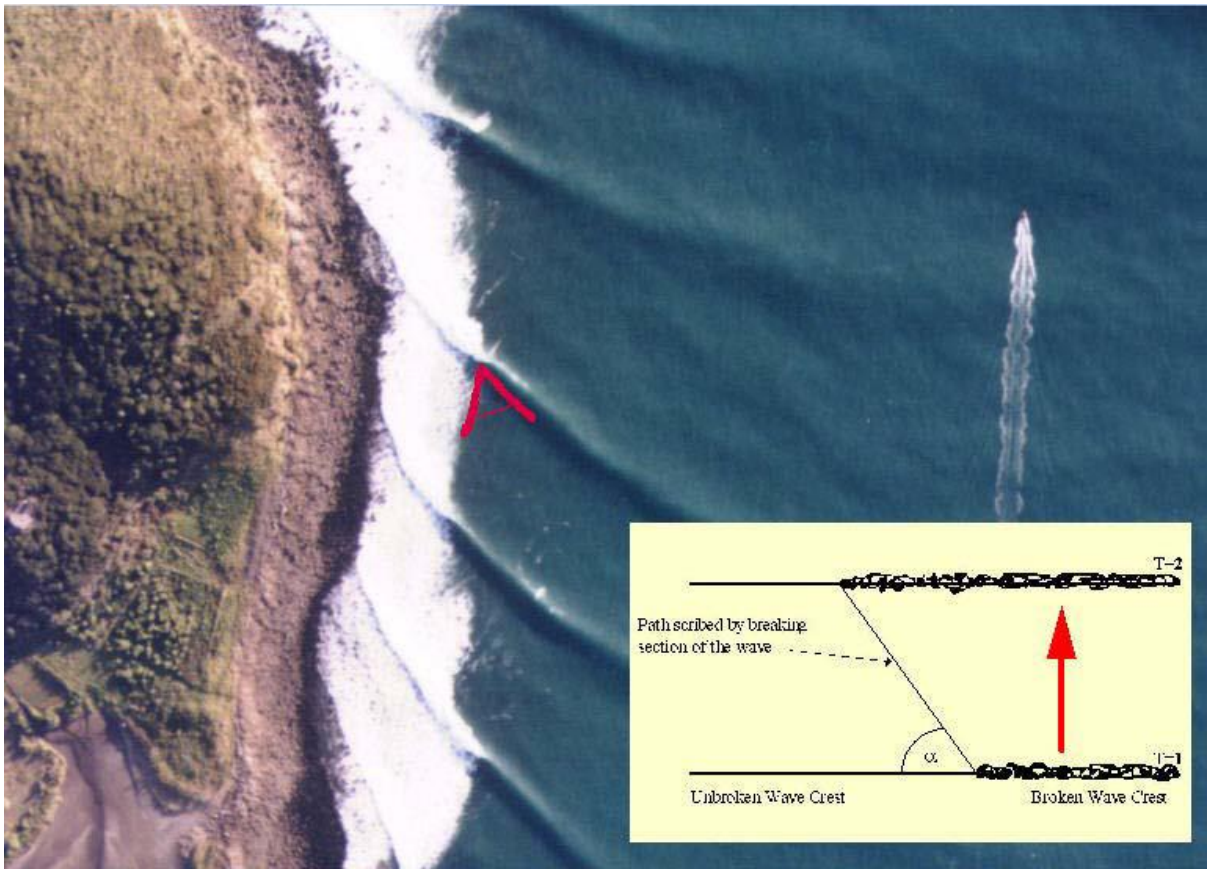

Figure 4-22: Schematic diagram of wave peel angle, α. [25]

The first comprehensive investigations into peel angles were undertaken by James Kimo Walker [26]at the University of Hawaii in the early 1970s. Walker classified a scheme that relates peel angle and wave height for three levels: beginner, intermediate and expert (Figure 4-23).

Later, Hutt undertook detailed investigations into wave peel angle at Raglan Point in New Zealand. He created a new surfing skill classification scheme using peel angles and wave heights [28] which defined 10 skill levels, from absolute beginner (1) to world's best surfers (10), and restricted wave heights to a maximum of 4m: Figure 4-24.

According to simulation results for different channel shapes (Figure 4-2 and Figure 4-9), the average peel angle was calculated. It is possible to classify the surfing skill for all channels by considering the wave height, the peel angle and Hutt diagram (Figure 4-24). Table 4-5 and Table 4-6 show the average peel angles and surfing skills for different Fr_h and different channel shapes. According to the results, the best way to change the required skill level for surfing is to change the pressure source speed and changing the channel shape does not have significant effect on required skill level for surfing.

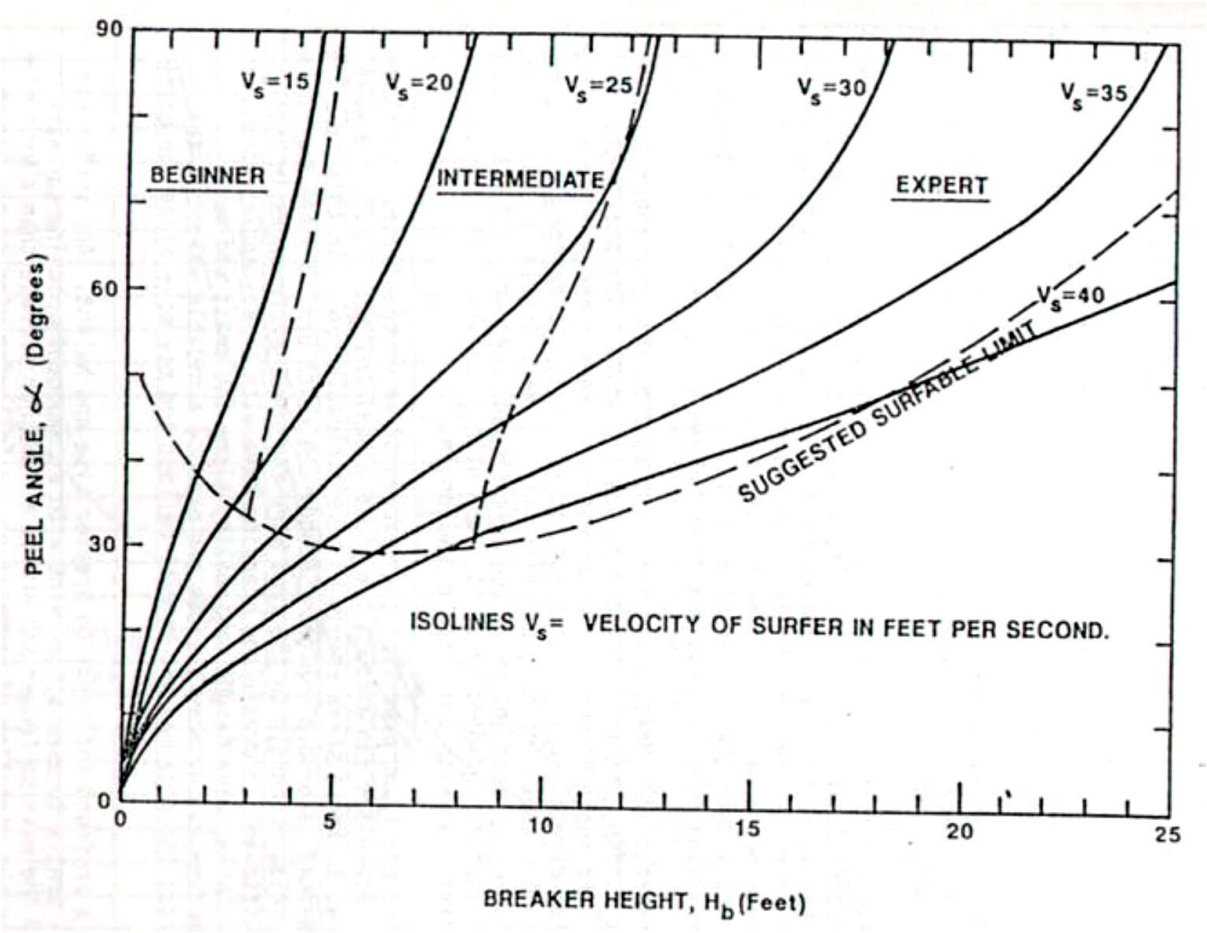

Figure 4-23: Classification of surfing skill by peel angle and wave height [25]

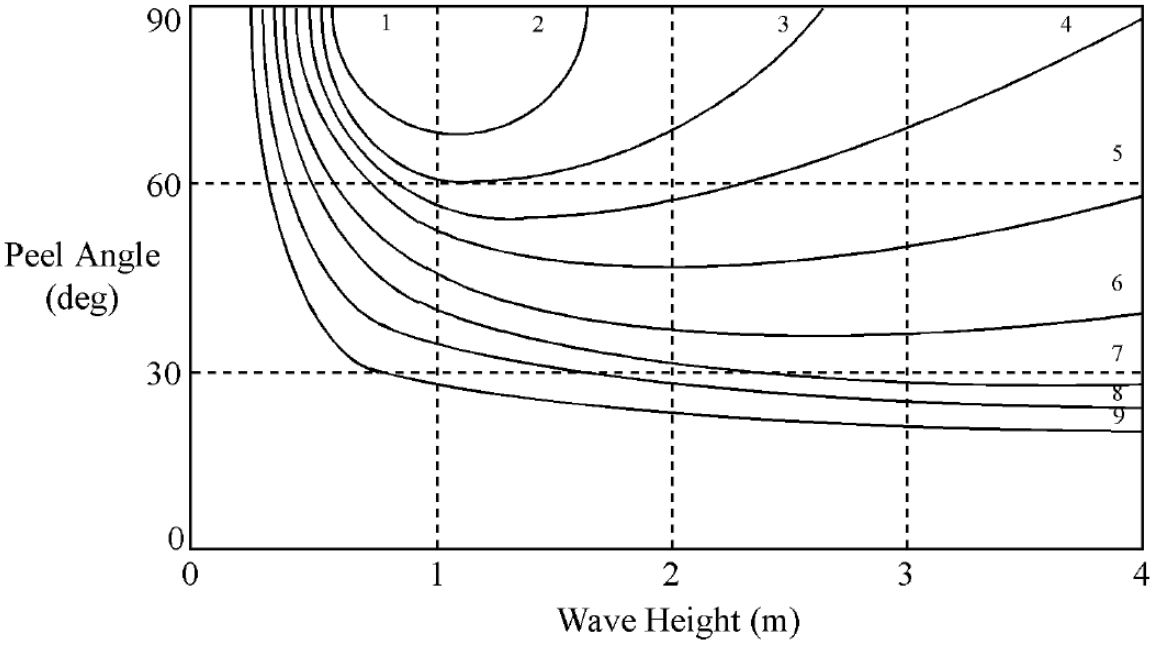

Figure 4-24: Classification of surfing skill as functions of peel angle and wave height [28]. The numbers defined 10 skill levels, from absolute beginner (1) to world's best surfers (10)

Table 4-5: Average Peel Angle for Channel 1 for Different Fr_h

Fr_h	Average peel angle (deg)	Average wave height (mm)	Surfing skill level
0.8	63	395	9
0.9	66	870	4
0.95	63	923	4
0.99	52	913	6

Table 4-6: Average Peel Angle for Different Channels at Fr_h=0.99

	Average peel angle (deg)	Average wave height (mm)	Surfing skill level
Channel 1	52	913	6
Channel 2	52	903	6
Channel 3	52	903	6
Channel 4	54	898	7

4.1. Wave wall length

Wave wall length is defined as the length of wave crest with a constant height (see Figure 4-25). Wave wall length is as important, if not more important, than wave height [10]. A long steep wall is required to provide surfers sufficient vertical and lateral space to perform different manoeuvres. The surfable wave wall length for different Fr_h and different channels were measured. Table 4-7 presents the surfable length for Channel 1 at different Fr_h. The surfable length at $Fr_h = 0.99$ for Channels 1 to 3 is between 7.9 to 14.0m lateral distance and for Channel 4 it is between 7.9 and 19.0m (Table 4-8). Therefore Channel 4 generates waves with the longest wave wall. The results show that channel shape can have a significant effect on the wave wall length.

Figure 4-25: Wave wall length definition[10]

Table 4-7: Surfable Wave Wall Length for Channel 1 at Different Fr_h

Fr_h	
0.8	12.1 m (Between 7.9 m to 20.0 m lateral distance)
0.9	7.1 m (Between 7.9 m to 15.0 m lateral distance)
0.95	6.1 m (Between 7.9 m to 14.0 m lateral distance)
0.99	6.1 m (Between 7.9 m to 14.0 m lateral distance)

Table 4-8: Surfable Wave Wall Length for Different Channels at Fr_h =0.99

Channel 1	6.1 m (Between 7.9 m to 14.0 m lateral distance)
Channel 2	6.1 m (Between 7.9 m to 14.0 m lateral distance)
Channel 3	6.1 m (Between 7.9 m to 14.0 m lateral distance)
Channel 4	11.1 m (Between 7.9 m to 19.0 m lateral distance)

4.2. Scale effects

It should be possible to build different size of wave pools, based on the clients' requests. Therefore it is necessary to find the scale factor effects on the wave heights, propagations and required power. To study the effect of scaling on the wave parameters and forces, the channel 4 and pressure source dimensions doubled and simulations were conducted at different Fr_h. The waves and forces results for two different scales were compared. Figure 4-26 presents the wave heights at different Fr_h for two different scaled channels.

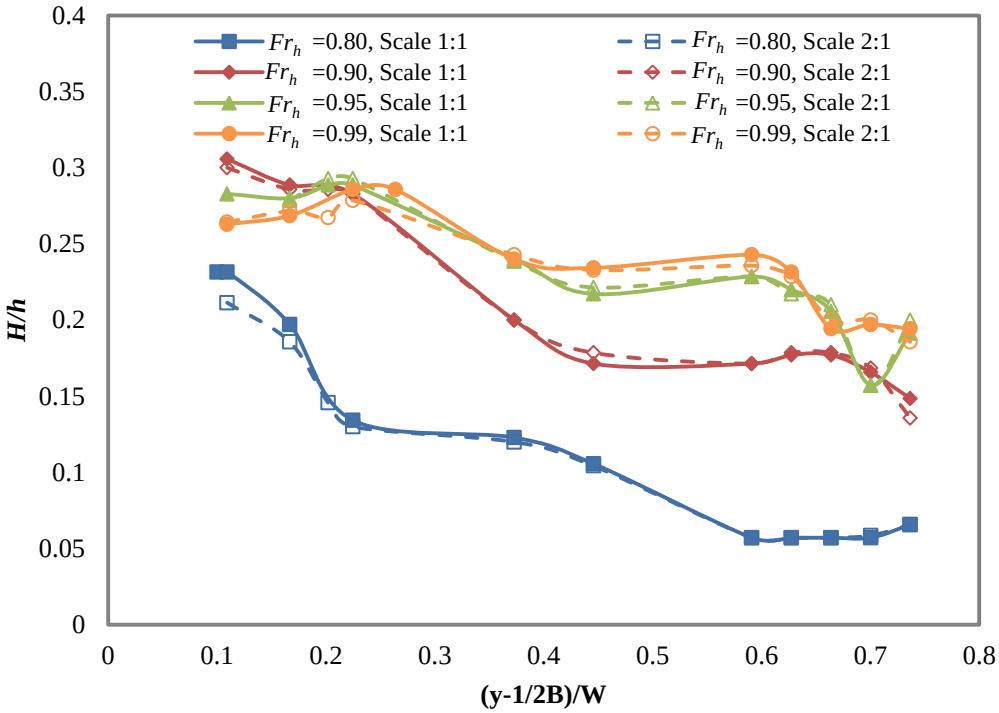

Figure 4-26: The wave heights at different depth Froude numbers for two different scales: Scale 1:1 is the results for channel 4 and Scale 2:1 which the dimensions of pressure source and channel were doubled.

Table 4-9: Drag and Vertical Forces for Two Different Scales

	Scale 1:1		**Scale 2:1**		**Ratio**	
Fr_h	Drag (KN)	Vertical force (KN)	Drag (KN)	Vertical force (KN)	Drag	Vertical force
0.8	9.58	76.22	79.34	631.95	8.28	8.29
0.9	10.81	82.66	85.77	658.36	7.94	7.96
0.95	12.47	94.73	99.08	756.32	7.95	7.98
0.99	14.14	107.15	112.13	857.03	7.93	8.00

According to the wave height results (Figure 4-26), the non-dimensional shape of the waves for two different scales are the same across the channel. It means the wave height for Scale 2:1 was twice of previous channel (Scale 1:1) and doubled at the different lateral distances for various Fr_h. The scaled wave height was found to be equal:

$$scale\ factor\ \times wave\ height \tag{4-1}$$

Table 4-9 shows the drag and vertical forces for two mentioned scales. According to the scale comparison, forces (drag and lift) for larger pressure source were 8 times bigger than forces for the smaller pressure source. Therefore the forces (drag and lift) can be obtained from following equation:

Forces (drag and lift) for scaled pressure source= Forces (drag and lift) for original (4-2)

pressure source times to scale factor to the power of 3

The residence on the pressure source is mainly due to the wave generation process, i.e. the mechanism mostly is due to the pressure distribution around the wavedozer as shown previously in Table 3-3. Therefore the influence of Reynolds number and Weber number is negligible and pressure distribution (C_p) should remain the same at model-scale and full-scale. Regarding to same Froude numbers for model-scale and full-scale:

$$Fr_{h_m} = Fr_{h_f} \tag{4-3}$$

$$\frac{V_m}{\sqrt{L_m}} = \frac{V_f}{\sqrt{L_f}} \rightarrow \frac{V_f}{V_m} = \sqrt{\frac{L_f}{L_m}} = \sqrt{\chi}$$

Where index m for model-scale and f is for full-scale and χ is scale factor.

Therefore the force for full-scale can be calculated:

$$F_f = 0.5 \times \rho \times C_p \times V_f^2 \times A_f \tag{4-4}$$

$$V_f^2 = \chi V_m^2 \quad and \quad A_f = \chi^2 A_m$$

$$F_f = \chi^3 F_m$$

Where ρ is water density, C_p is pressure force coefficient, V is speed of pressure source and A is area

4.3. Concluding remarks

In this chapter, the influences of channel parameters on wave characteristics were investigated. Four different full scale channel shapes were modeled, with the effect of beach slope and channel shape on the wave breaking location, wave breaking intensity, peel angles and wave water length investigated. The wave heights were almost the same for all four channels at the same pressure source speed. It was concluded that channel shape does not have significant effect on the maximum wave height. The width of the deep section of the channel has significant influence in breaking location and the channel slope has effect on the breaking intensity. The narrowest channel (Channel 1) was considered to be the best due to cheaper construction costs, while the wave wall length was longest in the channel with the widest deep part (Channel 4). In terms of wave breaking intensity, all four channels were able to generate barrel shaped breaking waves. It was concluded that Irribarren number could not be used to determine the wave breaking intensity in these cases. The cubic curve method was used to specify the wave breaking intensity. The vortex ratio for each breaking wave was measured. It was found that changing the beach slope had an effect on the barrel shape. The peel angles were extracted from simulation results for different Fr_h and different channels. Based on Hutt's chart, the surfing skill

level for different channels and different speeds were considered. According to the simulation results, it is possible to generate waves for intermediate to expert levels by changing the speed. The effect of scaling was investigated by doubling the channel 4 and pressure source dimensions. By comparing the results for two different scales, it was understood that scaling does not change the wave shape and following two formulae present the wave height (eq. 4-1) and forces (eq. 4-2) for scaled channel:

$$H_2 = scale\ factor \times H_1 \quad \text{4-1}$$

$$F_2 = (Scale\ factor)^3 \times F_1 \quad \text{4-2}$$

Previously was mentioned that the resistance of pressure source is mainly caused by the pressure drag and other sources are insignificant. Therefore it also mathematically was proven that the force scales with the cube of the scale factor for same Froude values.

5. Use for design

In the previous chapter (chapter 4) the effects of channel parameters on wave quality and propagation were investigated. In the experimental tests it was shown that regardless of channel parameters the pressure source has a strong influence on the generated wave parameters and the propagation. This chapter presents the numerical simulation results of the investigation of wavedozer parameters as a pressure source on wave characteristics in the straight track. The parameters investigated are the draught, angle of attack, beam and pressure source profile shape. In addition, two channel parameters were investigated: depth and blockage factor (κ) as the ratio of pressure source cross section area (A_s) and channel cross section area (A_c). The relationship between the scale factor and wave parameters and forces were investigated.

5.1. Pressure source

5.1.1. Pressure source parameters

The main parameters of the pressure source are its overall dimensions, i.e. length, draught and beam, and the pressure source profile shape, which all have an impact on the generated waves. The early experimental investigations demonstrated that the wavedozer shape is better than the parabolic shape pressure source. Wavedozer simulation results showed that about 95% of the total drag is pressure drag and the proportion of viscous drag is negligible. For the wavedozer, the water completely separates from the sides and the transom of the model and only the underneath of the model remains wet, so the reason for having small viscous drag is because of the small wetted area. About 95% of power required to drive the wavedozer converts to wave energy. It appears that the wavedozer shape is efficient in terms of energy consumption. To improve the wavedozer parameters, the main dimensions of the wavedozer were considered and simulations were conducted to determine if there is a better pressure source profile shape in terms of wave generated.

Wavedozer dimensions

Draught, beam and angle of attack are the main dimensions of the wavedozer which were investigated with respect to the wave generated height and propagation. Changing any of these parameters will alter the wavedozer's displacement. In this study, only one of the parameters was changed at a time and the rest kept constant in order to compare the results and examine the effect of the changed parameter.

Draught

Table 5-1 shows the dimensions of two wavedozers. Model 5-1 is the model which was used in the experimental tests and the previous simulations. To consider the effect of draught on generated waves,

a new model (Model 5-2) was simulated. The draught of Model 5-2 was 20% more than Model 5-1. These simulations were conducted in 1.5 m water depth. Since the tests were conducted in 1.5 m water depth, the draught change does not have a significant influence on the blockage factor. Blockage factor can be defined as (eq. 5-1):

$$Blockage\ factor\ (\kappa) = \frac{Model\ cross\ section\ area\ (A_s)}{Channel\ cross\ section\ area\ (A_c)} \qquad 5\text{-}1$$

The predicted wave heights generated by Model 5-2 at different lateral distances are presented in Figure 5-1. The comparison between Model 5-1 and Model 5-2 shows that increasing the draught causes an increase in wave height except at a depth Froude number of 0.99 (Figure 5-2 to Figure 5-6).

Since the portion of displacement close to the free surface has the greatest effect on the wave generated, it is expected that there is a limitation for effective draught and the draught larger than special amount does not have effect on wave generated height.

Table 5-1: Wavedozers Dimensions

	Draught (m)	**Beam (m)**	**Angle of attack (deg)**	**LWL (m)**	**Displacement (m^3)**	**Blockage factor**
Model 5-1	0.1	0.3	14	0.401	0.006015	0.0057
Model 5-2	0.12	0.3	14	0.481	0.00866	0.0068

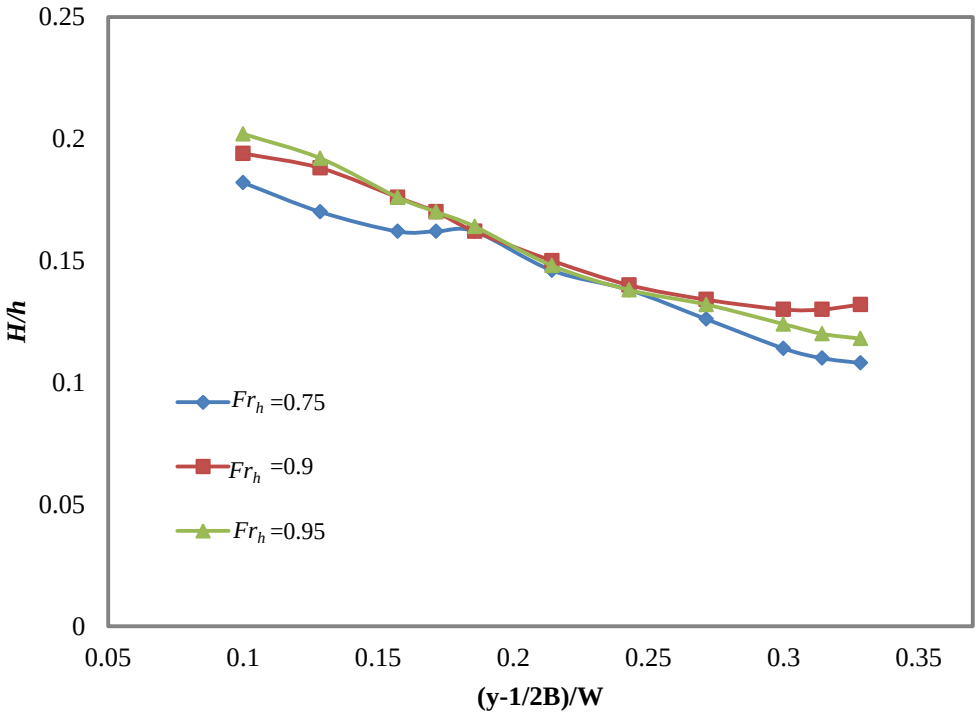

Figure 5-1: Predicted wave height generated by Model 5-2 at different lateral distances for different Fr_h

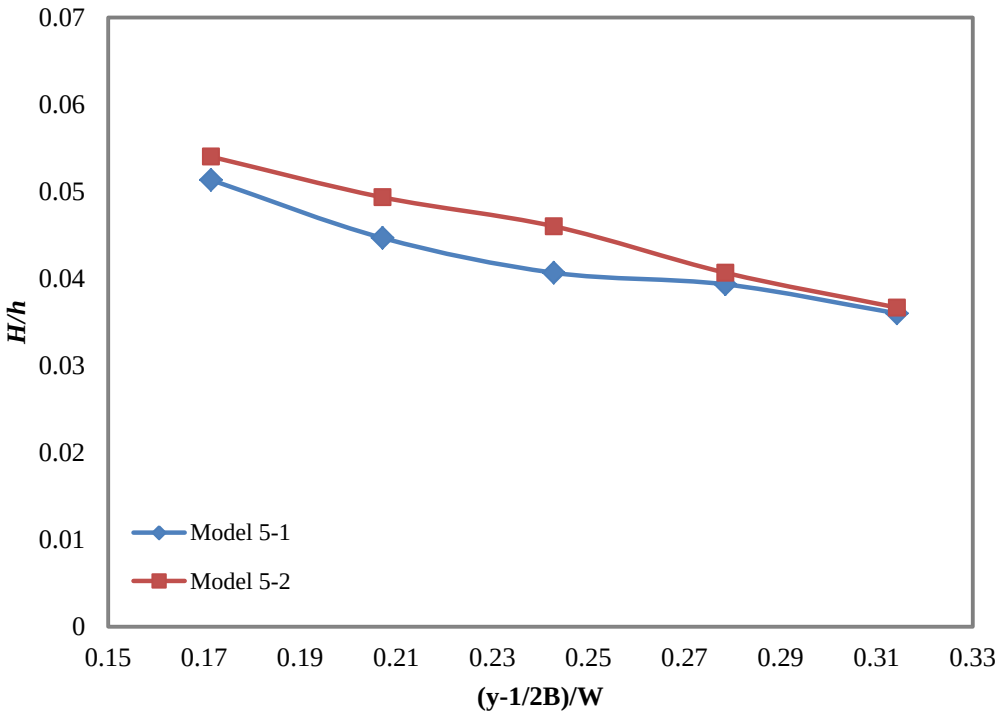

Figure 5-2: Wave height comparison for Model 5-1 and Model 5-2 at different lateral distances; Fr_h=0.75; model 5-1 has 0.1 draught m and model 5-2 has 0.12 m draught

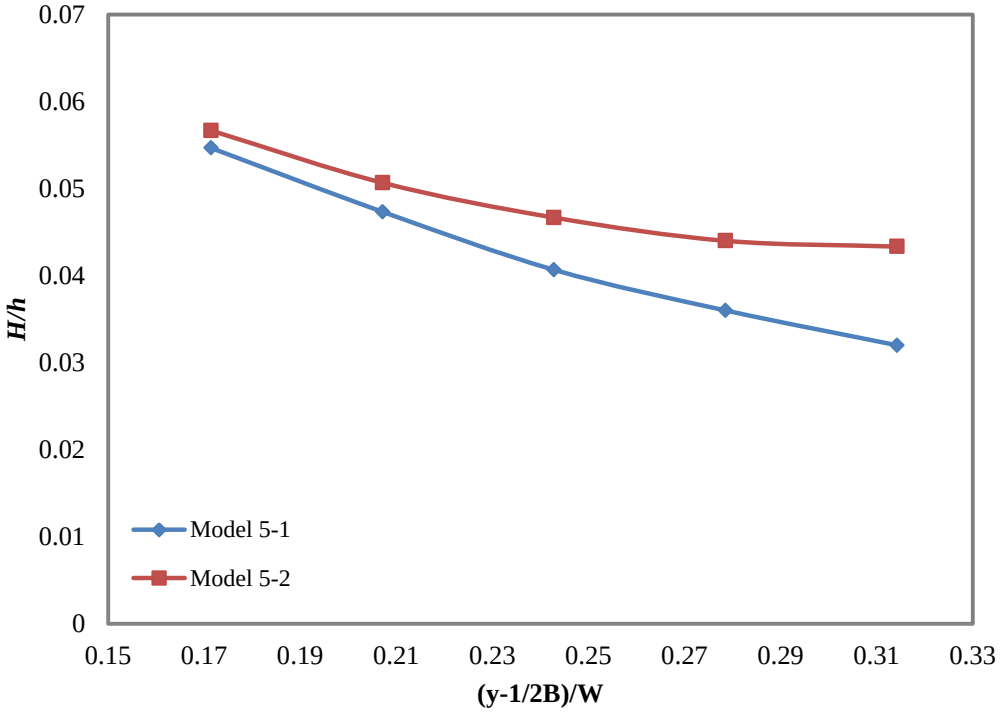

Figure 5-3: Wave height comparison for Model 5-1 and Model 5-2 at different lateral distances Fr_h=0.9; model 5-1 has 0.1 draught m and model 5-2 has 0.12 m draught

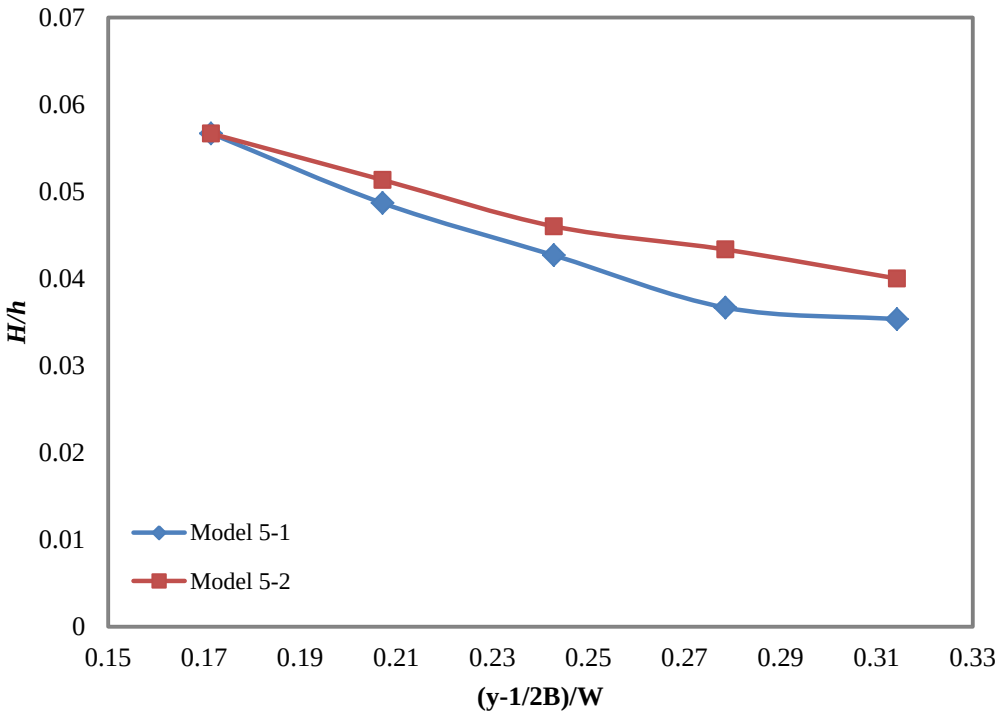

Figure 5-4: Wave height comparison for Model 5-1 and Model 5-2 at different lateral distances Fr_h=0.95; model 5-1 has 0.1 draught m and model 5-2 has 0.12 m draught

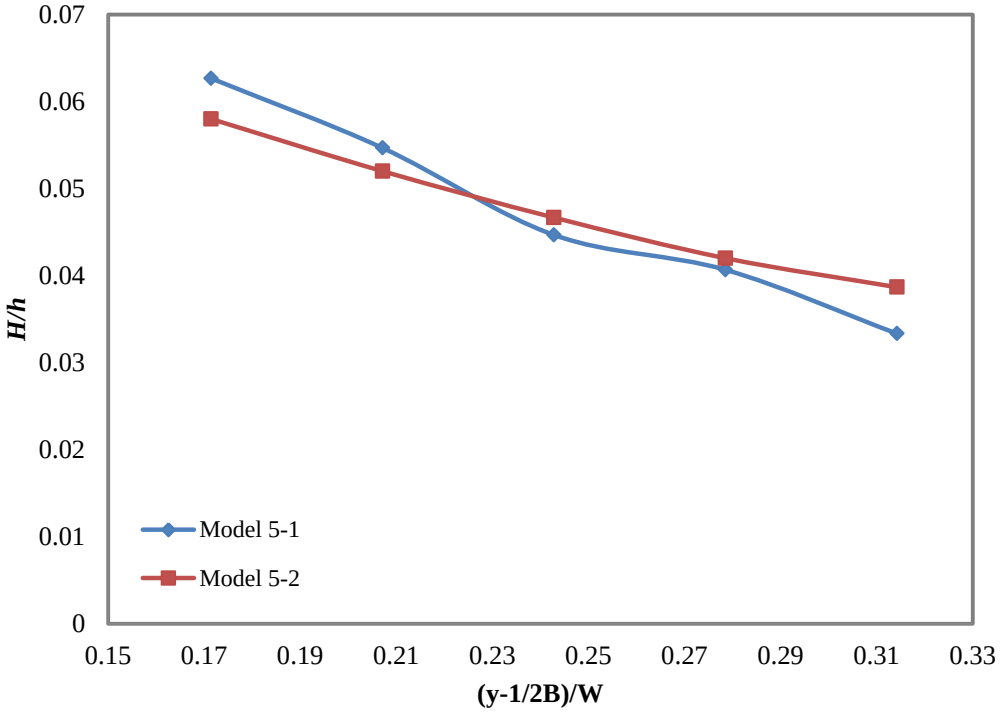

Figure 5-5: Wave height comparison for Model 5-1 and Model 5-2 at different lateral distances Fr_h=0.99; model 5-1 has 0.1 draught m and model 5-2 has 0.12 m draught

Angle of attack

Another potentially important dimension is the angle of attack. The angle of attack is the angle between the entry surface and the water surface. The previous studies were conducted with a wavedozer with a 14 degree angle of attack. In this study, wavedozers with different angles of attack were simulated. By altering the angle of attack, the length of water line (LWL) and the displacement were changed and the draught and beam remained constant. The wavedozer with the lowest angle of attack has the largest displacement and vice versa. Table 5-2 presents the wavedozers parameters. Figure 5-6 to Figure 5-9 illustrate the wave heights for different wavedozers at different Fr_h.

Table 5-2: Wavedozers with Different Angle of Attack Parameters

	Draught (m)	Beam (m)	Angle of attack (deg.)	LWL (m)	Displacement (m^3)	Blockage factor
Model 5-1	0.1	0.3	14	0.401	0.006015	0.0057
Model 5-3	0.1	0.3	10	0.567	.008505	0.0057
Model 5-4	0.1	0.3	7	0.814	0.01221	0.0057
Model 5-5	0.1	0.3	4	1.43	0.02145	0.0057

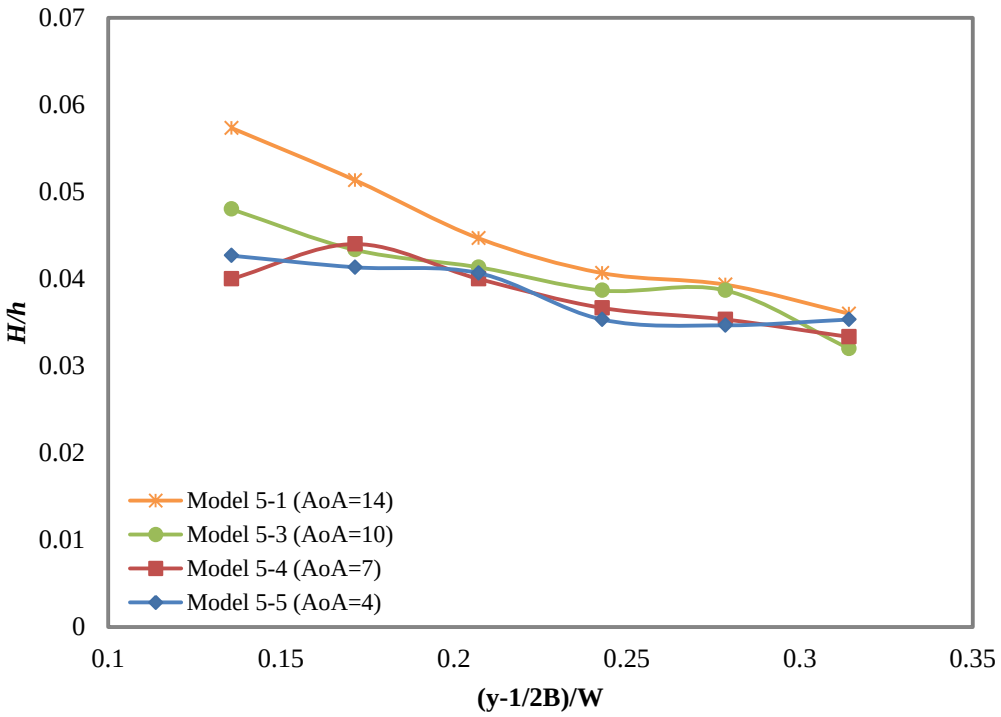

Figure 5-6: The wave height generated for different angle of attack (AoA) at different lateral distances for Fr_h=0.75

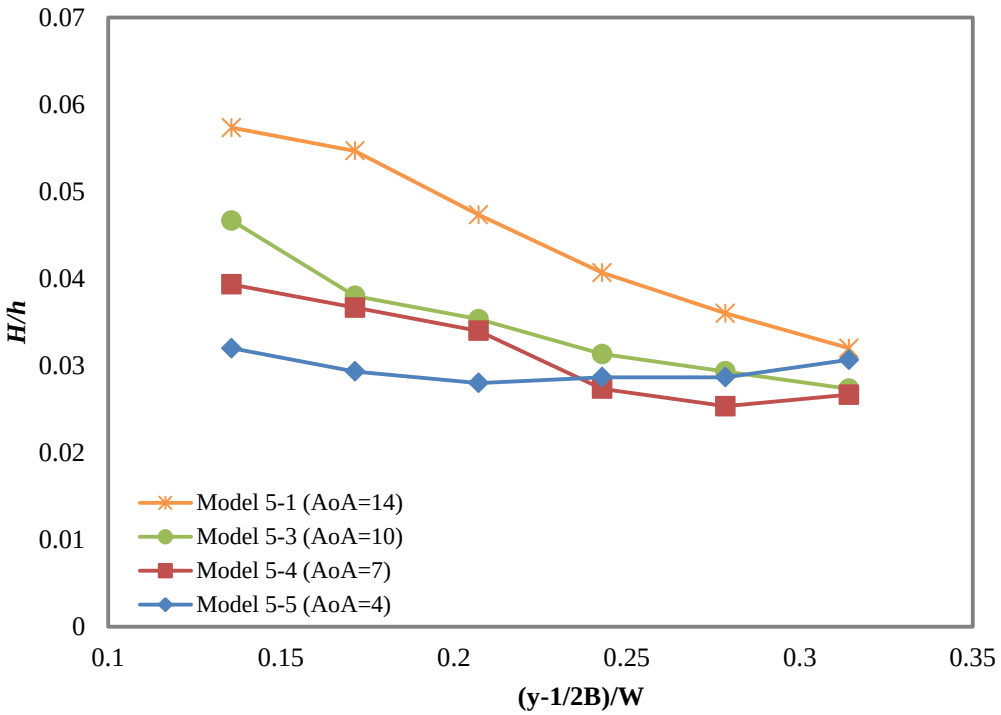

Figure 5-7: The wave height generated for different angle of attack (AoA) at different lateral distances for Fr_h=0.9

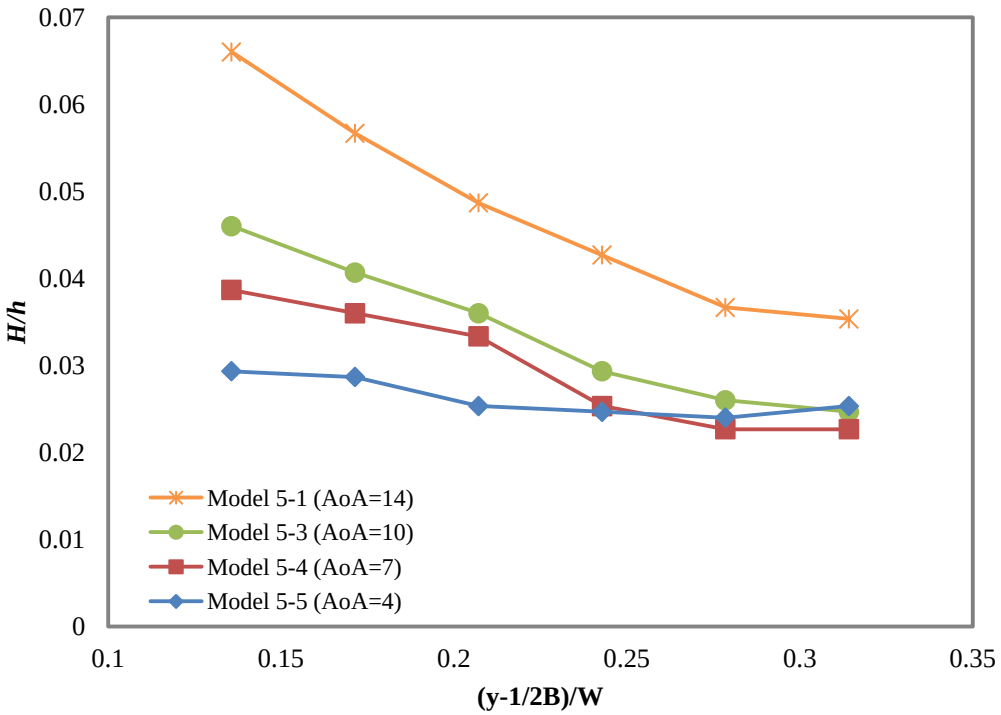

Figure 5-8: The wave height generated for different angle of attack (AoA) at different lateral distances for Fr_h=0.95

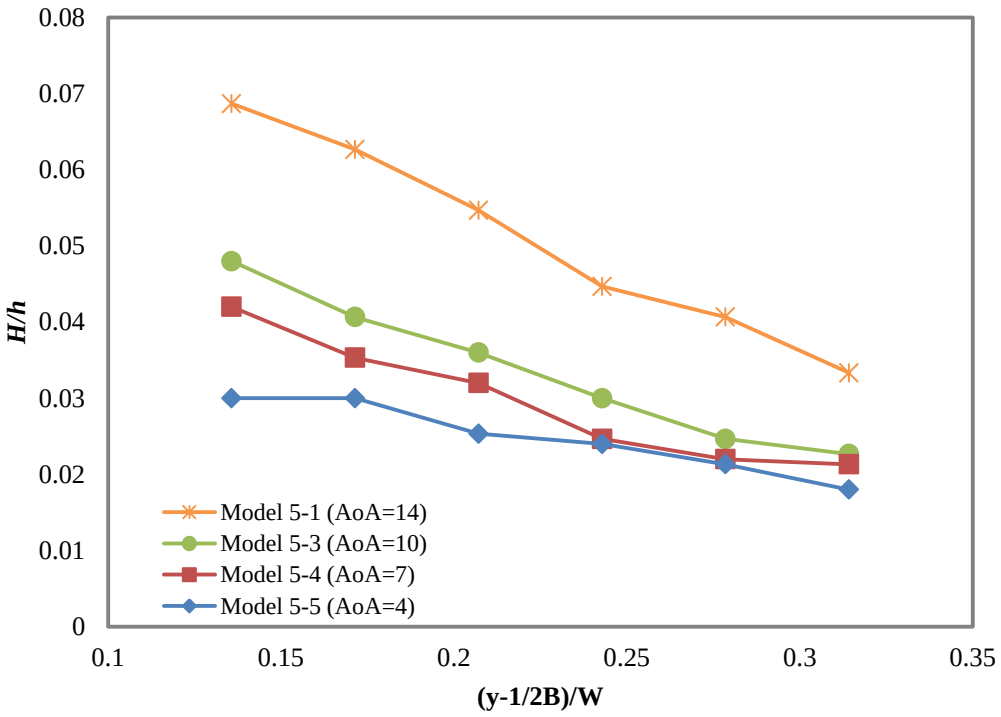

Figure 5-9: The wave height generated for different angle of attack (AoA) at different lateral distances for Fr_h=0.99

By decreasing the angle of attack, the variation of wave height with lateral distances decreases. For example, for Model 5-5 (angle of attack of 4 degrees) at $Fr_h = 0.9$, the wave height is almost constant for the entire width of the channel.

By increasing the angle of attack, the maximum wave height will be increased due to increasing the pressure gradient. It can be said that the pressure differential is proportional to the draught divided by length of waterline ($\frac{d}{LWL}\alpha\frac{\delta p}{\delta x}$), therefore by increasing the angle of attack for constant draught (d) the length of waterline (LWL) will decrease. It means that the pressure gradient will increase, and as a consequence, for given speed the wave generated height will increase.

Model 5-5 has the largest displacement while it generates the lowest wave height. Increasing the displacement by changing the angle of attack (or LWL) has the opposite effect on wave height. By decreasing the angle of attack the model drag decreases. Figure 5-10 and Figure 5-11 show the drag and lift coefficients for different angles of attack. Drag and lift coefficients defined as follows:

$$Drag\ Coefficient\ (C_d) = \frac{Drag\ force}{0.5 \times \rho \times V^2 \times B \times d} \quad 5\text{-}2$$

$$Lift\ Coefficient\ (C_l) = \frac{Lift\ force}{0.5 \times \rho \times V^2 \times LWL \times B} \quad 5\text{-}3$$

Where ρ is water density (kg/m^3), V is model speed (m/s), B is model beam (m), d is draught (m) and LWL is length of waterline (m). Need to be mentioned that wetted surface area at drag coefficient formula is equal $B \times d$, while at lift coefficient is equal $LWL \times B$.

As mentioned before, the large portion of total drag belongs to pressure drag. Increasing the angle of attack increases the pressure drag and decreasing the angle of attack increases the wetted area and as a result increases the viscous drag. It can be concluded that Model 5-5 with largest displacement generates the lowest wave height and has minimum drag, and in terms of wave quality it generates the best wave and Model 5-1 with lowest displacement generated the highest wave height and has maximum drag. The quality of wave can be measured by comparing the wave height across the channel; a wave with a lower decrease in the height across the channel has better quality.

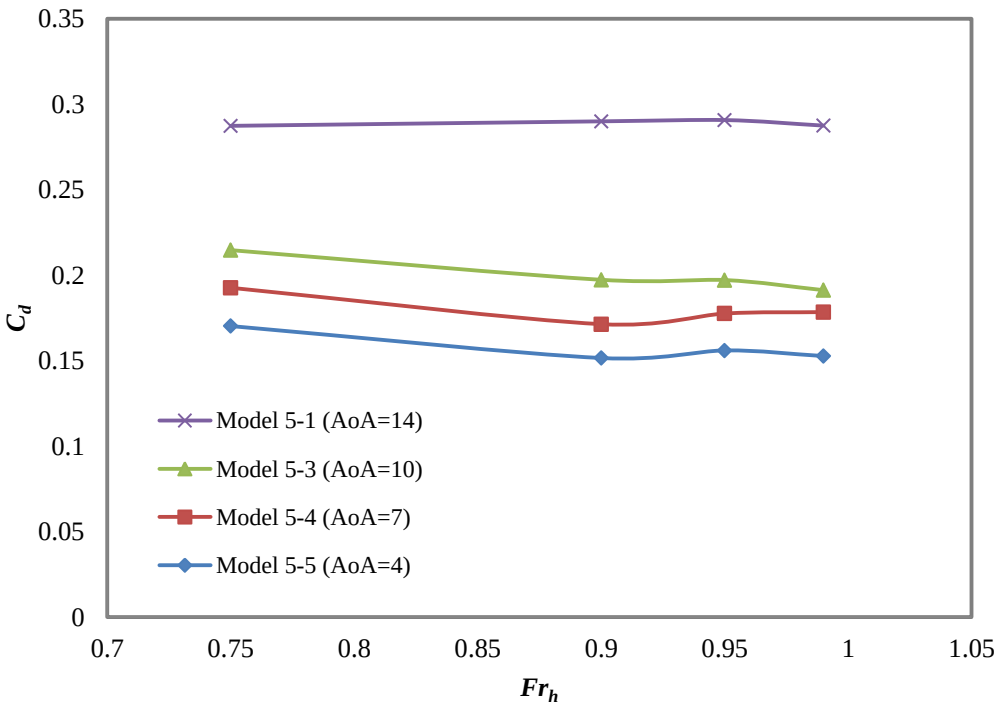

Figure 5-10: The drag coefficients for different models at different Fr_h

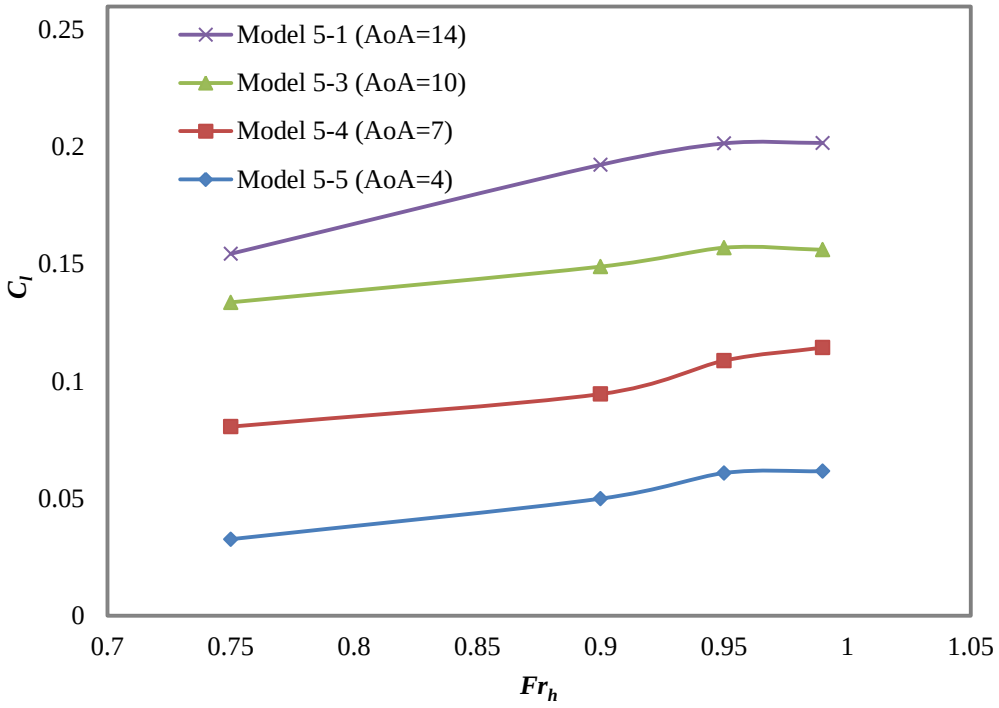

Figure 5-11: The lift coefficients for different models at different Fr_h

Beam

The beam of the pressure source is an important parameter affecting the generated wave height and quality. For this investigation, the wavedozer beam was increased from 300mm (model 5-1) to 433mm (model 5-6). In addition, it should be noted that the wavedozer with 433mm beam (Model 5-6) has the same displacement as the model with 120mm draught (model 5-2) which was used previously for the draught investigation. Table 5-3 presents the characteristics of these models. Therefore, by comparing models 5-1 and 5-6, it is possible to see the effect of beam and displacement change on wave height and by comparing models 5-2 and 5-6, make it possible to see the effect of altering beam and draught, but maintaining displacement. The simulations were conducted in a channel with 3.5m width and 1.5m depth. Figure 5-12 to Figure 5-15 illustrate the results for the aforementioned models at different Fr_h.

It is expected that there is a limitation for effective beam. Increasing the beam increases the wave height till the wave generated does not break.

Table 5-3: The Pressure Sources Characteristics

	Draught (m)	Beam (m)	LWL (m)	Water plane (m^2)	Angle of attack (degree)	Volume displacement (m^3)
Model 5-1	0.1	0.3	0.401	0.120	14	0.006
Model 5-2	0.12	0. 3	0.481	0.144	14	0.00866
Model 5-6	0.1	0.433	0.401	0.174	14	0.00866

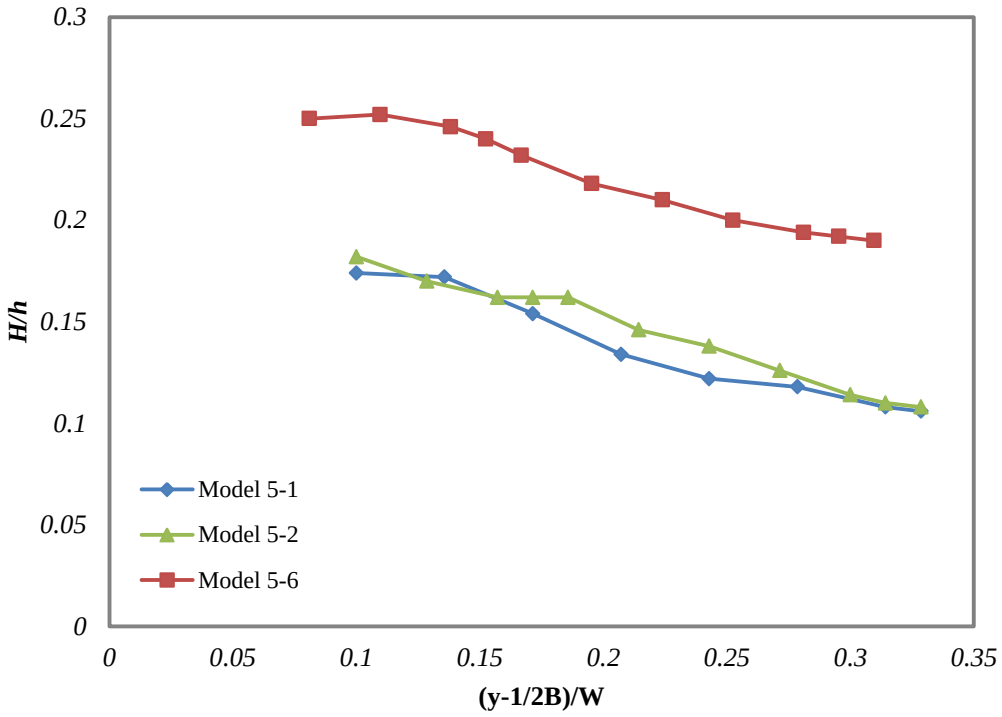

Figure 5-12: Comparison of wave height at different lateral distances for different models at Fr_h=0.75

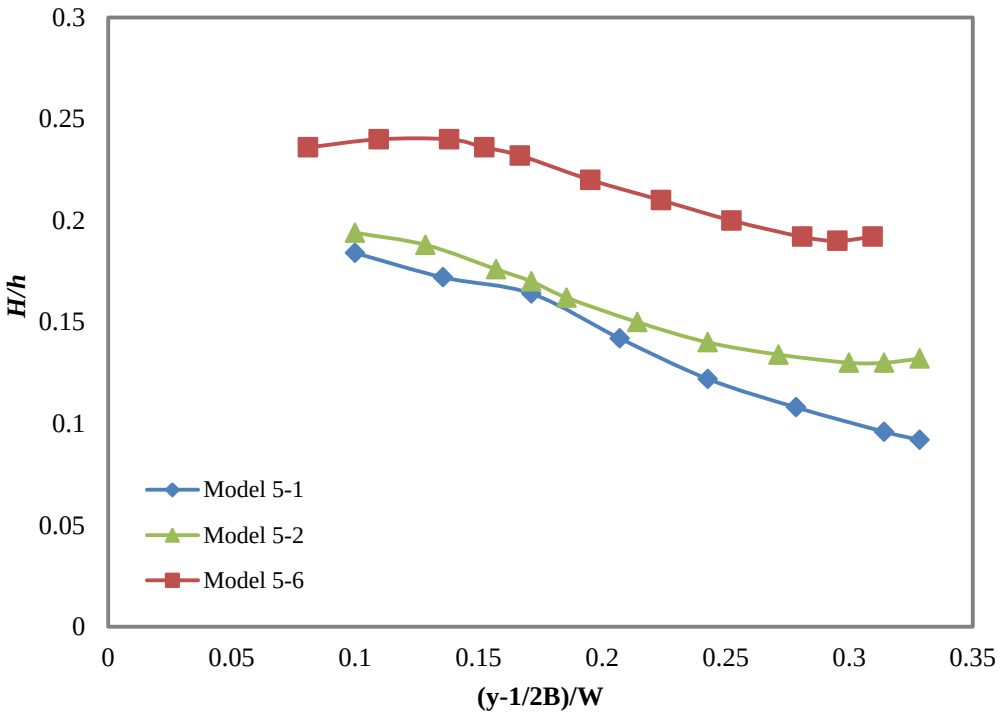

Figure 5-13: Comparison of wave height at different lateral distances for different models at Fr_h=0.9

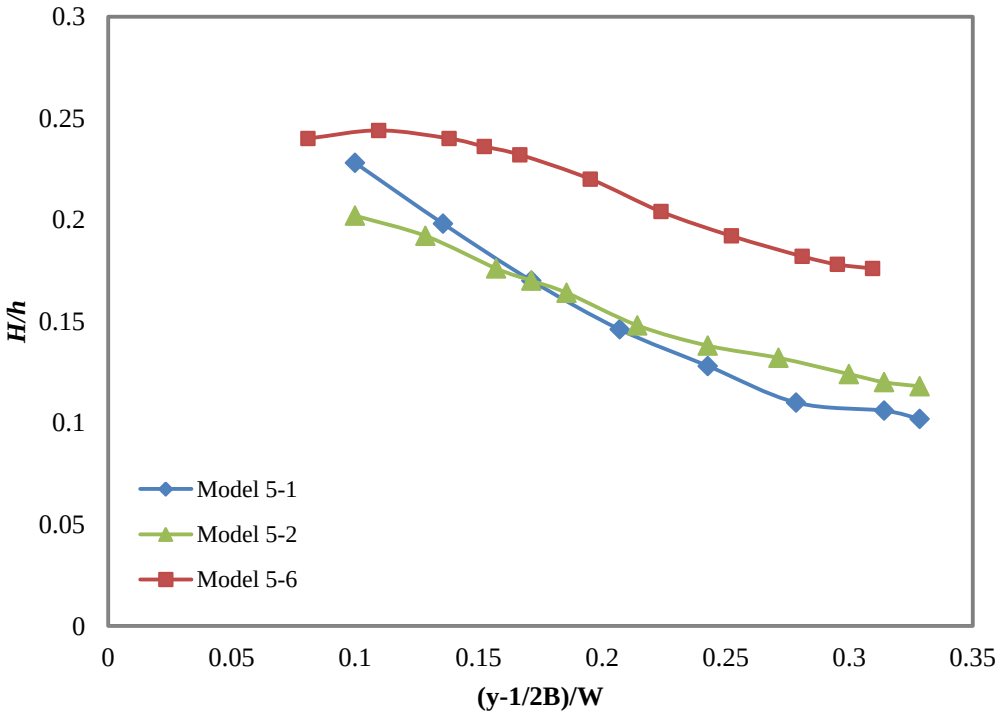

Figure 5-14: Comparison of wave height at different lateral distances for different models at Fr_h=0.95

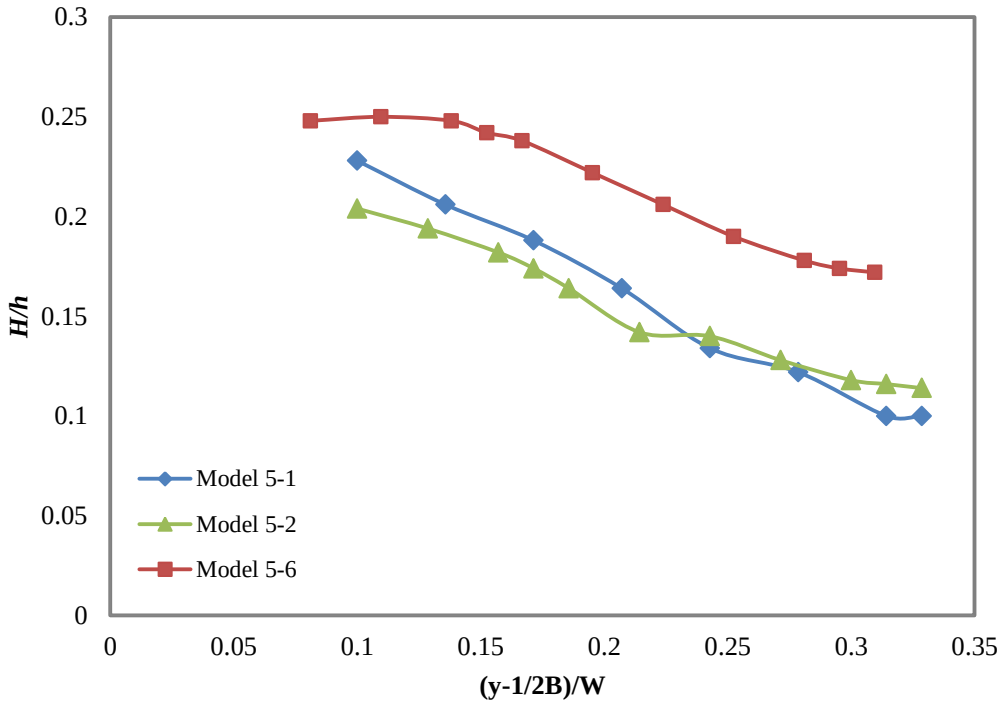

Figure 5-15: Comparison of wave height at different lateral distances for different models at Fr_h=0.99

The results show that by increasing the model beam, the generated wave height increases for all investigated Fr_h. An increase of about 44% of beam can increase the wave height form about 28% to 98% at different lateral distances. The comparison between models 5-2 and 5-6 shows that adding displacement increases wave height, however the increase by increasing draught is small, whereas the increase due to a beam increase is large. The author has hypothesised that the waterplane of Model 5-6 is larger than Model 5-2 (Table 5-3). Therefore increasing the displacement by increasing the beam is more effective than increasing the draught regarding to wave height. It is predicted that increasing the beam will increase the wave height till wave breaks.

5.1.2. Pressure source profile shape

In addition to the main parameters of pressure source such as draught, beam and angle of attack (or length of water line), the shape of the pressure source is important. As shown in the experimental investigation in the Towing Tank tests, two different profile shapes, parabolic and wavedozer, were investigated. It was concluded that generated waves by wavedozer have a better quality for surfing. A numerical approach was then used to investigate two other pressure source shapes by changing the plan and profile views of wavedozer.

Plan shape

According to the previous experimental results, the bow wave is not surfable and only the generated waves behind the model can be used for surfing [38]. By considering this conclusion, a new pressure source plan was designed. This profile shape has reduction in beam from 0.4m at stern to 0.1m at bow. The model beam in front is smaller than that at the stern. Table 5-4 presents the model characteristics and Figure 5-16 shows the different views of the model. This model was simulated at two Fr_h : 0.9 and 0.99. The wave heights at different lateral distances for this model were compared with two previous wavedozers: model 5-1 and model 5-6 (beam=0.3 m and beam=0.43 m). This model and model 5-1 have the same displacement and along with the other wavedozer (model 5-6) have almost the same beam at the stern. Figure 5-17 and Figure 5-18 show the simulation results for the three different models at Fr_h=0.9 and Fr_h=0.99. The generated wave by model 5-7 is much higher than the generated wave by model 5-1, while both have the same displacement. Comparison between model 5-6 and model 5-7 shows that waves generated by model 5-7 are higher than those generated by model 5-6, but these waves disperse faster than those generated by model 5-6. The wave run up in front of model 5-7 is another problem for this model. Figure 5-19 shows the wave run up for model 5-7 and wavedozer (model 5-1) at Fr_h=0.99 for two different views. For instance the bow wave height for this model for Fr_h=0.99 at 750mm lateral distance is about 150mm, while for wavedozer at the same condition is 20mm.

Table 5-4: Characteristics of Model 5-7

Beam at stern	0.4 m
Beam on the waterline at bow	0.1 m
Angle of attack (α)	14 degree
Side angle (β)	21.0 degree
Length	0.54 m
Draught	0.1 m

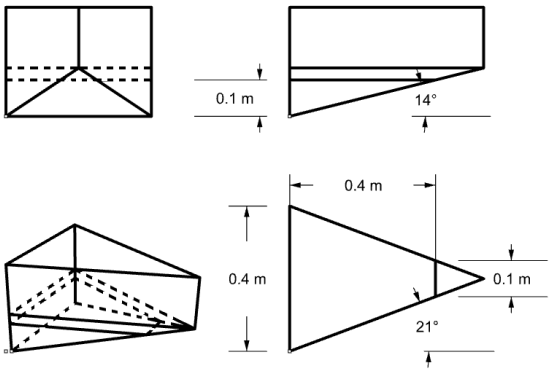

Figure 5-16: Model 5-7 of B=0.4m, LWL=0.4m, α=14 degrees, β=21 degrees and *d*=0.1m

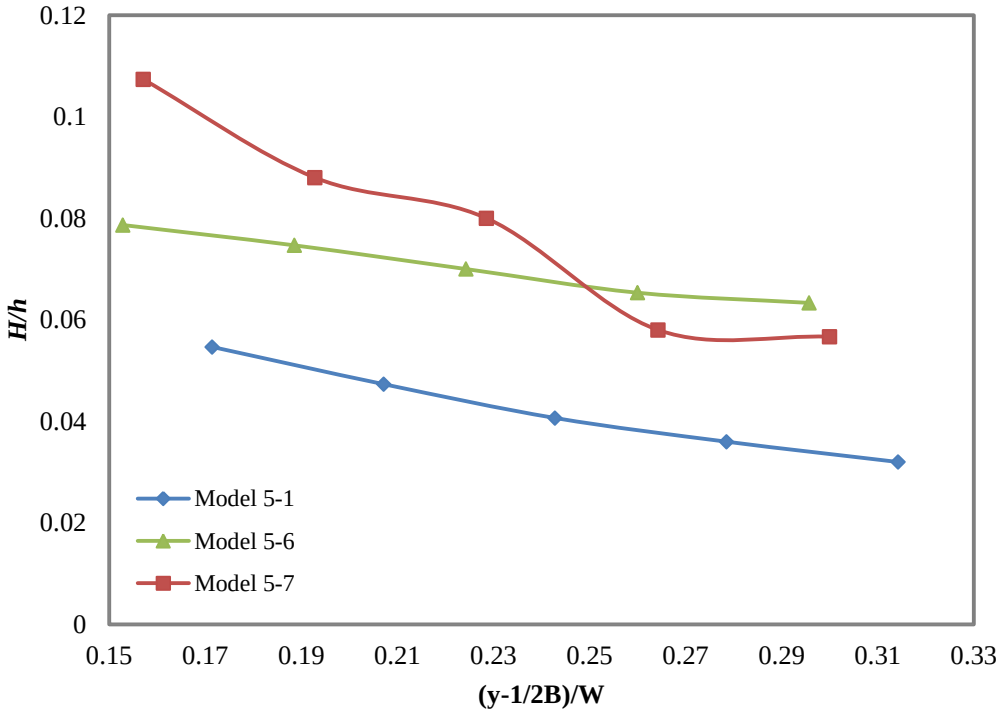

Figure 5-17: wave height comparison at different lateral distances for Fr_h=0.9

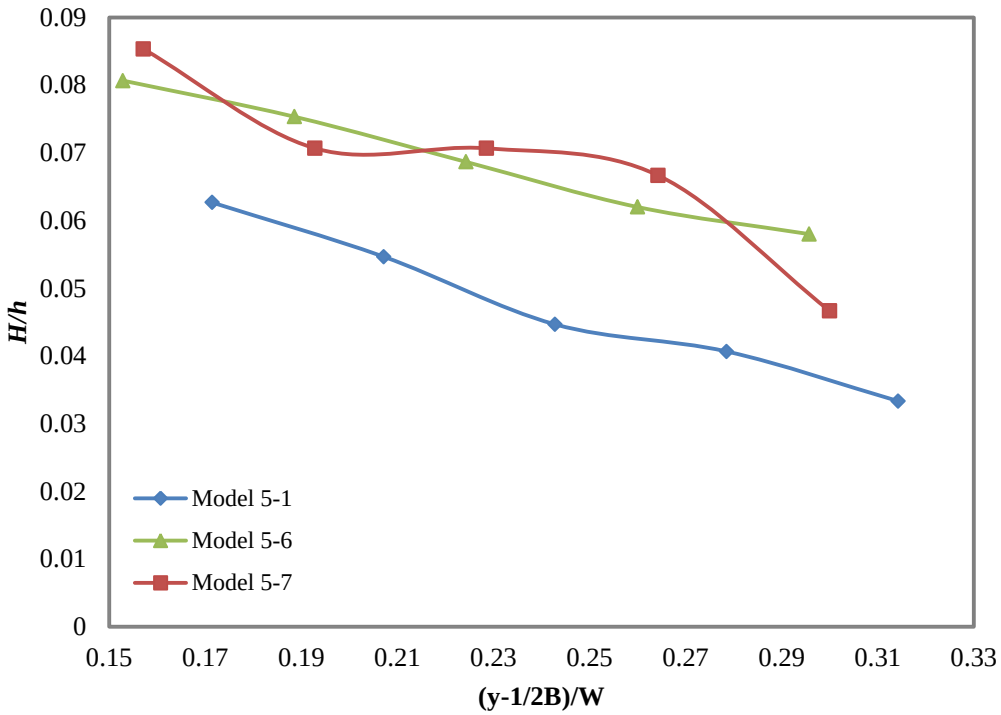

Figure 5-18: wave height comparison at different lateral distances for Fr_h=0.99

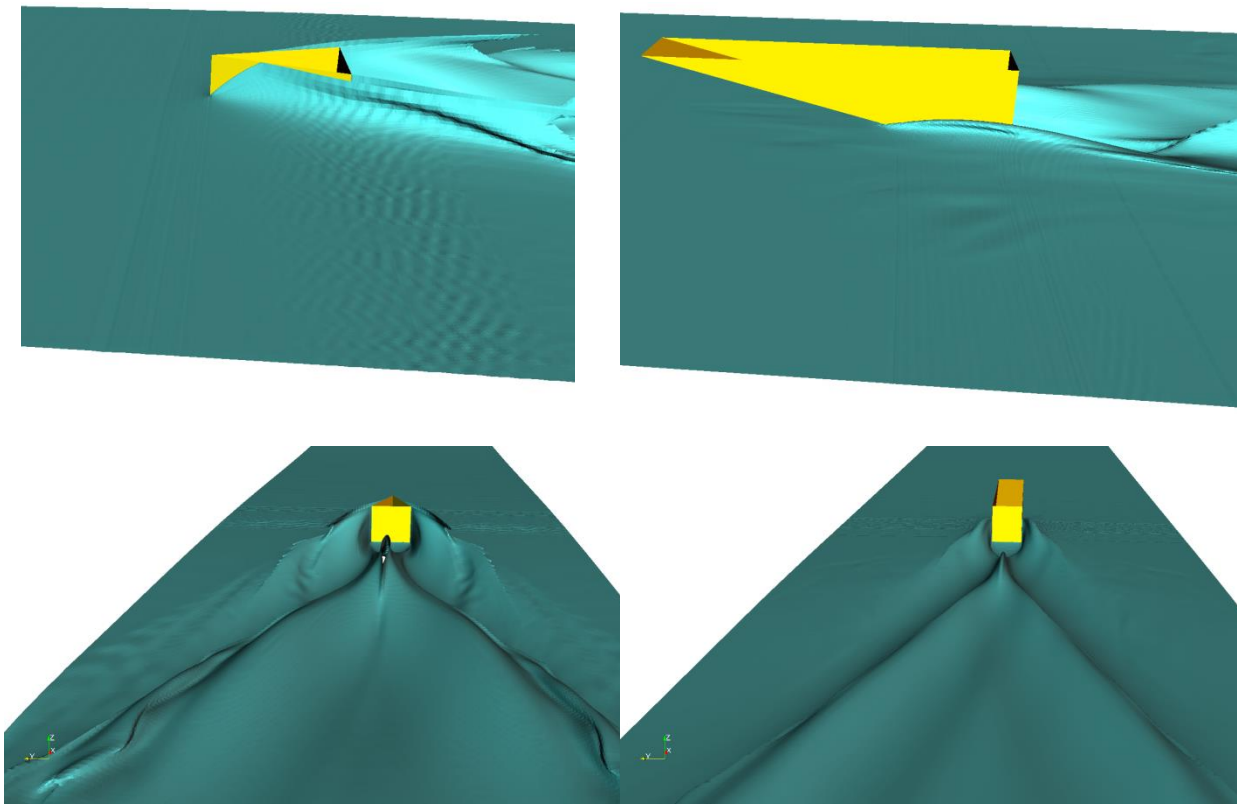

Figure 5-19: Comparing the wave run up for Model 5-1 and Model 5-7

Profile shape

According to the angle of attack study results, it was seen that the quality of waves generated by a 4 degree angle of attack model were better than those generated by an angle of attack of 14 degrees. However the bow waves generated by the 4 degree angle of attack were larger than those of the 14 degree angle of attack. A new profile shape (model 5-8) was generated. This model has a constant beam, with a 14 degree angle of attack at the front and a 4 degree angle of attack at the stern (Table 5-5). Figure 5-20 shows model 5-8 schematically. Figure 5-21 to Figure 5-24 show the results between model 5-1 (14 degree angle of attack), model 5-5 (4 degree angle of attack) and model 5-8. The wave generated heights for model 5-8 are smaller than those of model 5-1, but the wave height decrease of between 1.0 m and 1.25 m lateral distances is slightly less compared to model 5-1.

Table 5-5: The Characteristics Model 5-8

Beam (m)	0.3
Length of water line (m)	0.4
Angle of attack in front (degree)	14
Angle of attack in stern (degree)	4
Draught (m)	0.1

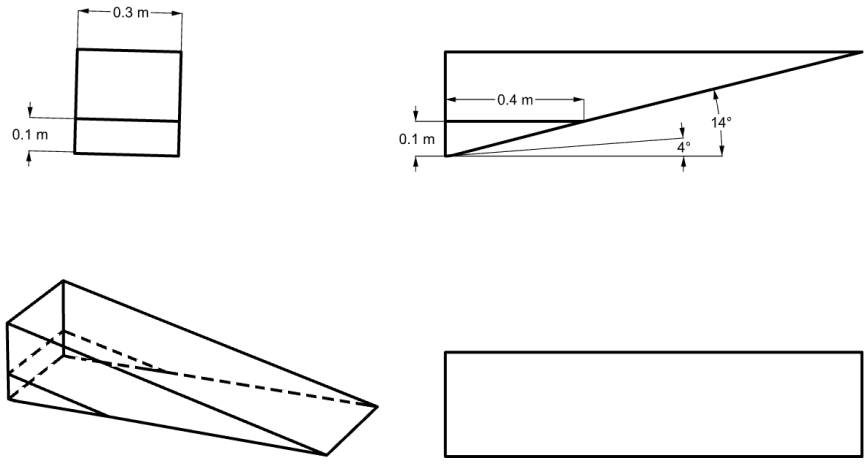

Figure 5-20: Model 5-8 of B=0.3m, LWL=0.4m, α at transom=4 degrees, α at front=14 degrees and d=0.1m

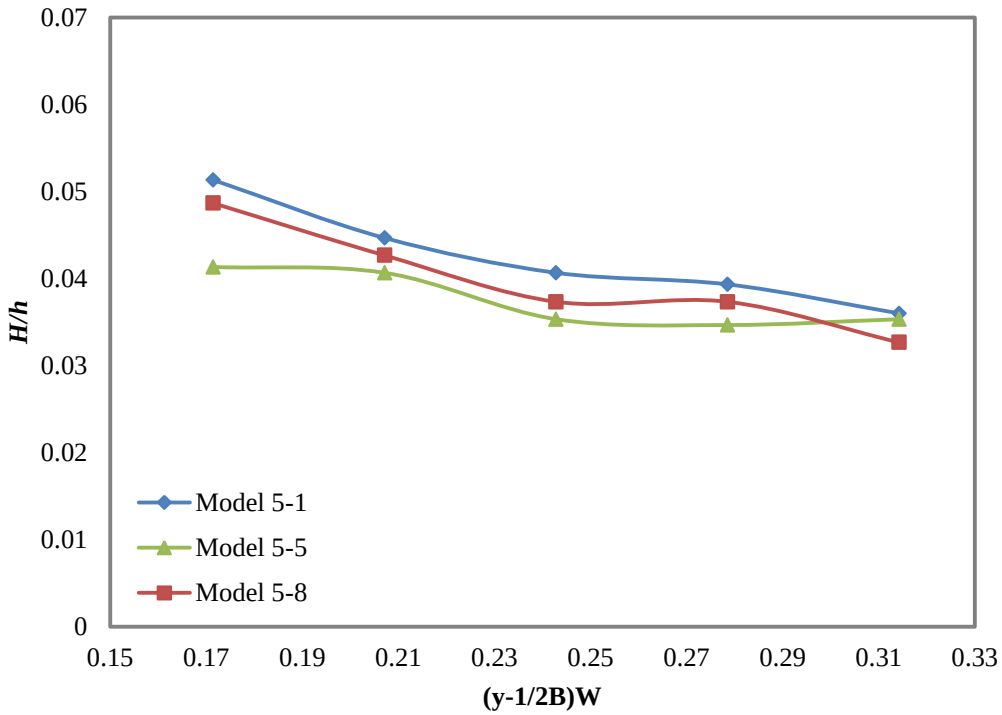

Figure 5-21: Results comparison for model 5-1 and 5-8 at different lateral distances for Fr_h=0.75; model 5-1 has 14 degrees constant angle of attack and model 5-8 has 14 degrees angle of attack at front and 4 degrees at transom

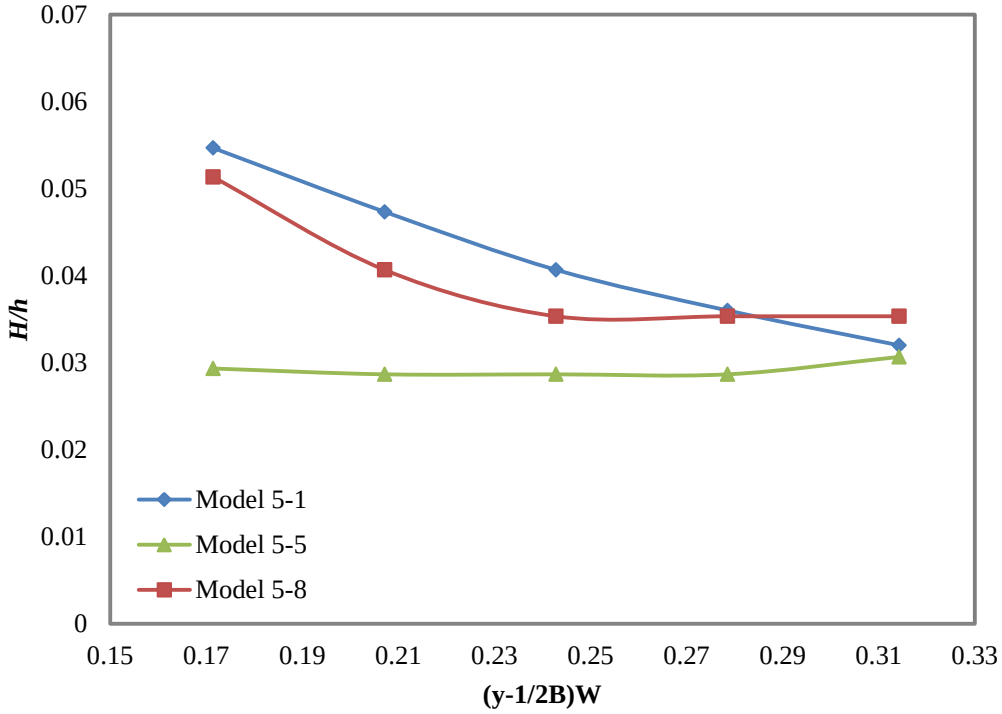

Figure 5-22: Results comparison for model 5-1 and 5-8 at different lateral distances for Fr_h=0.9; model 5-1 has 14 degrees constant angle of attack and model 5-8 has 14 degrees angle of attack at front and 4 degrees at transom

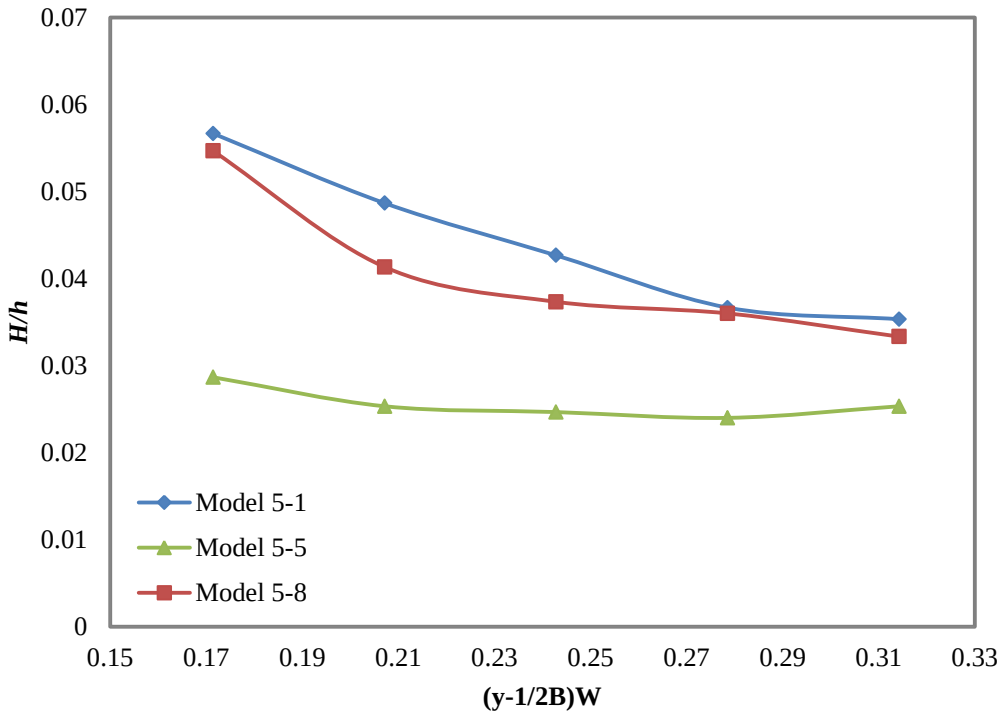

Figure 5-23: Results comparison for model 5-1 and 5-8 at different lateral distances for Fr_h=0.95; model 5-1 has 14 degrees constant angle of attack and model 5-8 has 14 degrees angle of attack at front and 4 degrees at transom

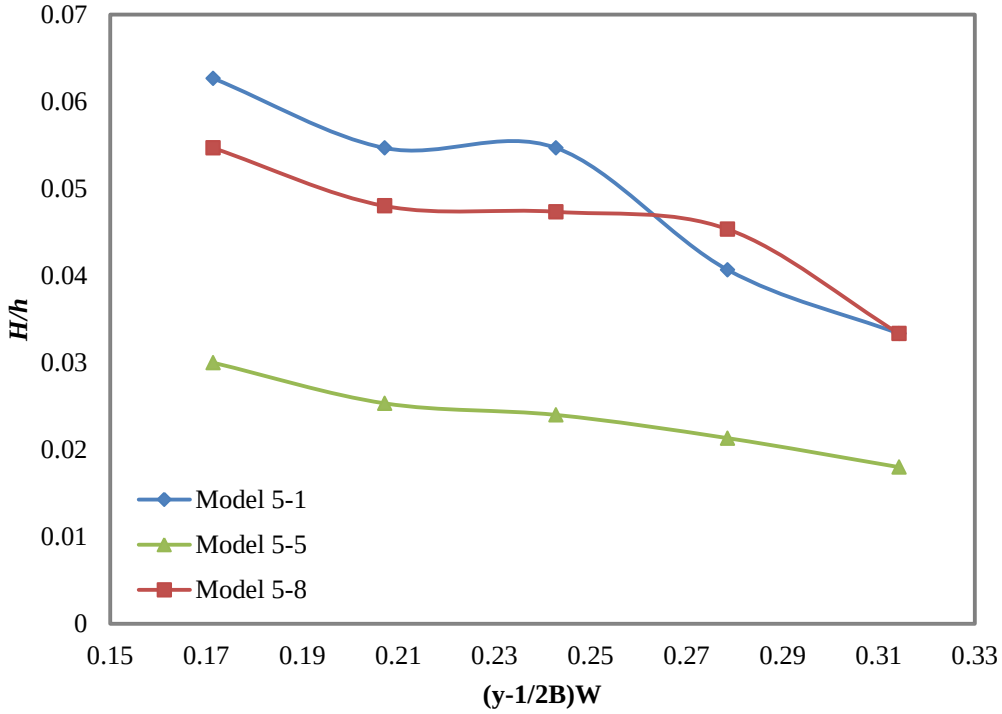

Figure 5-24: Results comparison for model 5-1 and 5-8 at different lateral distances for Fr_h=0.99; model 5-1 has 14 degrees constant angle of attack and model 5-8 has 14 degrees angle of attack at front and 4 degrees at transom

According to the results, it can be concluded that the angle of attack in front of model (stagnation point) is more effective in the height of generated wave. While the angle of attack at transom can effect wave quality. The wave quality means, the wave height decrease of between 1.0 m and 1.25 m lateral distances is slightly less compared to model 5-1 and more than model 5-8.

5.2. Channel parameters

5.2.1. Depth

Previous experimental and numerical studies showed that it is possible to generate higher waves for a given speed by decreasing the water depth (2.1.3). Two more water depths were considered and the wavedozer with 0.1 m draught and 0.3 m beam was simulated at three different speeds. The only difference between channels were the water depths and channel shape and width are same as Towing Tank dimensions (see section 3.3.1). Table 5-6 presents Fr_h for the given speeds at different water depths. Fr_h values at 1.66 m/s forward speed for all three different depths are less than 1 (sub-critical Fr_h) . Figure 5-26 shows the wave height results at 1.66 m/s speed for the three different water depths. According to the results, the wave generated in the shallowest water has the largest wave height, because it has the highest Fr_h. Figure 5-25 shows the time history of surface elevation at 0.75 lateral distances for 1.66 m/s speed at three different water depths.

The Fr_h at 1.99 m/s speed and 0.4 m water depth is equal to 1. The simulation results show the bow wave generated (soliton wave) at this condition is larger than for the two other conditions (Figure 5-27). The wave behind the pressure source has the lowest height at Fr_h=1.0 (Figure 5-28). The wave generated at Fr_h=0.9 is higher than two other Fr_h; 0.95 and 1.0. Figure 5-29 presents the results for 2.66 m/s at different water depths. The Fr_h for all three conditions are larger than 1. The results show that water depth does not have an effect for Fr_h larger than 1.2 (super-critical Fr_h). Figure 5-30 shows the time history of surface elevation at 0.75 lateral distances for 2.6 m/s speed at three different water depths. It can be seen that the shape of the waves are the same for Fr_h larger than 1.2. The water depth does not influence the wave shape at supercritical Froude depth values because the pressure source speed is greater than wave propagation speed.

Table 5-6: Fr_h for Different Speeds at Different Water Depth

	***V* [m/s]** / ***h* [m]**	**1.66**	**1.99**	**2.66**
Channel 5-1	0.4	0.838	1	1.343
Channel 5-2	0.45	0.79	0.947	1.266
Channel 5-3	0.5	0.75	0.9	1.2

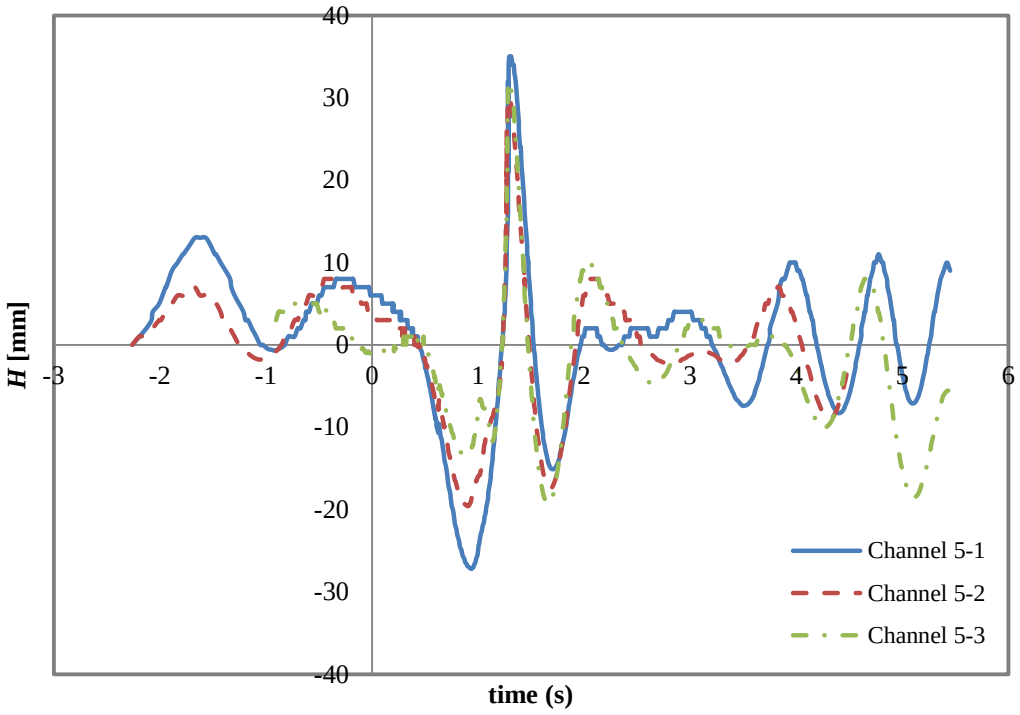

Figure 5-25: History of wave height at 0.75 m lateral distances at 1,66 m/s speed for three different water depths; Channels 5-1, 5-2 and 5-3 have 400mm,450 and 500 mm water depth respectively

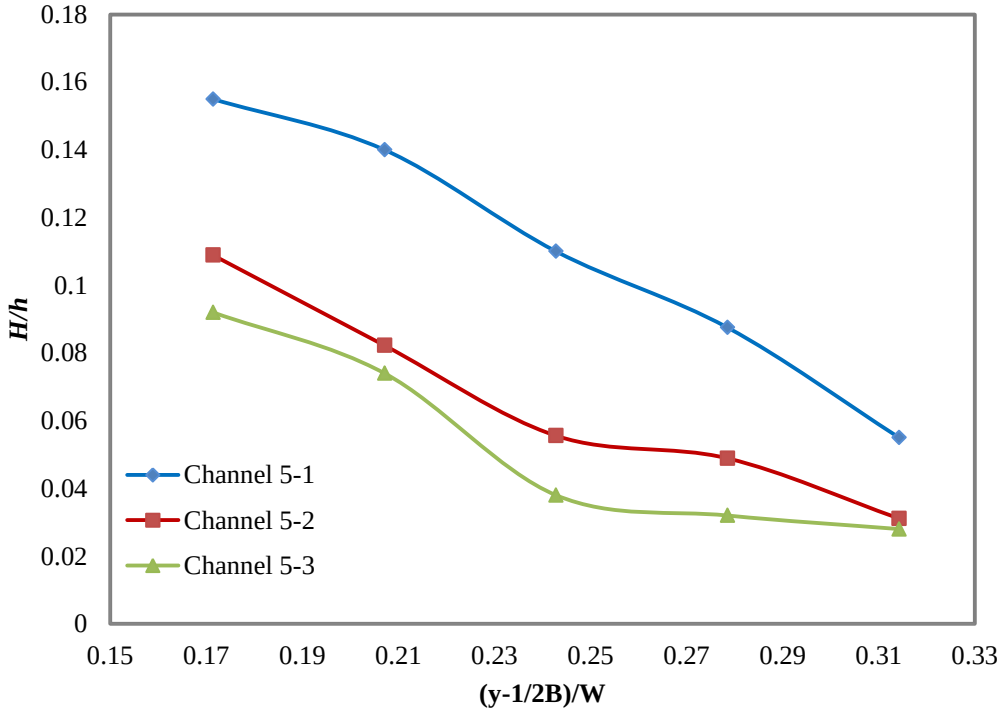

Figure 5-26: Wave heights at diffirent lateral distances for three different water depths at 1.66 m/s speed; Channels 5-1, 5-2 and 5-3 have 400mm,450 and 500 mm water depth respectively

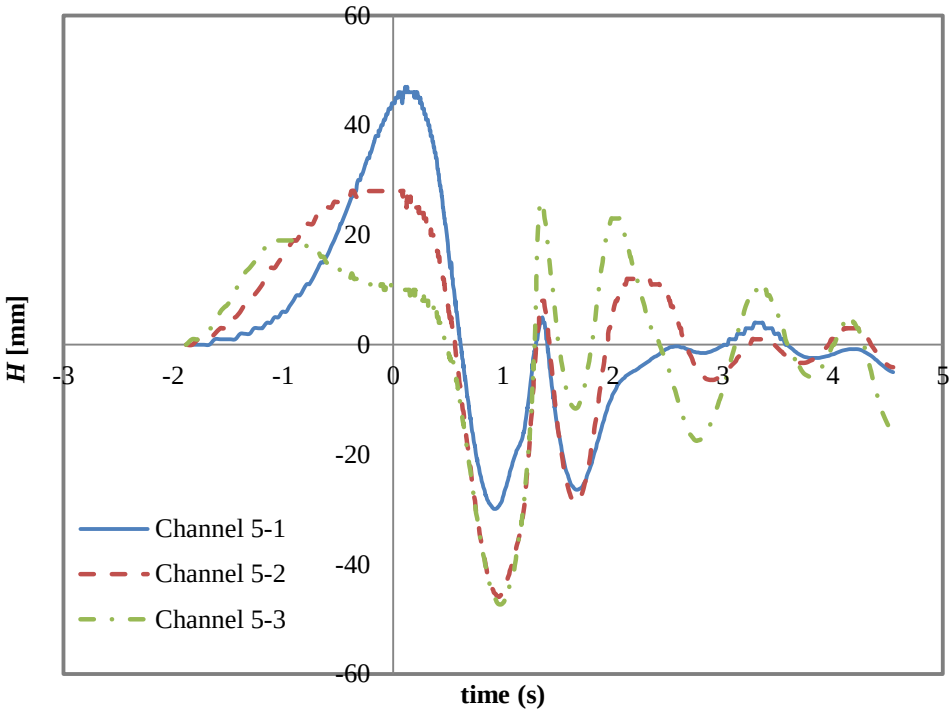

Figure 5-27: History of wave height at 0.75 m lateral distances at 1,99 m/s speed for three different water depths; Channels 5-1, 5-2 and 5-3 have 400mm,450 and 500 mm water depth respectively

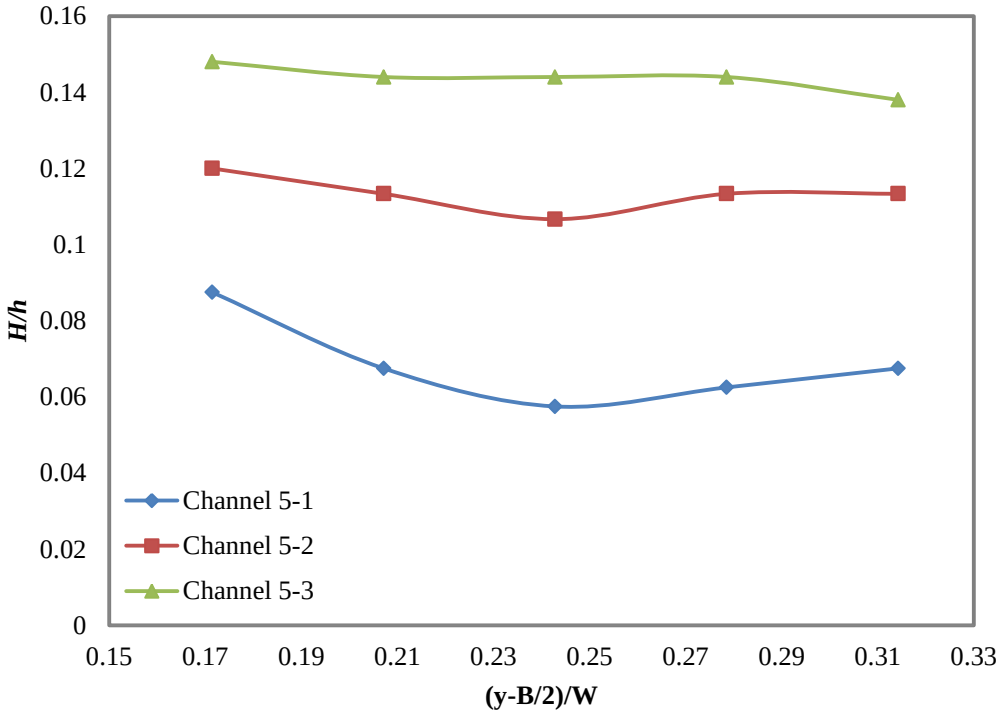

Figure 5-28: Wave heights at diffirent lateral distances for three different water depths at 1.99 m/s speed; Channels 5-1, 5-2 and 5-3 have 400mm,450 and 500 mm water depth respectively

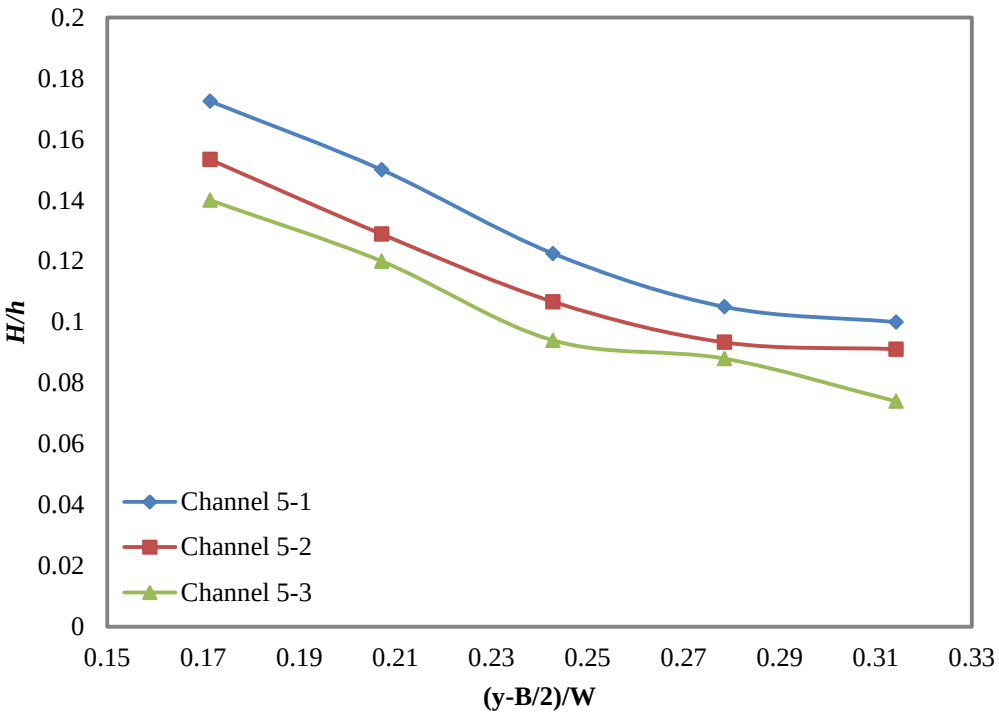

Figure 5-29: Wave heights at diffirent lateral distances for three different water depths at 2.66 m/s speed; Channels 5-1, 5-2 and 5-3 have 400mm,450 and 500 mm water depth respectively

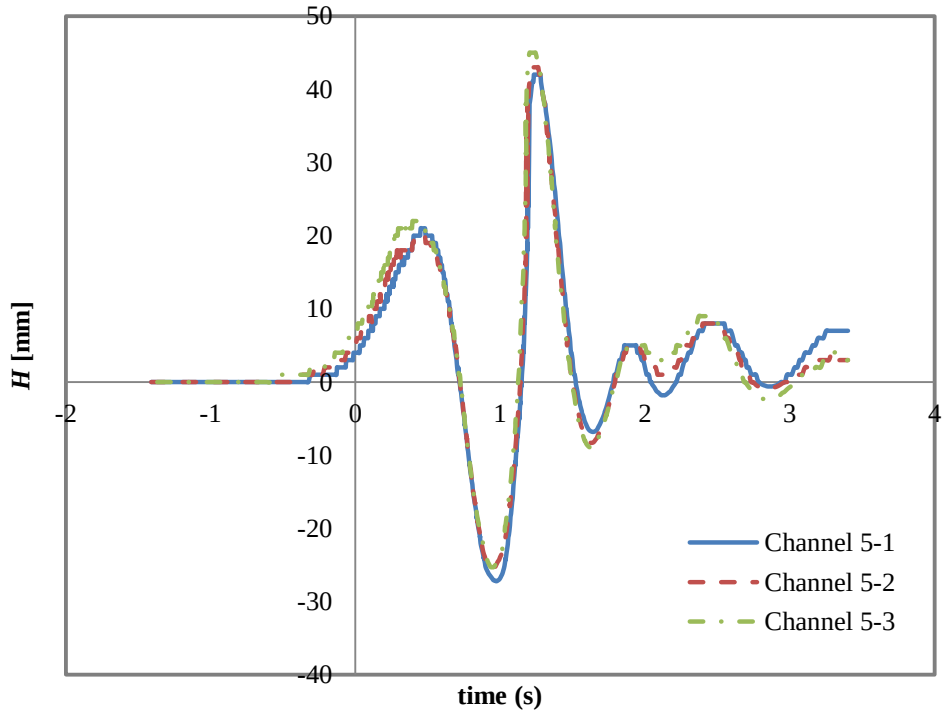

Figure 5-30: History of wave height at 0.75 m lateral distances at 2.66 m/s speed for three different water depths; Channels 5-1, 5-2 and 5-3 have 400mm,450 and 500 mm water depth respectively

5.2.2. Blockage factor

By changing the water depth, depth Froude number and blockage factor will change simultaneously. It was shown in the previous section that changing the water depth has an effect on the generated wave characteristics. To separate the effect of depth Froude number and blockage factor by changing the water depth, a new channel was modelled (channel 5-4) and the results were compared with the two other channels results. Table 5-7 presents the parameters of the three channels which were used for this comparison. Channels 5-1 and 5-4 have the same water depth, and channels 5-3 and 5-4 have the same blockage factor but different water depths. The results for the three different speeds 1.66, 1.99 and 2.66 m/s are presented in Figure 5-31 to Figure 5-33. The depth Froude number for channels 5-1 and 5-3 at V=1.66 m/s are 0.838, while for channel 5-3 at the same speed is equal 0.75, therefore the wave generated height for channels5-1 and 5-4 are larger than channel 5-3 (Figure 5-31) and the blockage factor does not have significant effect for subcritical Fr_h. Figure 5-32 presents the wave height at different lateral distances at V=1.99 m/s. The depth Froude number for channel 5-1 and 5-4 are equal 1.0 and for channel 5-3 is 0.9. As it can be seen the wave generated height for channel 5-3 is larger than two other channels and the effect of depth Froude number is more important than the blockage factor. The Fr_h for all three channels at V=2.66 m/s are more greater than 1.2. In the depth effect study (section 5.2.1) was shown that water depth does not have influence the wave shape at supercritical Froude depth values. According to Figure 5-33, it is possible to generate the higher wave at supercritical Froude depth values by decreasing blockage factor (wider channel).

Table 5-7: Three Different Channels Parameters for Blockage Factor Investigation

	Width (m)	**Depth (m)**	**Blockage factor (κ)**
Channel 5-1	3.5	0.4	0.0214
Channel 5-3	3.5	0.5	0.0171
Channel 5-4	4.375	0.4	0.0171

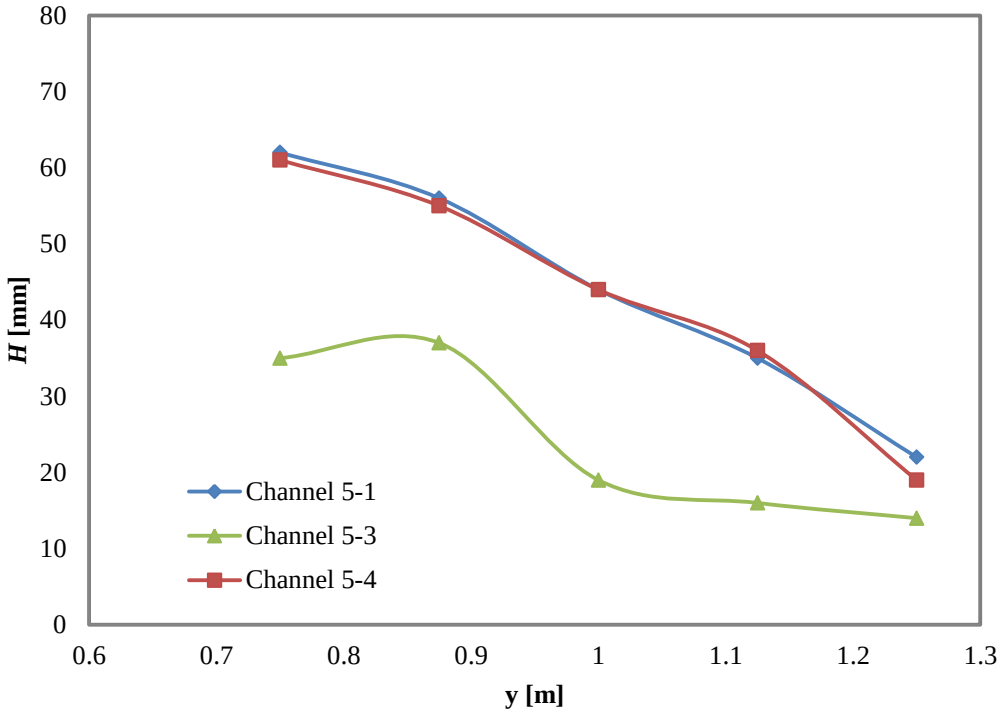

Figure 5-31: Wave heights at different lateral distances for three different water depths at 1.66 m/s speed

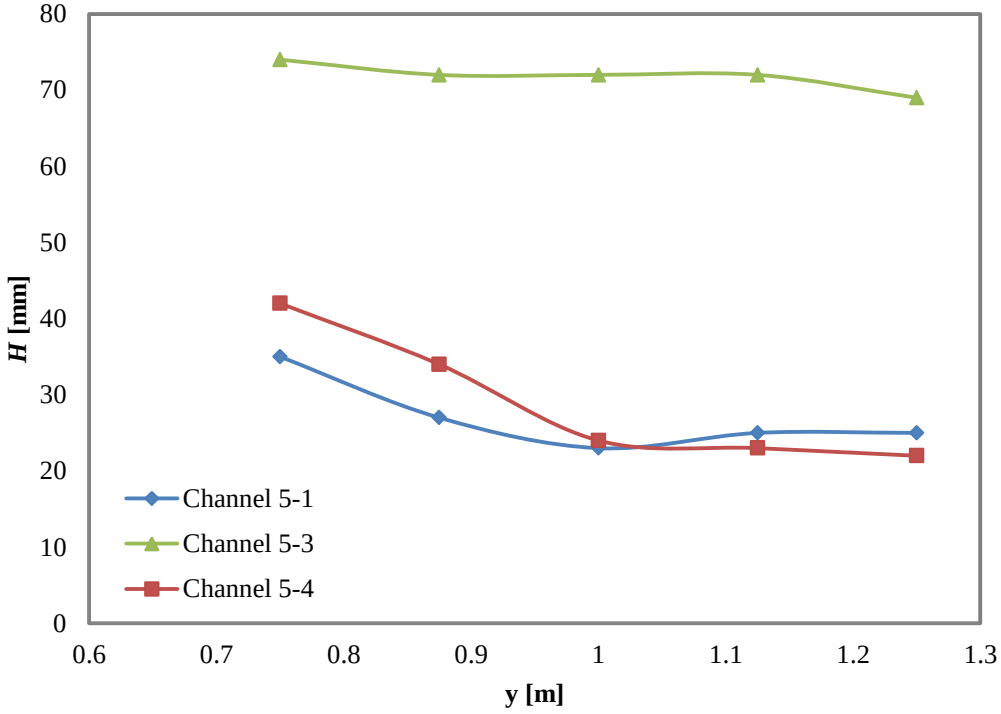

Figure 5-32: Wave heights at different lateral distances for three different water depths at 1.99 m/s speed

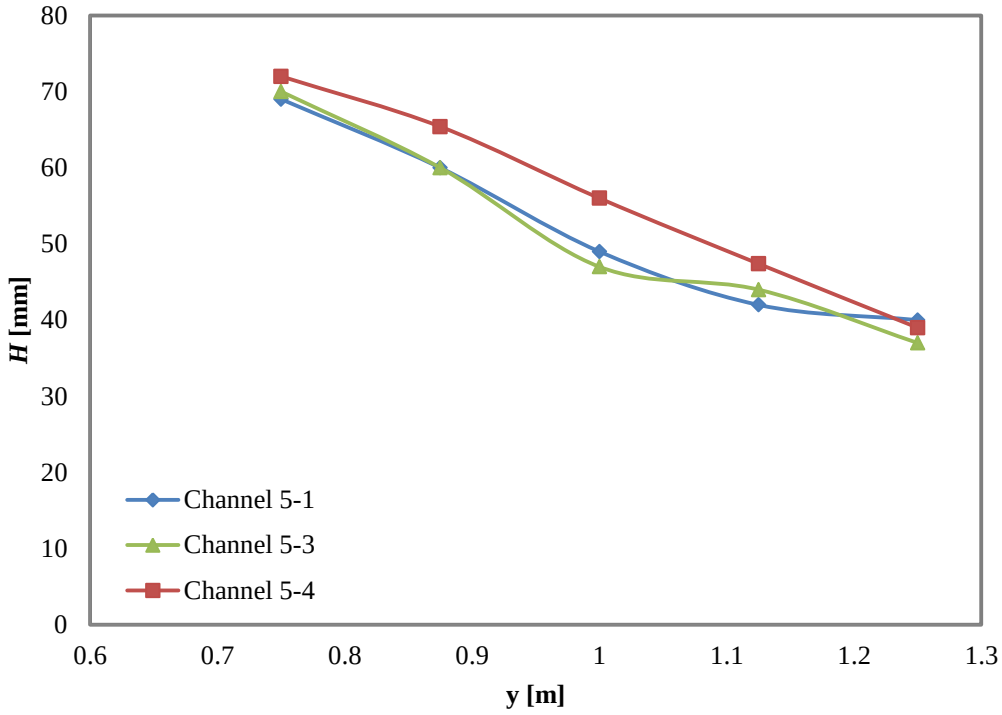

Figure 5-33: Wave heights at different lateral distances for three different water depths at 2.66 m/s speed

The results indicate that the effect of depth Froude number on wave height is more important than the blockage factor for Fr_h<1.0 and the blockage factor at this range is negligible. At supercritical Froude depth values the channel with lowest blockage factor generates the highest wave. More investigations are required to find the highest ineffective blockage factor. At highest ineffective blockage factor the channel cross section would be smallest cross section which does not have influence on the wave generated parameters.

5.3. Concluding remarks

In this chapter the influence of pressure source parameters, depth and blockage factors were investigated. Draught, angle of attack, beam and profile shape were investigated as the effective parameters of pressure source on wave height.

The investigation indicated that increasing draught, angle of attack and beam will increase the wave height generated. It was shown that the quality of waves generated by a lower angle of attack is improved and wave height variation across the channel for a lower angle of attack is less than a higher angle of attack. The pressure gradient will increase by increasing the angle of attack. Hence the predicted wave generated by a wavedozer with a higher angle of attack is greater than those generated from a wavedozer with a smaller angle of attack. Comparing the results for the two different wavedozers with the same displacement and angle of attack, but different beam and draught showed that the model with the wider beam generates a higher wave than the model with larger draught. This means that the effect of beam on generated waves is greater than the effect of draught. The model

with larger beam has larger water plane and consequently the volume of displacement close to free surface for model with larger beam is bigger than the model with larger draught. It is expected that there is a limitation for the effective draught and the draught larger than that amount does not have effect on wave generated height because only the portion of displacement close to free surface has effect on the wave generated. Increasing the beam increases the wave height till the wave generated does not break.

A new profile shape of pressure source was investigated. This pressure source has a wider beam in the transom and is slimmer in front. The displacement, draught and angle of attack of this model was the same as the wavedozer model with the 300 mm beam, 100 mm draught and a 14 degree angle of attack. The waves generated by this new profile shape were higher than that of the standard wavedozer, but the wave run-up in front of this model was much higher than that of the wavedozer.

The water depth study showed that it is possible to generate a larger wave height by decreasing the water depth for a given speed as long as the Fr_h is subcritical and the maximum wave height generated at Fr_h=0.9. When Fr_h=1 the bow (soliton) wave generated is higher than the wave behind the pressure source. It was also shown that water depth does not have an effect on the wave height for Fr_h more than 1.2. It means for this range of Fr_h the downstream does not have influence on upstream, because the pressure source moves faster than wave speed.

The blockage factor was investigated. The results indicate that the effect of depth Froude number on wave height is more important than the blockage factor for subcritical Froude depth values and the blockage factor at this range is negligible. At supercritical Froude depth values the channel with lowest blockage factor generates the highest wave. Further simulations are needed to find the highest ineffective blockage factor. The highest ineffective blockage factor would be useful in terms of construction, which presents the smallest channel section area without affecting the wave parameters.

6. Conclusions and recommendations

In this thesis a novel method for generating surfable waves has been described and investigated. This is a new surf pool concept to generate continuous surfable waves, with one or more pressure sources being rotated within an annular pool to generate waves. The circular channel has sloping bathymetry with the outer side being deeper; the waves are generated in the deep water and break in the shallow water on the inner island. Previous studies, that were primarily experimentally based, demonstrated that it is possible to generate the surfable waves with this method. However due to a lack of knowledge concerning waves generated in such a restricted environment, the influence of many parameters on the generated waves needed to be considered. For successful circular wave pool design many aspects need a much improved level of understanding, for example: the waves generated by moving pressure sources, the waves' propagation and the effect of bathymetry on the wave quality for surfing. Studying all these parameters by experimental means would be exceptionally time consuming and expensive, so computational fluid dynamics was proposed as an effective alternative approach. All previously proposed numerical methods were not able to predict the behaviour of these waves accurately. Therefore the core research question of this thesis was to investigate whether a new numerical method could be used as a research tool to gain insight into the production of highly controlled waves suitable for surfing and subsequently for proposed designs, in particular to numerically investigate the shape of the pressure source and wave pool bathymetry.

To validate the numerical approach several series of experimental tests were conducted at the Australian Maritime College, these experiments also provided valuable data on wave generation limitations, including pressure source shape and channel parameters. To investigate the numerical method's capability to predict the wave generation and breaking characteristics, the finite volume approach was chosen. To examine the accuracy and stability of the numerical scheme, different configurations were simulated and compared with the experimental data. In this part of the study different pressure sources and channel shapes that had been experimentally tested were numerically simulated. It was found that the numerical approach used is capable of accurately predicting wave height, propagation and forces on the pressure sources (drag and lift) with the differences between the experimental and numerical results in relation to wave height being less than 10% and in relation to the forces less than 4%.

An extensive grid study was conducted to improve the accuracy of the results and decrease the simulation cost by optimising the cell size. In this mesh study the effect of aspect ratio, the number of cells per wave length and wave height were also investigated. It was shown that mesh quality has a significant effect on wave height prediction. According to the numerical results, an average aspect ratio of about 7 is required to efficiently predict wave height. It was assumed that the flow is more perpendicular to cell faces and thus numerical diffusion is the lowest in this aspect ratio. In terms of

the number of cells per wave height, the results showed that 10 cells are sufficient to predict wave height and increasing this value does not result in increased accuracy in the wave height prediction. It was thus concluded that mesh quality (aspect ratio) is much more important than the number of cells in the computational domain. Using the new mesh domain resulting from the mesh study, the previous simulations were re-modelled and it was shown that it is possible to obtain results with the same level of accuracy, but with significantly fewer cells.

After ascertaining that the numerical method was appropriate (thus answering the main research question), the numerical method was used to gain an improved understanding of the influence of the pressure source parameters on generating high quality surfable waves and the effect of channel bathymetry on wave propagation.

In order to define the pressure source parameters for generating high quality surfable waves, various pressure source shapes were modelled and the results compared. The effects of wavedozer parameters such as draught, angle of attack and beam were investigated and it was shown that increasing the draught, angle of attack and beam increases the height of the generated waves. The comparison between two wavedozers with the same displacement and angle of attack but different beam and draught showed that increasing the beam is more effective than increasing draught in terms of increasing the wave height. The wider pressure source has a larger waterplane that causes higher waves to be generated. The waves generated by a higher attack angle wavedozer were found to be larger than the lower attack angle, but the quality of the waves generated by the lower angle of attack was better. Increasing the attack angle for constant draught increases the pressure gradient and thus the generated wave height will increase.

Two further pressure sources with different plan and profile shapes were investigated: a wedge with variable beam and a wedge shape with constant beam but convex profile at the bottom. The wedge shaped pressure source with variable beam generated the highest waves, but there was large wave run up in front of this pressure source. According to the results for the convex shape, it was concluded that the angle of attack in front of the pressure source (stagnation point) is more effective than the attack angle at the transom.

The effect of channel bathymetry on the wave breaking location, wave breaking intensity, peel angle and wave wall length in full scale were examined. From the channels studied it was concluded that channel shape does not have a significant effect on the maximum wave height, but the width of the deep section of the channel has a significant influence on the breaking location and the channel slope has an effect on the breaking intensity. The narrowest channel was considered to be the best, due to its cheaper construction costs, while the wave wall length was longest in the channel with the widest deep-section. In terms of wave breaking intensity, all four investigated channels were capable of generating barrel-shaped breaking waves, which is the required wave quality for surfing. It was shown

that high quality continuous breaking waves, with the desired plunging shape and long wave length, were able to be generated and it is possible to create waves suitable for surfers from beginner to expert level by changing the pressure source speed.

To find the relationship between scale factor and wave parameters, two different scales were modelled and wave height, shape and forces were compared and relationships were developed for each of the parameters. According to the scale comparison, by scaling the pressure source and channel the shape of the wave does not change. The wave height was found to scale with the scale factor and the pressure source forces (drag and lift) scaled by the scale factor to the power of 3.

The water depth and blockage factor effects on the waves generated were also investigated. Decreasing the water depth was found to increase the wave height for a given speed until the Fr_h was subcritical. It was concluded that in supercritical Fr_h the water depth does not have an influence on wave height. The results indicate that the effect of depth Froude number on wave height is more important than the blockage factor for subcritical depth Froude numbers and the influence of blockage factor is negligible. However at supercritical depth Froude number values the channel with the lowest blockage factor generates the highest wave. Further simulations would be needed to find the highest blockage factor that is ineffective.

The following are recommendations for future research:

- It was proved that the numerical approach is able to predict the wave-generated parameters. In addition, it was shown that mesh quality has significant effect on the result accuracy. In order to improve the accuracy and further decrease the simulation time other parameters effects such as turbulence modelling, order of discretisation and free surface modelling approach should be considered.
- It was shown that mesh aspect ratio of approximately 7 is required to accurately predict the wave height. It is recommended to further work should be conducted to determine how the aspect ratio affects the result accuracy and why an aspect ratio of about 7 is appropriate.
- While some investigations were conducted into improving the pressure source performance, there are other designs that should be investigated further. For example, since increasing the angle of attack increases the generated wave height; it is recommended that the effect of angles of attack greater than 14 degrees should be studied.
- Increasing beam will increase the wave height, but it was predicted that there are limitations to this increase, as wave breaking will occur. As a future study, it is recommended that the maximum effective beam is found.
- The study showed that increasing the draught increases the height of the generated wave. Since the volume of the pressure source close to the free surface has an effect on the wave generated, there is clearly a limit for draught, and increasing the displacement past this limit

does not have an effect on the wave generated. It is suggested that an investigation is conducted to find the maximum effective draught.

- Finding the maximum effective blockage factor is another case to study, since establishing the narrowest channel width without affecting the wave parameters will help to minimise construction costs.

References:

1. *Surfing Statistics*. 2.19.2014]; Available from: http://www.statisticbrain.com/surfing-statistics/.
2. *Andrew Stark - The Man Who Runs Surfing Australia*. 31 Jan, 2013; Available from: http://www.coastalwatch.com/news/article.aspx?articleId=7745&cateId=3.
3. Stark, A. *Surfing Australia Fast Facts*. 2012; Available from: http://www.surfingaustralia.com/statistics.php.
4. Black, K. and S. Mead, *Field Studies Leading to the Bathymetric Classification of World-Class Surfing Breaks.* Journal of Coastal Research, 2001: p. 5-20.
5. Schmied, S., et al., *A Novel Method for Generating Continuously Surfable Waves.* Marine Technology Society Journal, 2010: p. 7-12.
6. *Cruise Ahead*. 2010 04/06/2010]; Available from: http://www.cruiseahead.co.uk/offer-of-the-week/canaries-cruise-4th-may-2011/.
7. Webber, G., *Wave Generation Apparatus*, I.P. Australia, Editor 2004: Australia.
8. Webber, G., W.I.P. Organization, Editor 2006: Switzerland.
9. Schmied, S., et al. *A Novel Method For Generating Continuously Surfable Waves-Comparison Of Predictions With Experimental Results*. in *30th International Conference on Ocean, Offshore and Arctic Engineering*. 2011. Rotterdam, Netherlands.
10. Schmied, S., *Limitations On The Creation of Continuously Surfable Waves Generated By A Pressure Source Moving In A Circular Path*, in *Australian Maritime College*2014, University of Tasmania.
11. Georgiadis, C., *Modeling Boat Wake Loading on Long Floating Structures.* Computers & Structures, 1984. **18**(4): p. 6.
12. Sorensen, R.M., *Investigation of Ship-Generated Waves.* Waterways and Harbors Division, 1967: p. 14.
13. Sorenson, R.M., *Waves Generated by Model Ship Hull.* Waterways and Harbors Division, 1969: p. 26.
14. Pianc, *Guidlines for Managing Wake Wash from High-Speed Vessels*, in *Marcom Report of Working Group 41*2003, International Navigation Associaltion.
15. Melsheimer, C., H. Lim, and C. Shen. *Observation and Analysis of Ship Wakes in ERS-SAR and Spot Images*. in *20th Asian Conference on Remote Sensing*. 1999. Hong Kong, China.
16. Imani, A.A., et al., *Approximate Traveling Wave Solution for Shallow Water Wave Equation.* Applied Mathematical Modeling, 2012. **36**(4): p. 8.
17. Molland, F., S.R. Turnock, and D.A. Hudson, *Ship Resistance and Propulsion: practical estimation of ship propulsive power*. 2011: Cambridge.
18. Dam, K.T., et al., *Numerical Study of Propagation of Ship Waves on a Sloping Coast.* Ocean Engineering, 2006. **33**: p. 15.
19. Jiankang, W., T.S. Lee, and C. Shu, *Numerical Study of Wave Interaction Generated by Two Ships Moving Parallely in Shallow Water.* Computer Methods in Applied Mechanics and Engineering, 2001. **190**: p. 12.
20. Macfarlane, G. and G. Cox. *The Development of Vessel Wave Wake Criteria for the Noosa and Brisbane Rivers in Southeast Queensland*. in *5th International Conference on Coastal Environment*. 2004. Alicante, Spain.
21. Macfarlane, G. and N. Bose, *Wave Wake: Focus On Vessel Operations Within Sheltered Waterways.* SNAME, 2012. **006**.
22. Varyani, K.S., *Full scale study of the wash of high speed craft.* Ocean Engineering, 2006. **33**(5-6): p. 18.
23. Macfarlane, G., G. Cox, and J. Bradbury, *Bank Erosion From Small Craft Wave Wake in Sheltered Waterways.* RINA Transactions, International Journal of Small Craft Technology, 2008. **Part B**.

24. Nanson, G.C., et al., *Experimental Measurements of River-Bank Erosion Caused by Boat-Generated Waves on the Gordon River, Tasmania.* Regulated Rivers; Research and Management, 1994. **9**.
25. Mead, S. *Surfing Science*. in *3rd International Surfing Reef Symposium*. 2003. Raglan, New Zealand.
26. Walker, J.R. and R.Q. Plamer, *A General Surfe Site Concept*, 1971, LOOk Laboratory TR-18, department of Ocean Engineering, University of Hawaii.
27. Black, K. and S. Mead, *Beach amenity options and coastal protection at bournemouth*, 2000, Leisure and Tourism Service: Bournemouth Borough Council.
28. Hutt, J.A., K.P. Black, and S.T. Mead, *Classification of surf breaks in Relation to Surfing Skill.* Journal of Coastal Research, 2001(29): p. 16.
29. Battjes, J.A., *Surf Similarity*, in *14th Coastal Engineering Conference*1974. p. 15.
30. Sayce, A., k. Black, and R. Gorman, *Breaking Wave Shape on Surfing Reefs* in *14th Australian Conference on Coastal Engineering*1999. p. 596-603.
31. Dally, W.R., *Stochastic Modeling of Surfing Climate*, in *22nd Coastal Engineering Conference*1990.
32. Pengzuin, L. Philip, and F. Liu, *A Numerical Study of Breaking Waves in the Surf Zone.* Journal of Fluid Mechanics, 1998. **359**: p. 25.
33. Mortensen, S.B., *Detailed Investigation of Surfing Amenity Using CFD*, 2010, DHI Water & Environment. p. 12.
34. Scarfe, B.E., et al., *The Science of Surfing Waves and Surfing Breaks- a review*, 2003.
35. Schmied, S. and M. Meier, *Surfin' in Circles.* Eng World, 2007.
36. Schipper, M.A., *On the Generation of Surfable Ship Waves in a Circular pool: Part I Physical background & Wave pool design* 2007, Delft University of Technology.
37. Vries, T., *On the Generation of Surfable Ship Waves in a Circular Pool, part II*, 2007, Delft University of Technology.
38. Schmied, S., *Test Plan-Tow Tank Testing*, 2009, Australian Maritime College.
39. Schmied, S., *Test Plan- Scale Model- Second Test Session*, 2011, Australian Maritime College.
40. Doyle, N., *The Circular Wave Pool- Predicting Curved Path Wave Patterns*, in *Australian Maritime College*2010, University of Tasmania.
41. Essen, S.V., *RAPID Non-linear Potential Flow Wave Height Prediction*, 2011, Australian Maritime College.
42. Versteeg, H.K. and W. Malalasekera, *Introduction to Computational Fluid Dynamics. The Finite Volume Method*. 1995: Longman.
43. Tannehill, J.C., D.A. Anderson, and R.H. Pletcher, *Computational Fluid Mechanics and Heat Transfer*. 1997: Taylor & Francis.
44. Driscoll, A. and M.R. Renilson, *The Wavedozer. A System of Generating Stationary Waves in a Circulating Water Channel.* AMTE(H) TM80013, 1980.
45. *ANSYS FLUENT User's Guide*, 2011, ANSYS, Inc.
46. Yang, Q., O.M. Faltinsen, and R. Zhao, *Wash Of Ships In Finite Water Depth*, in *FAST*2001, The Royal Institution Of Naval Architects: Southhampton, UK. p. 181-196.
47. Raven, H.C., *Numerical Wash Prediction Using A Free-Surface Panel Code*, in *International Conference on Hydrodynamics of High-Speed Craft - Wake Wash and Motion Control*2000, The Royal Institution Of Naval Architects: London, UK.
48. Chandraprabha, S. and A.F. Molland, *A Numerical Preiction Of Wash Wave And Wave Resistance Of High Speed Displacement Ships In Deep And Shallow Water*, in *Conference Of Mechanical Engineering Network Of Thailand*2004: Khon Kaen, Thailand.
49. Kofoed-Hansen, H., T. Jensen, and O.R. Sørensen, *Wake Wash Risk Assessment Of High-Speed Ferry Routes – A Case Study And Suggestions For Model Improvements*, in *International Conference on Hydrodynamics of High-Speed Craft - Wake Wash and Motion Control*2000, The Royal Institution of Naval Architects: London, UK.
50. Kim, Y., *Artificial Damping In Water Wave Problems II: Application to Wave Absorption.* International Journal of Offshore and Polar Engineering, 2003. **13**: p. 5.
51. *ANSYS FLUENT User's Guid*, 2011, ANSYS, Inc.

52. Wilcox, D.C., *Turbulence Modeling for CFD*. 1994: DCW Industries, Inc.
53. Andersson, B., et al., *Computational Fluid Dynamics for Engineers*. 2012: Cambridge University Press.
54. Muzaferija, S., et al. *A Two-Fluid Navier-Stokes Solver to Simulate Water Entry*. in *International Proceeding 22nd Symposium on Naval Hydrodynamics*. 1998. Washington, DC.
55. Richardson, l.F. and J.A. Gaunt, *The Deferred Approach to the Limit. Part I. Single Lattice. Part II. Interpenetrating lattices*, in *Philosophical Transactions of the Royal Society of London. Series A, Conatining Papers of a Mathematical or Physical Charatcter*. 1927, The Royal Society. p. 299-361.
56. Karcz, J. and L. Kacperski, *An Effect Of Grid Quality On The Results Of Numerical Simulations Of The Fluid Flow Field In An Agitated Vessel*, in *14th European Conference on Mixing*2012: Warsaw, Poland.
57. Diskin, B. and J.L. Thomas, *Effects of Mesh Irregularities on Accuracy of Finite-Volume Discretization Schemes.* American Institute of Aeronautics and astronautics, 2012.
58. Mastin, C.W. *Error Induced by Coordinate Systems*. in *Numerical grid generation*. 1982. Nashville, United States.
59. Lee, J. and Y.M. Tsuei, *A Formula for Estimation of Truncation Errors of Convection Terms in a Curvilinear Coordinate System.* Computational Physics, 1992. **98**: p. 90-100.
60. Diskin, B. and J.L. Thomas, *Comparison of Node-Centered and Cell-Centered Unstructured Finite-Volume Discretizations: Viscous Fluxes.* AIAA Journal, 2010. **48**: p. 1326-1338.
61. Mavriplis, D.J., *Revisiting the Least-Square Procedure for Gradient Reconstruction on Unstructured Meshes*, in *AIAA Computational Fluid Dynamics*2003.
62. ANSYS, *Solving the Linear System*, in *Ansys Fluent*2009.
63. Galvin, C.J.J., *Breaker Type Classification on Three Laboratory Beaches.* J. Geoph. Res., 1968(73): p. 3651-3659.
64. Walker, J.R., *Recreational Surf Parameters*, 1974, LOOk Laboratory TR-30, department of Ocean Engineering, University of Hawaii.
65. Hutt, J.A., *Bathymetry and Wave Parameters Defining The Surfing Quality of Five Adjacent Reefs*, 1997, The University of Waikato.
66. *Lump- Instatnt galleries to share with friends*. Available from: http://lump.co/surfing.
67. Bremner, J. *World's 50 best surf spots*. Available from: http://www.cnn.com/2013/06/30/travel/50-surf-spots/.
68. Black, K. and S. Mead, *Predicting the Breaking Intensity of Surfing Waves.* Special Issue of the Journal Coastal Reseach on Surfing, 2001.

Appendices

Appendix A

Number of cells per wave length= number of cells which cover the first wave in the X direction

$$Average\ cells\ size\ in\ the\ X\ direction = \frac{Number\ of\ cells\ per\ wave\ length}{wave\ length}$$

Number of cells per wave height= number of cells which cover the first wave in the Z direction

$$Average\ cells\ size\ in\ the\ Z\ direction = \frac{Number\ of\ cells\ per\ wave\ height}{wave\ height}$$

$$Aspect\ ratio = \frac{Average\ cells\ size\ in\ the\ X\ direction}{Average\ cells\ size\ in\ the\ Z\ direction}$$

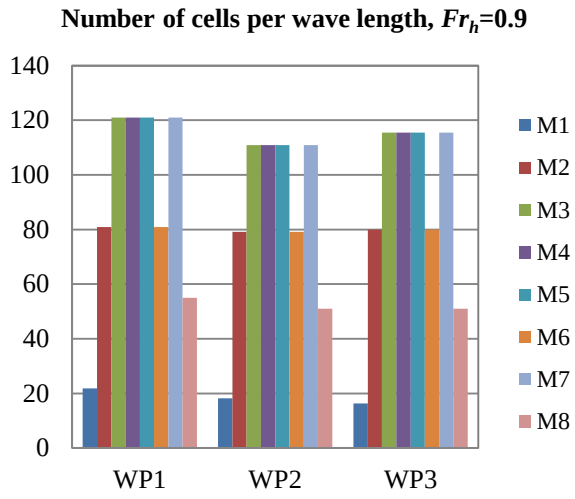

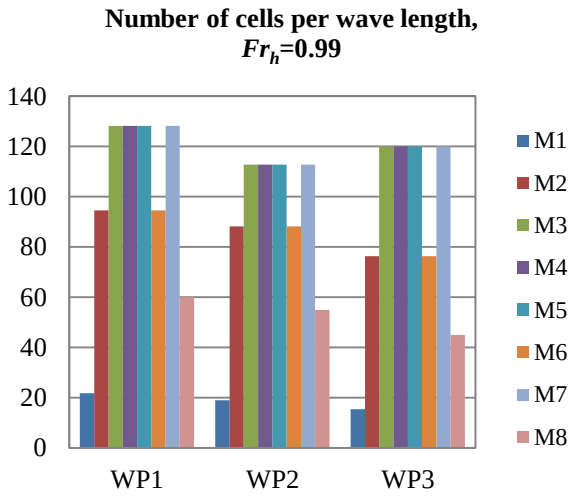

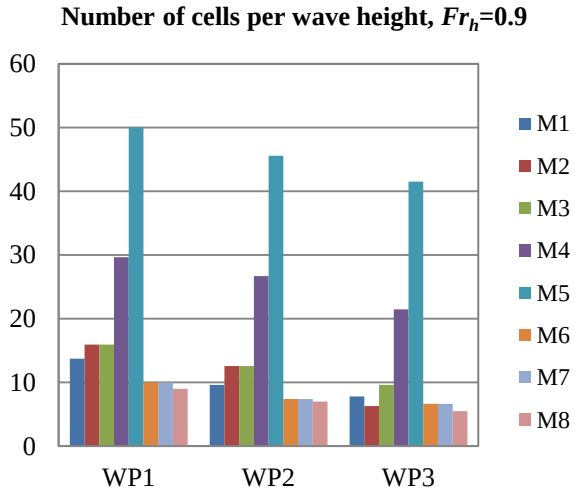

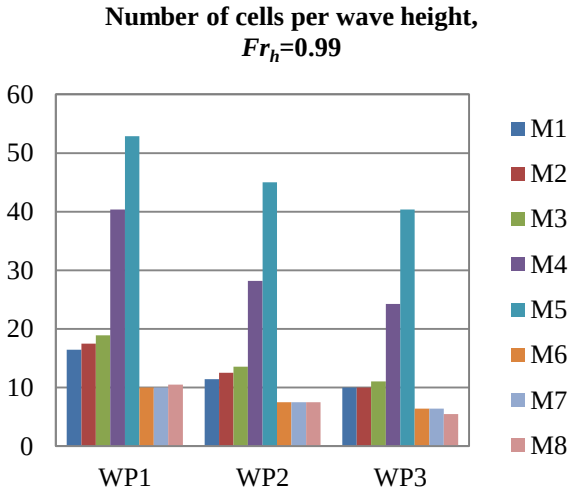

Average cells size in the Z direction (mm), Fr_h=0.9

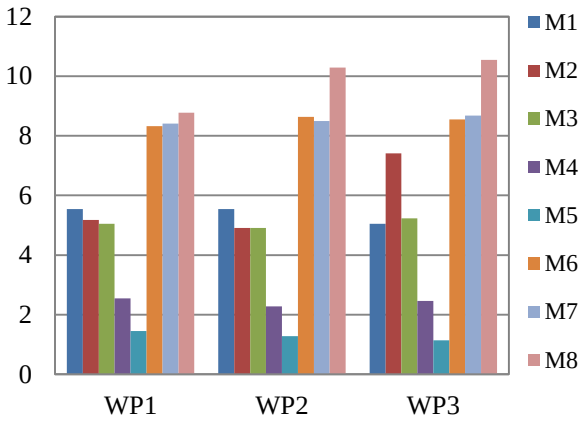

Average cells size in the Z direction (mm), Fr_h=0.99

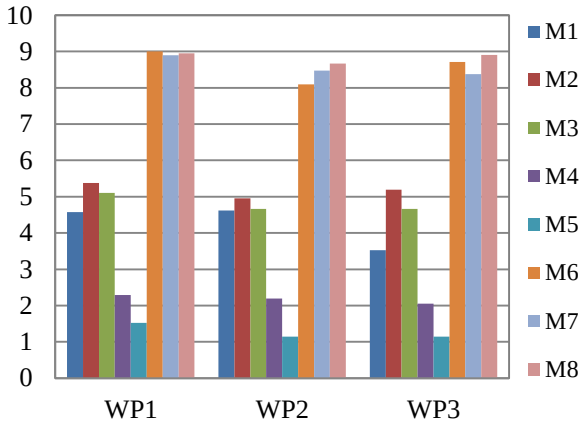

Average cells size in the X direction (mm), Fr_h=0.9

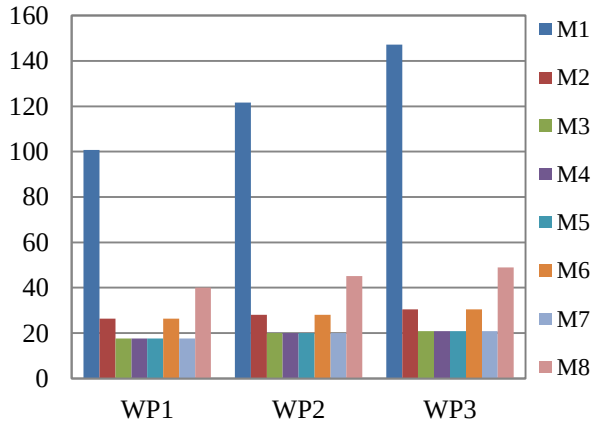

Average cells size in the X direction (mm), Fr_h=0.99

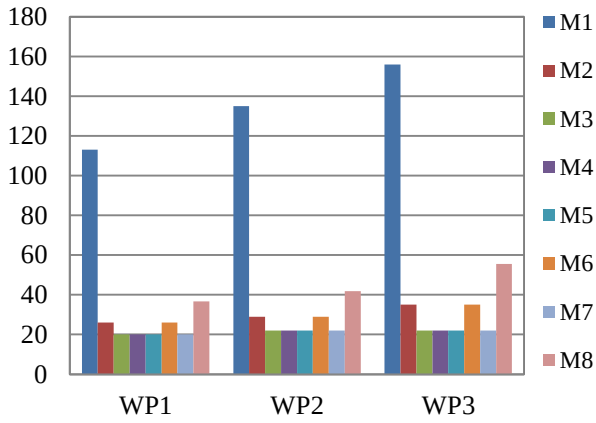

Aspect ratio (x/z), Fr_h=0.9

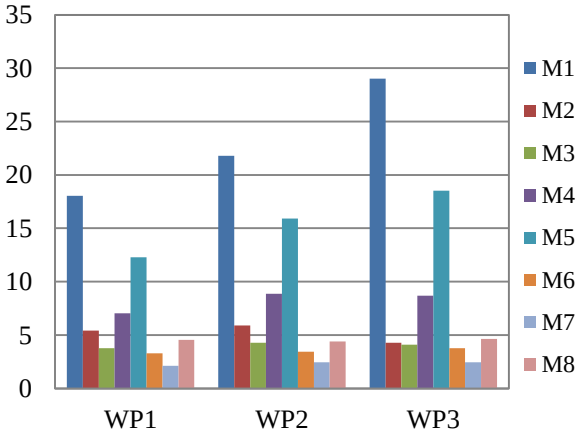

Aspect ratio (x/z), Fr_h=0.99